A Hybrid Electronic Nose System for Monitoring the Quality of Potable Water

Hyun Woo Shin

Submitted in fulfillment of the requirements
for the degree of Doctor of Philosophy

University of Warwick
School of Engineering

October 1999

Contents

List of Figures

List of Tables

To my wife, Nan Kyung and
my daughters, Hye Jin and Young Jin

Acknowledgements

I would like to thank my supervisor, Prof. Julian Gardner, for his guidance, advice and inspiration during my MRes and PhD. I also thank LG Corporate Institute of Technology for giving me the opportunity of studying at Warwick University and for financial support. I would like to acknowledge the British Council for my scholarship and the British Embassy for the UK-Korea Science and Technology Collaboration Fund.

Many people have kindly helped me throughout my stay at Warwick.
School of Engineering, Warwick University: Dr. Evor Hines, Mr. Frank Courtney, Mr. James Covington, Mr. Ian Griffith, Mr. Craig Lloyd, Mr. Doo Won Choi, Dr. Yong-Tae Jun, Mr. Pascal Boilot, Mr. Sherzad Al-Khalifa and Mr. Reza Tamadoni for their assistance and valuable comments.
Department of Biological Sciences, Warwick University: Dr. Crawford Dow, Dr. Uthaya Swoboda and Mrs. Jenny Flint for providing the environment for the cyanobacteria data collection experiments.
Department of Chemistry, University of Southampton: Prof. Phillip Bartlett and Miss Isabelle Besnard for conducting polymer deposition.
Department of Electronic Engineering, Universitat Rovira i Virgili: Dr. Eduard Llobet for valuable discussions.

Special thanks to Prof. Choon Sik Kang (Seoul National University) and Dr. Sung-Tae Kim (LG CIT) for their concern and encouragement. Many thanks to Dr. Hyung-Ki Hong (LG CIT) for his assistance.

Finally, I would like to thank my parents, family and friends for their continual support and encouragement.

Declaration

This thesis is presented in accordance with the regulations for the degree of doctor of philosophy. The work described by the author is entirely original and my own unless otherwise indicated.

Summary

This PhD thesis reports on the potential application of an electronic nose to analysing the quality of potable water. The enrichment of water by toxic cyanobacteria is fast becoming a severe problem in the quality of water and a common source of environmental odour pollution. Thus, of particular interest is the classification and early warning of toxic cyanobacteria in water. This research reports upon the first attempt to identify electronically cyanobacteria in water. The measurement system comprises a Cellfacts instrument and a Warwick e-nose specially constructed for the testing of the cyanobacteria in water. The Warwick e-nose employed an array of six commercial odour sensors and was set-up to monitor not only the different strains, but also the growth phases, of cyanobacteria. A series of experiments was carried out to analyse the nature of two closely related strains of cyanobacteria, *Microcystis aeruginosa* PCC 7806 which produces a toxin and PCC 7941 that does not. Several pre-processing techniques were explored in order to remove the noise factor associated with running the electronic nose in ambient air, and the normalised fractional difference method was found to give the best PCA plot. Three supervised neural networks, MLP, LVQ and Fuzzy ARTMAP, were used and compared for the classification of both two strains and four different growth phases of cyanobacteria (lag, growth, stationary and late stationary). The optimal MLP network was found to classify correctly 97.1 % of unknown non-toxic and 100 % of unknown toxic cyanobacteria. The optimal LVQ and Fuzzy ARTMAP algorithms were able to classify 100% of both strains of cyanobacteria. The accuracy of MLP, LVQ and Fuzzy ARTMAP algorithms with 4 different growth phases of toxic cyanobacteria was 92.3 %, 95.1 % and 92.3 %, respectively.

A hybrid e-nose system based on 6 MOS, 6 CP, 2 temperature sensors, 1 humidity sensor and 2 flow sensors was finally developed. Using the hybrid system, data were gathered on six different cyanobacteria cultures for the classification of growth phase. The hybrid resistive nose showed high resolving power to discriminate six growth stages as well as three growth phases. Even though time did not permit many series of the continuous monitoring, because of the relatively long life span (30–40 days) of cyanobacteria, improved results indicate the use of a hybrid nose. The HP 4440 chemical sensor was also used for the discrimination of six different cyanobacteria samples and the comparison with the electronic nose. The hybrid resistive nose based on 6 MOS and 6 CP showed a better resolving power to discriminate six growth stages as well as three growth phases than the HP 4440 chemical sensor. Although the mass analyser detects individual volatile chemicals accurately, it proves no indication of whether the volatile is an odour.

The results demonstrate that it is possible to apply the e-nose system for monitoring the quality of potable water. It would be expected that the hybrid e-nose could be applicable to a large number of applications in health and safety with a greater flexibility.

Publications from this thesis

The following is a list of publications, in chronological order, of publications from this thesis:

1. H. W. Shin, C. Lloyd, and J. W. Gardner, “Combined resistive and calorimetric sensing of gases using a single micromachined device”, Transducers ‘97, Chicago, 16-19 June 1997, pp.935-938

2. H. W. Shin, C. Lloyd, and J. W. Gardner, “A combined resistive and calorimetric gas sensor”, The 3rd East Asia Conference on Chemical Sensors, Seoul, 5-6 November 1997, pp.466-469.

3. H. W. Shin, J. W. Gardner, E. L. Hines, and C. S. Dow, “Classification of cyanobacteria in water with an electronic nose”, The 6th International Symposium, Olfaction & Electronic Nose 99, Tübingen, 20-22 September 1999, pp. 366-367.

4. J. W. Gardner, C. S. Dow, H. W. Shin, G. Searle, and M. J. Chappell, “Dynamical signal processing techniquesfor bioprocess monitoring”, The 6th International Symposium, Olfaction & Electronic Nose 99, Tübingen, 20-22 September 1999, pp. 331-335.

5. H. W. Shin, J. W. Gardner, E. L. Hines, and C. S. Dow, “An electronic nose system for monitoring the quality of potable water”, Sensors and Actuators B, (accepted).

6. H. W. Shin, E. Llobet, J. W. Gardner, E. L. Hines, and C. S. Dow, “The classification of the strain and growth phase of cyanobacteria in potable water using an electronic nose system”, IEE - Sci. Meas. Technol., (submitted).

7. H. W. Shin, J. W. Gardner, and E. L. Hines, “An electronic nose system to diagnose illness”, Sensors and Actuators B, (accepted).

List of Author's Publications

JOURNALS

1. Hyun Woo Shin, Choon-Sik Kang and Zin-Hyoung Lee, "Composite by the Centrifugal Casting Process," The Journal of the Korean Foundrymen's Society, Vol. 9, No. 2, pp. 143-151, 1989.

2. Kyuchung Lee, Dong Hyun Yun, Hyeon Soo Park, Hyun Woo Shin, Hyung-Ki Hong, Chul Han Kwon and Sung-Tae Kim, "Thin film Micro-Gas-Sensor for Detecting CH_3SH," Sensors and Materials, Vol. 7, No 1, pp. 35-41, 1995.

3. Hyeon Soo Park, Hyun Woo Shin, Dong Hyun Yun, Hyung-Ki Hong, Chul Han Kwon, Kyuchung Lee and Sung-Tae Kim, "Tin oxide micro-gas-sensor for detecting CH_3SH," Sensor and Actuators B, Vol. 25, No. 1-3, pp. 478-481, 1995.

4. Hyun Woo Shin, Hyeon Soo Park, Dong Hyun Yun, Hyung-Ki Hong, Chul Han Kwon and Kyuchung Lee, "Fabrication of ZnO thin film gas sensor for detecting $(CH_3)_3N$ gas," The Journal of the Korean Institute of Electrical and Electronic Material Engineers, Vol. 8, No. 1, pp. 21-26, 1995.

5. Hyung-Ki Hong, Hyun Woo Shin, Hyeon Soo Park, Dong Hyun Yun, Chul Han Kwon, Kyuchung Lee, Sung-Tae Kim and Toyosaka Moriizumi, "Gas identification using micro-gas-sensor array and neural-network pattern recognition," Sensors and Actuators B, Vol. 33, pp. 68-71, 1996.

6. Hyung-Ki Hong, Hyeon Soo Park, Dong Hyun Yun, Hyun Woo Shin, Chul Han Kwon and Kyuchung Lee, "Technical trend of Electronic Nose System," accepted to the Journal of the Korean Institute of Electrical and Electronic Material Engineers.

7. Dong Hyun Yun, Chul Han Kwon, Hyung-Ki Hong, Hyun Woo Shin, Seung-Ryeol Kim, Kyuchung Lee "Abnormal current-voltage characteristics of WO_3-doped SnO_2 oxide semiconductors and their applications to gas sensors," Sensors and Actuators B, Vol. 35-36, pp. 48-51, 1996.

8. Hyung-Ki Hong, Hyun Woo Shin, Dong Hyun Yun, Seung-Ryeol Kim, Chul Han Kwon, Kyuchung Lee and Toyosaka Moriizumi, "Electronic nose system with micro gas sensor array," Sensors and Actuators B, Vol. 35-36, pp. 338-341, 1996.

CONFERENCES

1. Kyuchung Lee, Dong Hyun Yun, Hyeon Soo Park, Hyun Woo Shin, Hyung-Ki Hong, Chul Han Kwon and Sung-Tae Kim, "Microelectronic Thin Film Gas Sensor for Detecting CH_3SH," The Fourth Conference on Sensor Technology, Vol. 4, No. 1, pp. 242-245, 1993.

2. Hyun Woo Shin, Hyeon Soo Park, Dong Hyun Yun, Hyung-Ki Hong, Chul Han Kwon, Kyuchung Lee and Sung-Tae Kim, "Fabrication of $ZnO/A1_2O_3$ thin film gas sensor for detecting $(CH_3)_3N$ gas," The 1st Korean Semiconductor Conference, pp. 401-402, 1994.

3. Kyuchung Lee, Dong Hyun Yun, Hyeon Soo Park, Hyun Woo Shin, Hyung-Ki Hong, Chul Han Kwon and Sung-Tae Kim, "Fabrication and Characterization of Si-based Microsensors for Detecting CH_3SH and $(CH_3)_3N$ gases," Korea-Australia Joint Symposium on Sensor and Membrane Technology for Environmental Management, pp. 151-160, 1994.

4. Hyeon Soo Park, Hyun Woo Shin, Dong Hyun Yun, Hyung-Ki Hong, Chul Han Kwon, Kyuchung Lee and Sung-Tae Kim, "Tin Oxide Microelectronic Gas Sensor for Detecting CH_3SH," The 5th International Meeting on Chemical Sensors, pp. 612-615, 1994.

5, Hyung-Ki Hong, Hyun Woo Shin, Hyeon Soo Park, Dong Hyun Yun, Chul Han Kwon, Kyuchung Lee, Sung-Tae Kim and Toyosaka Moriizumi, "Gas identification using oxide semiconductor gas sensor array and neural-network pattern recognition," Transducer '95, Stockholm, vol. 1, pp.687-690, 25-29 June 1995.

6. Dong Hyun Yun, Chul Han Kwon, Hyung-Ki Hong, Hyun Woo Shin, Hyeon Soo Park, Kyuchung Lee and Sung-Tae Kim "Abnormal current-voltage characteristics of oxide semiconductors and their application to gas sensors," The 2nd East Asia Conference on Chemical Sensors '95, Xian, pp. 34-36, 5-8 October, 1995.

7. Dong Hyun Yun, Chul Han Kwon, Hyung-Ki Hong, Hyun Woo Shin, Seung-Ryeol Kim, Kyuchung Lee “Abnormal current-voltage characteristics of WO_3-doped SnO_2 oxide semiconductors and their applications to gas sensors," The 6th International Meeting on Chemical Sensors, Gaithersburg, MD, USA, pp. 48-51, 22-25 July, 1996.

8. Hyung-Ki Hong, Hyun Woo Shin, Dong Hyun Yun, Seung-Ryeol Kim, Chul Han Kwon, Kyuchung Lee and Toyosaka Moriizumi, "Electronic nose system with micro gas sensor array," The 6th International Meeting on Chemical Sensors, , Gaithersburg, MD, USA, pp. 338-341, 22-25 July, 1996.

Abbreviations

ADC	Analogue to digital converter
ANN	Artificial neural network
ART	Adaptive resonance theory
ATP	Adenosine triphosphate
BAW	Bulk acoustic wave
BP	Back-propagation
BPN	Back-propagation neural network
CA	Cluster analysis
CP	Conducting polymer
DAC	Digital to analogue converter
DAQ	Data acquisition
DFA	Discriminant function analysis
DI	De-ionised
DSA	Decanesulfonic acid
EC	Electrochemical
ENT	Ears, nose, and throat
FNN	Fuzzy neural network
G	Granule cell
GC	Gas chromatograph
HCA	Hierarchical cluster analysis
HpSA	Heptanesulfonic acid
IDC	Inter-digital capacitive
IR	Infra-red
LDA	Linear discriminant analysis
LPCVD	Low pressure chemical vapour deposition
LPM	Low-power multifunction

LVQ	Learning vector quantisation
M	Mitral cell
MLP	Multi-layer perceptron
MOS	Metal oxide semiconductor
MOSFET	Metal oxide semiconductor field effect transistor
MS	Mass spectroscopy
MSD	Mass selective detector
OSN	Olfactory sensory neurone
P	Pyramidal cell
PAN	Polyaniline
PARC	Pattern recognition
PCA	Principal components analysis
PCR	Principal components regression
PE	Polyethylene
PEs	Processing elements
PG	Periglomerular cell
PLS	Partial least-squares regression
PnP	Plug and play
PPY	Polypyrrole
PSA	Pentanesulfonic acid
PTFE	Polytetrafluoroethylene
PVC	Polyvinyl chloride
QCM	Quartz crystal microbalance
RH	Relative humidity
SAW	Surface acoustic wave
SCE	Saturated calomel electrode
SIMCA	Soft independent modelling of class analogy
SOM	Self-organising map
SRL	Sensors Research Laboratory
T	Tufted cell
TTL	Transistor-transistor logic
VI	Virtual instrument
VOC	Volatile organic compound

Glossary of Symbols

δ_k	Error signal at the output of *k*th
ΔH	Heat of combustion
Δ_p	Gradient descent vector component for weight
ΔP	Change in the electrical power
η	Learning-rate parameter
λ	Eigenvalues
σ	Population standard deviation
a_{ip}	Eigenvectors
A_{eff}	Catalytically active area
b	Bias
d	Distance in the data set
dr/dt	Reaction rate
eV_s	Potential barrier
f_i	Normalisation factor for the *i*th sample
i	Sensor *i*
j	Odour *j*
m/z	Mass-to-charge ratio
N	Number of feature vectors
o_k	Actual output from the *k*th output unit
Q	Gas flow rate
T_d	Time delay
T_s	Temperature of sensor
Var	Covariance

V_T	Voltage ouput of temperature sensor
V_d	Dead volume
w	Weight
$\bar{x}$	Average value of x
x_i^{norm}	Normalised array parameter
x_{ij}	Components of the input vector
$x_{ij(mc)}$	Mean-centre
X	Linear combinations of the orthogonal vectors
y_{pk}	Target value from the kth output unit
z_{min}	Global minimum
z_1	Local minimum.
Z_p	pth principal component

Chapter 1

Introduction

The purpose of this chapter is both to introduce the electronic nose technology upon which the research is based and provide an outline of this thesis. The term ‘electronic nose’ describes an electronic system that is able to mimic the human sense of smell [1]. Electronic noses have been the subject of much research at the University of Warwick over the past 17 years [2]. The research described here covers the development of an electronic nose system to analyse water quality, based upon a hybrid modular approach, which consists of an array of metal oxide semiconductor resistive gas sensors and conducting polymer gas sensors.

1.1 Electronic Nose Technology

Generally, the system comprises the chemical sensor array, signal interfacing electronic units, and a pattern recognition sub-system. At present many applications of electronic nose have been reported [3-30]. This has led to improvements in both sensor technology and pattern recognition techniques resulting in several commercial electronic nose systems. These systems use a number of different gas sensors depending on the applications, e.g. metal oxide chemoresistors, conducting polymer

chemoresistors, SAW devices, and catalytic gate MOSFETs. Some commercial electronic nose systems reported to date are listed below in Table 1.1.

Table 1.1 Some commercial electronic noses (at Sept. 1999).

Product name	Supplier	Sensor type(s)	No. of odour sensors
Fox 3000/4000/5000 αCentauri αPrometheus	Alpha MOS, France	Metal Oxide Resistive, SAW, Conducting Polymer Resistive	6/12/18
AromaScanner	Osmetech., UK	Conducting Polymer Resistive	32
Olfactometer	HKR Sensor System GmBH, Germany	Quartz Microbalance	6
eNOSE 5000	EEV Ltd, UK	Metal Oxide Resistive, BAW Conducting Polymer Resistive	12
MOSES II [3]	Lennartz Electronics GSG, Germany	Quartz Microbalance, Metal Oxide Resistive, Calorimeter, Electrochemical Sensor	24
Nordic Electronic Nose	Nordic Sensor AB, Sweden	MOSFET, IR CO_2 sensor, Metal Oxide Resistive	15
The Rhino	Mosaic Industries Inc., USA	Metal Oxide Resistive	4
BH 114 [4]	Bloodhound Sensors Ltd, UK	Conducting Polymer Resistive	14
Scentinel	Mastiff Electronic Systems Ltd, UK	Conducting Polymer Resistive	16
Hand held Electronic Nose	Cyrano Science Inc., USA	Composite Resistive Polymer	32

While classical gas chromatograph (GC) / mass spectroscopy (MS) techniques separate, quantify and identify individual volatile chemicals, they cannot tell us

whether the compounds have an odour. Therefore the electronic nose was developed not to replace traditional GC/MS analytical instrumentation or indeed human sensory analysis, but to augment these. The electronic nose allows people to transfer expert knowledge from highly trained sensory panels and very sophisticated analytical techniques to the production floor for the control of quality. Researchers are at present developing the second generation of artificial electronic nose that will be smaller and cheaper and thus will also find applicability in the consumer marketplace. A more detailed description of the electronic nose system is given in chapter 2.

1.2 Applications of the Electronic Nose System

During the past few years, the food and beverage industries have been the largest users of electronic nose technology [5]. Table 1.2 summarises some of the reported applications of electronic noses (research and commercial) pertaining to the food industry which are listed from seafood, such as oysters and squid, through to cheeses, such as cheddar. At present, the broad range of applications for electronic noses is constantly expanding on the market of several competing electronic devices. By the automated identification of volatile chemicals, the electronic nose can assess an aroma for many purposes, which include the grading of larger, beers and whiskeys [5, 6, 7], identifying perfumes [8], controlling cheese ripening, evaluating seafood quality [5, 6, 9] and the grading of coffee beans [6]. The product packaging, pharmaceutical, environmental [3], petrochemical, agricultural [5, 10], personal care and medical area [4, 11] also use electronic noses. Continuous process control systems, food security,

Table 1.2 Some reported applications of electronic noses in the food industry.

Food	Test	Sensors/type	Year [Ref.]
Seafood (oyster, sardine, squid)	Freshness	1/MOS†	1991 [12]

Fish (cod, haddock)	Freshness	4/MOS	1992 [13]
Fish	Freshness	1/MOS†	1994 [14]
Fish (trout)	Freshness	8/EC	1994 [15]
Grains	Classification	15/mixed	1995 [16]
Ground Pork/Beef	Discriminate and effect of ageing	15/mixed	1993 [17]
Boar	Taints in meat	14/MOS	1995 [18]
Sausage meats	Discriminate	6/MOS	1995 [19]
Food Flavours (orange, apple, strawberry, grape, peach)	Flavour identification	8/BAW	1993 [8]
Wheat	Grade quality	4 x 4/EC	1993 [20]
Wheat and Cheese	Discriminate and ageing	20/CP	1994 [21]
Tomatoes	Effect of irradiation and stress	7/mixed	1995 [22]
Cheese	Maturity of cheddars	20/CP	1997 [23]
Cheese	Discriminate	8/CP	[24]

†Strictly not an electronic nose (as defined here) but an odour monitor. Key: MOS = Metal Oxide Semiconductor, EC = Electrochemical, BAW = Bulk Acoustic Wave, CP = Conducting Polymer.

environmental monitoring and medical diagnosis areas are quite likely to be the promising application fields of electronic noses in the near future. Monitoring of the spoilage of foodstuffs is closely related to monitoring the growth of bacteria, in a certain medium. In other words, an electronic nose may be able to recognise characteristic smells from diseases and bacteria cells due to cell metabolism which is the biological oxidation of organic compounds, such as glucose ($C_6H_{12}O_6$), to yield ATP and secondary metabolites, as shown in Figure 1.1. There is now great interest in the clinical application of an electronic nose; that is in the ability of an electronic nose

to diagnose illness. It is well-known that certain diseases are associated with characteristic smells, for example, diabetes produces the sweet smell of acetone on the breath and stomach ailments are often associated with halitosis. Other diseases, like cancers associated with the lungs, liver and intestine can also produce characteristic odours. Some reported clinical applications of electronic noses are listed in Table 1.3.

The Sensors Research Laboratory (SRL) group at Warwick University has carried out a number of experiments on the uses of electronic noses for medical applications: (i) the identification of pathogens that cause infectious disease of the upper respiratory tract and ears [25, 26]; (ii) diagnosing the presence of sub-clinical or clinical ketosis from the breath of dairy cows [28]. Recently, the electronic nose has been used as a new analytical tool that enables electronic olfactory discrimination and recognition in the water treatment industry. So far, water analysis has been carried out

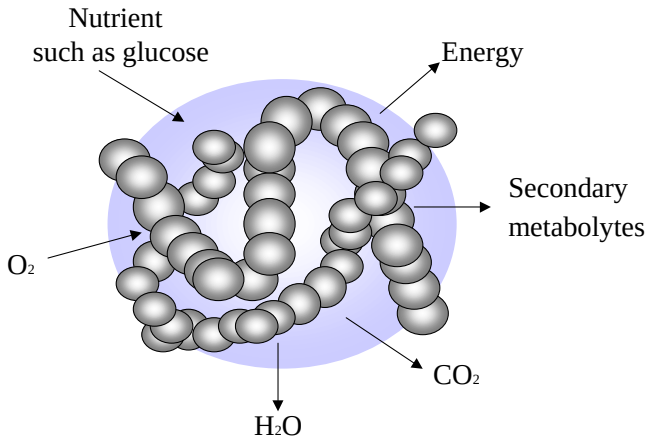

Fig. 1.1 Schematic diagram of the bacteria cell metabolism.

Table 1.3 Some reported applications of electronic noses in medical diagnostics.

Pathogens	Application	Sensors	Group	Year [Ref.]
6 micros	ENT Infections	6 MOS	Warwick	1994 [25]

4 micros	ENT infections	6 MOS	Warwick	1997 [26]
13 micros	Various	16 CP	Leeds	1996 [27]
Dietary problem	Ketosis in cows	6 MOS	Warwick	1997 [28]
Bacterial vaginosis	Vaginal infection	32 CP	UMIST	1997 [30]
E. coli; S. aureus	Infections	6 MOS	Warwick	1998 [11]
E. coli; Human factor VII	Batch process	MOSFET	Linkoping	1998 [31]

Key: ENT = Ears, Nose and Throat, *E. coli = Eschericha coli, S. aureus = Staphylococcus aureus.*

mostly by analytical instruments, which are based on liquid chromatography or optical microscopy in liquid phase. These instruments may give precise analytical data, but in most cases they need several days for data analysis. This disadvantage makes clear the importance of the electronic nose, employing gas sensors, as an alternative to analytical instrument and supports trials to replace if gas sensors can detect and classify odour components in water. The SRL group had applied the adaptive back propagation technique for the classification of several types of Severn Trent water and three types of mineral water using a 4-element electronic nose and the results were encouraging [29].

1.3 Objectives of the Project

The objectives of the project were to design an electronic nose, based upon a hybrid modular sensor system, and to construct a measurement system for the monitoring of the quality of potable water with data acquisition via virtual instrumentation (LabVIEW) and artificial neural networks.

Previously, Craven [26] reported on the use of an array of 6 MOS sensors to predict the class and phase of two potentially pathogenic micro-organisms, *Eschericha coli* (*E. coli*) and *Staphylococcus aureus* (*S. aureus*). The type and the growth phase of bacteria was correctly predicted for 96% and 81% of all samples taken during a 12 h incubation period, respectively. The results for the clinical application were promising but the flexibility in the choice of sensors and sensor materials was limited because he used a MOS array only.

Here a hybrid sensor system comprising a MOS array and a CP array has lead to a system with greater flexibility for the general aim of electronic noses. A number of different sensor technologies, sensor chambers and odour pattern recognition techniques have been investigated for the application of assessing water quality. The purpose being to correlate the odorous headspace of water to cyanobacteria[1] strain and growth phase.

The enrichment of water by inorganic plant nutrients is becoming both a severe problem in maintaining water quality, and a common source of odour pollution [32, 33]. Thus, it is very important to identify cyanobacteria in water, which can cause serious nuisance from an unpleasant odour and, in the case of reservoirs, taste. Many species of cyanobacteria have been observed to produce toxins, thus rapid analysis to detect and quantify these toxins in natural waters is also required.

[1]The cyanobacteria (blue-green algae) are the largest group of photosynthetic prokaryotes (Whitton, 1992) and contain chlorophyll which differ from the bacteriochlorophylls of the photosynthetic eukaryote. It is derived from the Greek for blue (Kyanos) because of their characteristic blue-green colour.

This research covered the first attempt to identify cyanobacteria in water made with an electronic nose. The modified Warwick Fox 2,000 has been used for the

continuous monitoring of the growth of cyanobacteria over a period of 40 days [34, 35].

1.4 Outline of Thesis

This thesis is presented in two parts. In the first part, an electronic nose, comprising an array of six commercial odour sensors, has been used to monitor not only different strains, but also the growth phase, of cyanobacteria (i.e. blue-green algae) in water. In the second part, it outlines the modification of the electronic nose system to include a new sensor chamber with conducting polymer sensors, hence producing a hybrid electronic nose for superior discrimination.

Chapter 1 contains a brief description of the electronic nose technology including the various applications reported so far. It highlights the potential importance of the electronic nose employing gas sensors for the monitoring of an environmental problem such as water enrichment.

Chapter 2 is a review of electronic nose systems. It details a historical background of the electronic nose, odours and a mammalian olfactory system and an artificial olfactory system.

Chapter 3 describes the original experimental set-up for applying the electronic nose to water analysis. This describes the procedures for testing and characterisation of the modified Fox 2,000 system, the methods of data collection, and the characterisation of a discrete thin film sensor.

Chapter 4 describes the initial data analysis, which consists of data processing and classification using MATLAB and NeuralWorks Professional II/Plus (NeuralWare Inc., USA). Principal component analysis (PCA), three supervised classifiers, multi-layer perceptron (MLP), learning vector quantisation (LVQ) and

Fuzzy ARTMAP were used to explore the data and classify the cyanobacteria samples in water.

Chapter 5 details the design and fabrication of a new sensor chamber and other modifications to the electronic nose. Although a MOS-based sensor array - based on one class of sensor - is good for the simplicity of the electronic nose system, its range of application was found to be limited. Therefore a mixed or hybrid array comprising different types of sensor, such as MOS and conducting polymers was investigated. This chapter also describes further a second set of experiments carried out after the modification of the electronic nose system.

Chapter 6 describes a HP 4440 chemical sensor, which has been installed to determine the gases present. The relevant performances of the two units, the electronic nose and the HP 4440 chemical sensor, are examined from the classification of cyanobacteria samples.

Chapter 7 contains the principal conclusions drawn from the results achieved. Also possible future explorations are discussed.

1.5 References

1. J. W. Gardner, and P.N. Bartlett, A brief history of electronic nose, Sensors and Actuators B, 18-19 (1994) 211-220.
2. K. C. Persaud, and G. H. Dodd, Analysis of discrimination mechanisms of the mammalian olfactory system using a model nose, Nature, 299 (1982) 352-355.
3. H. Ulmer, J. Mitrovics, G. Noetzel, U. Weimar, and W. Göpel, Odours and flavours identified with hybrid modular sensor systems, Sensors and Actuators B, 43 (1997) 24-33.

4. T. D. Gibson, O. Prosser, J. N. Hulbert, R. W. Marshall, P. Corcoran, P. Lowery, E. A. Ruck-Keene, and S. Heron, Detection and simultaneous identification of microorganisms from headspace samples using an electronic nose, Sensors and Actuators B, 44 (1997) 413-422.
5. P. N. Bartlett, J. M. Elliott, and J.W. Gardner, Electronic Noses and Their application in the Food Industry, Food Technology, Vol. 51, No.12, December (1997).
6. J. W. Gardner, and P.N. Bartlett, Sensors and Sensory Systems for an Electronic Nose, Kluwer Academic Publishers (1992).
7. T. C. Pearce, J. W. Gardner, S. Friel, P. N. Bartlett, and N. Blair, Electronic nose for monitoring the flavour of beers, Analyst, 118 (1993) 371-377.
8. T. Nakamoto, A. Fukuda, and T. Moriizumi, Perfume and flavour identification by odor sensing system using quartz-resonator sensor array and neural-network pattern recognition, Sensors and Actuators B, 10 (1993) 85-90.
9. M. Egashira, Y. Shimizu, and Y. Takao, Trimethylamine sensor based on semiconductive metal oxides for detection of fish freshness, Sensors and Actuators B, 1 (1990) 108-112.
10. F. Winquist, H. Arwin, E. Lund, R. Forster, C. Day, and I. Lundström, Screening of irradiated tomatoes by means of an electronic nose, The 8th International Conference on Solid-State Sensors and Actuators, and Eurosensors IX, Stockholm, Sweden, June (1995) 691-694.
11. J. W. Gardner, M. Craven, C. Dow, and E. L. Hines, The prediction of bacteria type and culture growth phase by an electronic nose with a multi-layer perceptron network, Meas. Sci. Technol. 9 (1998) 120-127.

12. H. Nanto, H. Sokooshi, T. Kawai, and T. Usuda, Freshness detection of seafoods using ZnO thin film gas sensor, The 10th Sensor Symposium, Japan, (1991) 195-198.
13. R. Olafsson, E. Martinsdottir, G. Olafdottir, S. I. Sigfusson, and J. W. Gardner, Monitoring of fish freshness using tin oxide sensors, in Sensors and Sensory Systems for an Electronic Nose, J. W. Gardner, P. N. Bartlett, eds. Dordrecht: Kluwer Academic Publishers, (1992) 257-272.
14. M. Egashira, Y. Shimizu, and Y. Takao, Fish freshness detection by semiconductor gas sensors, in Olfaction and Taste XI, Sapporo, Japan, K. Kurihara, N. Suzuki, and H. Ogawa, eds. Springer-Verlag, (1994) 715-719.
15. M. Schweizer-Berberich, S. Vaihinger, and W. Göpel, Characterisation of food freshness with sensor arrays, Sensors and Actuators B, 18-19 (1994) 282-290.
16. J. Olsson, T. Borjesson, and J. Schnurer, Penicillium identification using an electronic nose, Personal communication of conference abstract, (1995).
17. F. Winquist, E. G. Hornsten, H. Sundgren, and I. Lundström, Performance of an electronic nose for quality estimation of ground meat, Meas. Science Technol., 4 (1993) 1493-1500.
18. B. Bourrounet, T. Talou, and A. Gaset, Application of a multigas sensor device in the meat industry for boar-taint detection, Sensors and Actuators B, 26-27 (1995) 250-254.
19. T. Tan, Q. Lucas, L. Moy, J. W. Gardner, and P. N. Bartlett, The electronic nose - a new instrument for sensing vapours, LC-GC International, 8 (1995) 218-225.
20. J. R. Stetter, M. W. Findlay, K. M. Schroeder, C. Yue, and W. R. Penrose, Quality classification of grain using a sensor array and pattern recognition, Analytica Chem. Acta, 284 (1993) 1-11.

21. A. Pisanelli, A. A. Qutob, P. Travers, S. Szyszko, and K. C. Persaud, Applications of multi-array sensors to food industries, Life Chemistry Reports, 11 (1994) 303-308.

22. F. Winquist, H. Arwin, E. Lund, R. Forster, C. Day, and I. Lundstrom, Screening of tomatoes by means of an electronic nose, The 8th Int. Conf. On Solid State Sensors and Actuators, and Eurosensors IX, Stockholm, Sweden, (1995) 691-694.

23. K. C. Persaud, and P. J. Travers, Arrays of broad specificity films for sensing volatile chemicals, in Handbook of biosensors and electronic noses: medicine, food and the environment, E. Kress-Rogers, ed. Ohio: CRC Press Inc., (1997) 563-592.

24. D. J. Strike, G. Fiaccabrino, N. F. de Rooij, and M. Koudelka-hep, Headspace measurement of cheese samples using an electronic nose, Mat. Sci. Eng. C.(In press.).

25. M. Craven, E. L. Hines, J. W. Gardner, P. Horgan, D. Morgan and I. A. Ene, Bacteria detection and classification using artificial neural networks in conjunction with an electronic nose, Int. Conf. on Neural Networks and Expert systems in Medicine and Healthcare, E. C. Ifeachor and K. G. Rosen, eds. Plymouth: Bluestone Design Ltd., (1994).

26. M. Craven, Bacteria Classification with an electronic nose employing artificial neural networks, PhD thesis, University of Warwick, UK, (1997).

27. T. D. Gibson, O. Prosser, J. N. Hulbert, R. W. Marshall, P. Corcoran, P. Lowery, and E. A. Ruck-Keene, Detection and simultaneous identification of microorganisms from headspace samples using an electronic nose, Proceedings of Eurosensors X, Leuven, Belgium, 8-11 September (1996) 1341-1344.

28. R. J. Elliott-Martin, T. T. Mottram, J. W. Gardner, P. J. Hobbs, and P. N. Bartlett, Preliminary investigation of breath sampling as a monitor of health in dairy cattle, J. Agri. Eng. Res., 67 (1997) 267-275.
29. I. A. Ene, E. L. Hines, and J. W. Gardner, Detecting water odours with a neural network based electronic nose, Project report, University of Warwick, UK, (1993).
30. S. Chandiok, B. A. Crawley, B. A. Oppenheim, P. R. Chadwick, S. Higgins, and K. C. Persaud, Screening for bacteria vaginosis: a novel application of artificial nose technology, J. Clincal Pathology, 50 (1997) 790-791.
31. C. Mandenius, A. Hagman, F. Dunas, H. Sundgren, and I. Lundstrom, A multisensor array for visualizing continuous state transitions in biopharmaceutical processes using principal component analysis, Biosensor & Bioelectronics, 13(2) (1998) 193-199.
32. W. W. Carmichael, The toxins of Cynanobacteria, Scientific American, January (1994) 64-72.
33. W. W. Carmichael, Cyanobacteria secondary metabolites-the cyanotoxins, Journal of Applied Bacteriology, 72 (1992) 445-459.
34. H. W. Shin, J. W. Gardner, E. L. Hines, and C. S. Dow, Classification of cyanobacteria in water with an electronic nose, The 6th International Symposium, Olfaction & Electronic Nose 99, Tübingen, 20-22 September (1999) 366-367.
35. H. W. Shin, E. Llobet, J. W. Gardner, E. L. Hines, and C. S. Dow, The Classification of the strain and growth phase of cyanobacteria in potable water using an electronic nose system, IEE - Sci. Meas. Technol., (submitted, 1999).

Chapter 2

Review of Electronic Nose System

The objective of this chapter is to detail a historical background of the electronic nose, the chemical properties of odours, a mammalian olfactory system and an artificial olfactory system.

Until recently, the mammalian nose has been the best sensing system to discriminate odours, such as foods, beverages and perfumes. The structure of the mammalian olfactory system can be crudely compared with an electronic system, which is composed of various kinds of sensors, and an artificial neural network system. Three distinct phases - detection, signal processing and recognition/interpretation - of activity allow the mammalian nose to detect, analyse and react to changes in the smell of its environment. Attempting to detect complex odours by conventional analytical techniques is not only very expensive but sometimes impossible. It is therefore not surprising that traditional (organoleptic) methods of odour assessment are still in use. Recently, significant interest in the use of electronic nose systems instead of human sensory systems has arisen. Here the brief history and technology of electronic nose systems are introduced. Also the relationship between mammalian and artificial olfaction is outlined.

2.1 Historical Review of an Electronic Nose

Gardner and Bartlett [1] defined an 'electronic nose' as: ‘an instrument, which comprises an array of electronic chemical sensors with partial specificity and an appropriate pattern recognition system, capable of recognising simple or complex odours’. Lundström et al. [2] described it as: ‘an electronic nose consists of an array of gas sensors with different selectivity patterns, a signal collecting unit and pattern recognition software applied to a computer’, but there are also various synonyms such as artificial olfactory system, odour monitor, odour-sensing system, mechanical nose, and artificial intelligent nose. In this research, the term, ‘electronic nose system’, is used to avoid confusion. Research on electronic noses began at the University of Warwick in 1982 [3], although the use of the term 'electronic nose' appeared in 1985 [4] and it was also specifically used at a conference [5, 6]. The first work of an experimental instrument performed in this area was reported in 1954 by Hartman [7], this research described an electrochemical sensor. It was ten years later that the concept of an odour sensor was investigated by Wilkens and Hartman [8]. The idea of using metal and semiconductor gas sensors for odour sensors was published one year later by Buck *et al.* [9] and also the use of modulated contact potentials by Dravnieks [10]. Zaromb and Stetter [11] proposed the use of an array of gas sensors with partially overlapping sensitivities in the mid 1980s. Pattern recognition techniques and neural network analysis were also used to analyse the multi-dimensional data sets from sensor arrays. Table 2.1 shows a brief history of electronic nose technology.

Table 2.1 Brief history of electronic nose technology

Year	Electronic Nose Technology	Investigator
1954	First report of an experimental instrument	Hartman

1964	First electronic nose using a redox reaction	Wilkens, Hatman
1965	Detection by modulation of conductivity at an electrode	Buck, Allen, Dalton
1965	Detection by thermal modulation of contact potential	Dravieks, Trotter
1982	First intelligent chemical sensor array system	Persaud, Dodd
1985	Olfactory detection using integrated sensors [12]	Ikegami
1985	Application of conducting polymers as odour sensor [4]	Persaud, Pelosi
1985	Appearance of the term 'electronic nose'	Persaud, Pelosi
1989	Quartz resonator array and neural network [13]	Nakamoto, Moriizumi
1990	MOSFET gas sensor and pattern recognition [14]	Sundgren et al.
1991	Aroma discrimination by pattern recognition [15]	Aishima
1996	Electronic nose using a fuzzy neural network [16]	Singh, Hines, Gardner
1997	Electronic nose with hybrid modular sensor systems [17]	Göpel et al.

2.2 Odours and the Mammalian Olfactory System

Olfaction is known as a molecular sense, in which information carried in external signal molecules is transformed into patterns of brain activity that underlie odour perception. The nature of the mammalian olfactory system is much more complex than any of the other senses and the least understood in terms of the sensing mechanism and biological transduction[1]. For the application of an artificial electronic nose system, it is necessary to have a basic understanding of odours and the mammalian olfactory system.

[1]It is the process by which the events of the physical environment become represented as electrical activity in a sensory nerve cell.

2.2.1 Odours

An odour consists of one or more types of compounds, which is typically a small hydrophobic molecule with a molecular mass in the range of 18 to 300 Daltons. Recognisable odours arise from the specific combination of complex mixtures of many odour molecules, each of different concentrations. Most natural odours and flavours are complex mixtures of chemical species and so contain at least tens and more often hundreds of constituents. For example, coffee aroma consists of hundreds of different odorous molecules, typically: 108 furans, 79 pyrazines, 74 pyrroles, 70 ketones, 44 phenols, 31 hydrocarbons, 30 esters, 28 aldehydes, 28 oxazoles, 27 thiazoles, 26 thiophenes, 21 maines, 20 acids, 19 alcohols, 13 pyridines, and 13 thiols/sulfides [18].

Therefore, subtle differences in the relative amounts of these odorous molecules determine the characteristic smell of a substance. Moreover, the shape, size and polar properties of the molecule relate to its odorous properties. Figure 2.1 shows the properties and structures of some typical odorants. Typical properties that all odours have in common are that they are all volatile substances [19]. To stimulate the sense of smell materials must be airborne and in a finely divided state. For example, liquids can not be smelled until they vaporise. However volatility seems to be a necessary but not a sufficient condition for the generation of odour. Solubility is necessary because odour materials must be captured by the mucous lining of the nostrils before they can stimulate. In addition to volatility and solubility, a large number of other physical properties have been investigated by many people but no comprehensive structure-activity relationship has emerged.

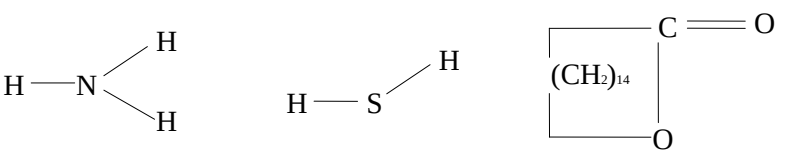

Ammonia (Pungent)

Hydrogen Sulfide

Cyclopentadecanone (Musk)

Fig. 2.1 The properties and structures of some typical odorants.

2.2.2 Architecture of the Mammalian Olfactory System

The architecture of the mammalian olfactory system consists of three main subsystems - the olfactory epithelium, the olfactory bulb and olfactory cortex. Figure 2.2 shows where the olfactory system in a human is sited and gives an overview of the mammalian olfactory pathway.

2.2.2.1 The Olfactory Receptor Cells – Gas Sensors

An odour is delivered to the olfactory epithelium through a series of nasal passages, or nares. The olfactory epithelium is composed mainly of three cell types: receptor cells, supporting cells and basal cells. The receptor cells are arranged like a mosaic between supporting cells and overlie a single layer of basal cells.

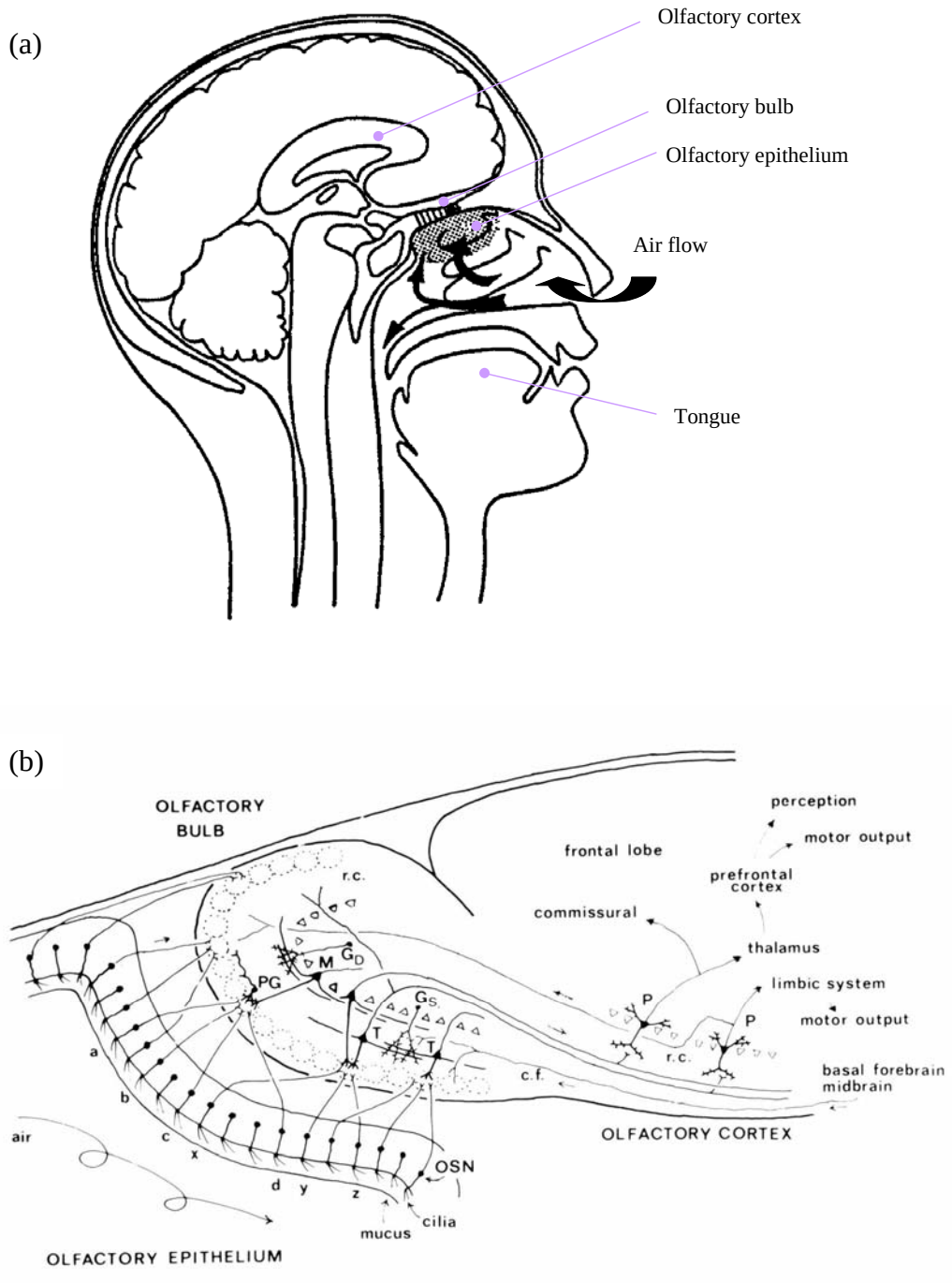

Fig. 2.2 Overview of (a) the human and (b) the mammalian olfactory pathway. Olfactory epithelium: OSN = olfactory sensory neurone. Olfactory bulb: *PG* = periglomerular cell; *M* = mitral cell; *T* = tufted cell; *Gs* = superficial granule cell; G_D = deep granule cell; *r.c.* = recurrent axon collateral; *c.f.* = centrifugal fiber. Olfactory cortex: *P* = pyramidal cell; *r.c.* = recurrent axon collateral [20].

Odorants diffuse through a layer of mucus to bind with the chemically sensitive membranes of the olfactory receptor cells in the epithelium. It is thought [21] that the first stage of signal generation occurs in an olfactory receptor and this reaction seems to be based on G-protein neurotransmitter receptors. The number of different receptor protein types is relatively small (about 1,000), while the number of receptor cells is relatively large (about 100 million). Therefore, there are overlapping sensitivities between individual receptor cells, i.e. receptors are not intrinsically specific to single odorants and do not have selectivity imposed on them by the mucus, later stages of the olfactory system must recognise the pattern of activity produced by that set of receptor cells that bear receptor proteins specific to molecules of a given odour[2].

2.2.2.2 The Olfactory Bulb – Signal Processing

The olfactory bulb is the first relay station for olfactory inputs, which is composed of three main layers: glomeruli, mitral cells, and granular layer [20, 22]. For example, there are about 2,000 glomeruli in the rabbit olfactory bulb and a convergence of the order of 1,000 to 1 for the olfactory input to mitral cells. The electrical signals produced are processed by the mitral cells and sent via the granular layer, which forms a thick layer, to the olfactory cortex. The mitral cells receive feedback signals from the brain that relate to the current emotional status. The granule cells have a superficial process that terminates in the external plexiform layer, forming numerous connections with the lateral dendrites of the mitral cells. The granule cells lack a true axon and their processes resemble dendrites in their

[2]It is reported that human is able to detect up to 10,000 odours and the life span of human receptor cells is about 3 to 4 weeks.

fine structural features, being covered with numerous small spines. The granular layer is believed to provide specificity in the olfactory system. Therefore, olfactory signals in this stage undergo considerable processing that reduces the noise associated with the signal and amplifies it, effectively increasing both the sensitivity and selectivity.

2.2.2.3 The Olfactory Cortex – Odour Recognition

The final stage of the mammalian olfactory system is the olfactory cortex of the brain. The primary olfactory cortex is still a relatively unexplored region of the brain, but it is known [20] to mainly be comprised of associative connections between pyramidal cells and the lateral olfactory tract. The output of the olfactory bulb goes to the olfactory cortex, a region on the basal and lateral surface of the forebrain. A basic circuit for this region was established by Haberly and Shepherd [21, 23]. Harberly suggested [23] that the "olfactory cortex serves as a content-addressable memory for association of odour stimuli with memory traces of previous odour stimuli." Therefore the olfactory information is transformed into a unified sensory experience, as well as creating and evoking memories of name, places and feelings, etc., which associate the current experience with previous experiences of the mixture.

The brain is a highly complex, non-linear, and parallel computer [24]. In the case of the human brain, it contains approximately 10^{11} neurones and 10^{4} interconnections per neurone. It has the capability of organising neurones so as to perform certain computation such as odour recognition many times faster than the fastest digital computer in existence today. Over the past ten years many attempts have been made to model the olfactory cortex in the brain with artificial neural network paradigms.

2.3 Artificial Olfactory System

Like the mammalian olfactory system, this electronic system incorporates sensors that are conceptually analogous to olfactory receptor cells, and a signal processing system that conceptually simulates the mammalian brain. This section describes how an artificial olfactory system in an electronic nose works and how it is related to the mammalian olfactory system.

2.3.1 Architecture of the Artificial Olfactory System

Figure 2.3 shows a comparison between an artificial olfactory system [1] and the mammalian olfactory system. The chemical sensor array and an analogue to digital convertor represent a group of olfactory receptor cells of the olfactory epithelium and produce time-dependent electrical signals in response to odours. Any noise and sensor drift may be reduced by using appropriate signal processing techniques, the odours can be recognised and classified by a PARC (pattern recognition) engine in a computer like the olfactory cortex of the mammalian brain.

2.3.2 Gas Sensors

A sensor is defined [25] as a device that converts a non-electrical physical or chemical quantity into an electrical signal and is classified by many different criteria, such as the transduction principle, measuring property, and application. Table 2.2 shows a number of typical sensor-active materials and applications. A gas sensor is one of the chemical sensors and has grown rapidly in importance encompassing a broad spectrum of technologies including food, safety, pollution, fuel economy, medical engineering and industrial processes.

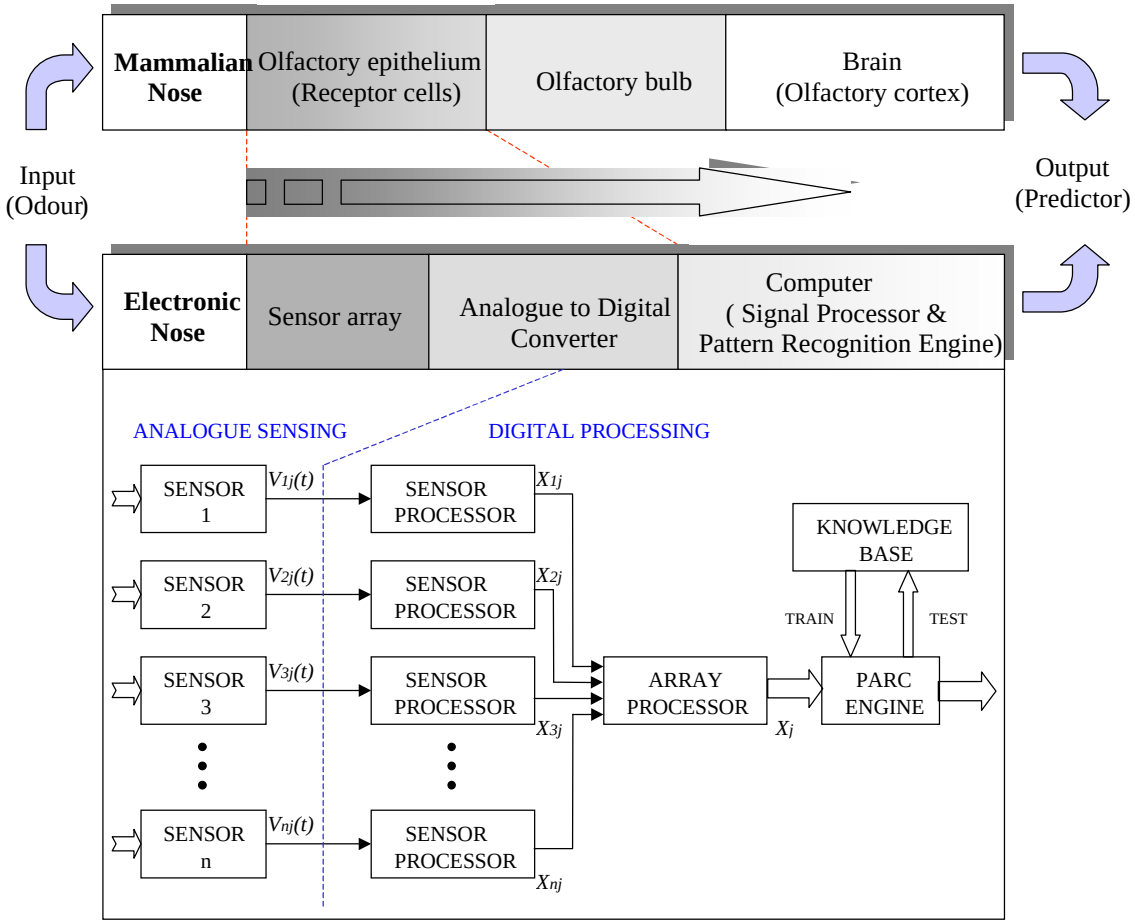

Fig. 2.3 A comparison between an artificial olfactory system and the mammalian olfactory system.

A large variety of gas sensor technologies have been developed for use in an artificial olfaction system. At present, the most common sensing materials for commercial electronic noses are metal oxide semiconductors (MOS) and conducting polymers (CPs) as shown in Table 1.1. This is due to their attractive material characteristics. Generally, MOS thick-film gas sensors have very good sensitivity at high operating temperature and are relatively easy to make and conducting polymers operate at room temperature and exhibit fast reversible changes in conductivity when exposed to gas species. Although CPs may have a lower sensitivity when

Table 2.2 Typical sensor materials and application fields [26].

Materials	Examples	Typical application fields
Metals	Pt, Pd, Ni, Ag, Au, Sb, Rh, …	
Semiconductors	Si, GaAs, InP, …	Industrial process control
Ionic compounds	Electronic conductors (SnO_2, TiO_2, Ta_2O_5, IrO_x, In_2O_3, $AIVO_4$ …) Mixed conductors ($SrTiO_3$, Ga_2O_3, … in general: perovskites) Ionic conductors (ZrO_2, LaF_3, CeO_2, CaF2, Na_2CO_3, β-alumina, Nacicon, …)	Exhaust gases
Molecular crystals	Phthalocyanines (PbPc, $LuPc_2$, LiPc, $(PcAlF)_n$, $(PcGaF)_n$, …)	Volatile organics in air and water, NO_x
Langmuir-Blodgett films	Polydiacetylene, Cd arachidate	Medical applications, Environmental monitoring
Cage compounds	Zeolite, calixarenes, cyclodextrins, Crown, ethers, cyclophanes, …	Food industry, flavour Monitoring, …
Polymers	Polyethers, polyurethanes, polypyrrole, Polysiloxanes, polythiophenes, PTFE, Polyfluorcarbons, polyolefins, Nafion, Cellulose, polyacetates, …	
Components of biomolecular systems	Synthetic: phospholipids, lipids, HMD and HIV epitopes, … Natural: glucose oxidase, lactose Permease, E.coli cell membrane, in General: enzymes, receptors, cells, transport proteins, membranes, ...	Water and blood analysis, pharmascreening, toxicity

compared to MOS, a wide variety of polymers are available and readily grown by electrochemical polymerisation of the monomer under controlled conditions. In order to understand the gas-sensing characteristics of the MOS and conducting polymers used in this research, the sensing mechanisms are described later in chapter 3.

They possess partial specificity, similar to the overlapping sensitivity of receptor cells in the mammalian nose. This lack of selectivity may be overcome by using a sensor array, where each sensor within the electronic nose produces a time-dependent electrical signal in response to a particular odour. For example, conductance variations resulting from the exposure of the sensors to an odour is a popular electrical signal to monitor and process in order to classify like the mammalian nose. Therefore the comparable partial specificity of a sensor array within the artificial olfaction system provides similar benefits of high order information like receptor cells.

2.3.3 Signal Processing

Signal processing [1, 4, 26] is used to condition input data from the sensor array prior to odour recognition by the PARC engine in a computer, like the mammalian olfaction system performs a comparable signal conditioning at the olfactory bulb. Any drift such as base-line drift of the sensors can be reduced at this stage. This means that the signal processing significantly affects the performance of the next stage of odour recognition. Each sensor *i* produces a time-dependent signal, $x'_{ij}(t)$, in response to odour j and it is often convenient to remove the time dependence of the signal output. Table 2.3 shows typical examples of sensor signal processing algorithms that have been applied for the application of sensors. Signal conditioning

Table 2.3 Some examples of signal processing algorithms used. i = sensor, j = odour, a = odour a, b = reference odour b, σ = population standard deviation, $\bar{x}$ =average value, N = the number of feature vectors in the feature-set with i component to each vector.

Signal processing algorithms	Formula
Difference signal	$x_{ij} = x'_{a,ij} - x'_{b,ij}$
Relative signal	$x_{ij} = x'_{a,ij} \big/ x'_{b,ij}$
Averaging	$\bar{x}_{ij} = \sum_{j=1}^{N} x'_{ij} \Big/ N$
Fractional difference	$x_{ij} = (x'_{a,ij} - x'_{b,ij}) \big/ x'_{b,ij}$
Linearisation	$x_{ij} = \log(x_{ij}'^{\max} - x_{ij}'^{\min})$, $x_{ij} = \sqrt{x_{ij}'^{\max} - x_{ij}'^{\min}}$
Normalisation	$k_{ij} = x_{ij} \Big/ \left\lvert x'_{a,ij} - x'_{b,ij} \right\rvert$, $k_{ij} = x_{ij} \Big/ \sum_{i=1}^{m} x_{ij}^{\,2}$
Autoscaling	$k_{ij} = (x_{ij} - \bar{x}_{ij}) \big/ \sigma_i$

is the link between the sensor output vector, X' and the input vector to the algorithms, $X = (x_{1j}, x_{2j}, ..., x_{ij}, ..., x_{mj})$. The components of the input vector, x_{ij}, may be scaled by a constant, k, in a normalisation algorithm. Various pre-processing algorithms are applied and related to the transduction mechanisms of particular types of sensor array or different types of pattern recognition techniques. For example, the difference signal algorithm, where the sensor parameter is the difference of sensor responses in air and in gas, has been used by many researchers [27, 28]. The fractional difference algorithm has been used with good results by Morrison [29] and Gardner *et al.* [27]. The relative signal algorithm is a very common model, which

defines the sensor parameter as the ratio of sensor response in air to the response in the odour being measured [27, 30, 31]. It has especially been used for considering drifts in the sensitivity coefficient. An averaging algorithm can be used to reduce noise effects and a linearisation technique may be usefully applied in odour sensing when odour component intensities are of particular importance. In a linearisation model, the log or root of the output has been used to linearise the sensor response as shown in Table 2.3 [25, 32]. The log function increases the relative contribution of sensor responses and the overall dynamic range of the system. Normalisation algorithms have also been used for the signal processing of sensors and sensor arrays [27]. Array normalisation divides each sensor value by the norm of the array vector. This technique is often used in order to reduce experimental error and the effect of variations in sample concentration. It improves overall pattern recognition performance but will enhance the noise with small signals. Array normalisation and autoscaling sets the length of all response vectors to unity[3] and puts the vector on the surface of a unit hypersphere.

Recently, dynamical signal processing [33, 34] has been employed in addition to those static parameters that were mentioned earlier. A combination of static and dynamic information in signal processing can be applied to obtain a signal vector more useful for the subsequent pattern recognition in most practical cases. Dynamic features may be represented by a set of parameters, some of which are specific for a specific gas and independent of the gas concentration. For example, derivative and equilibrium values processing algorithms which contain time domain information improve the selectivity of a specific sensor.

[3]Sensor normalisation removes concentration information in the data set and the output of each sensor over the entire data set lies in the range [0, 1] whereas autoscaling sets the mean value to 0 and the variance to 1.

2.3.4 Odour Recognition

Finally, a pattern recognition engine in the artificial olfactory system represents the olfactory cortex of the mammalian brain, which classifies and memorises odours. The output from the signal processor is fed into the PARC engine, which attempts to recognise and discriminate odours using chemometrics[4] and neural networks. Gardner et al. [27] have compared different methods of pattern recognition including multicomponent analysis, cluster analysis and neural networks in this field. PARC techniques has been widely split into two areas [1, 4, 35]; classical PARC and ANNs (Artificial Neural Networks). Figure 2.4 shows a simplified classification survey [26] of the most popular numerical methods which describe model-based and model-free methods used for qualitative and quantitative analysis. Also, this survey categorises supervised and unsupervised methods, referred to by the method of calibration. The following sections describe a more detailed methods commonly applied to electronic nose data.

2.3.4.1 Classical Pattern Recognition

Classical PARC is a statistical method described by the application of a probability model and was first developed and used in the field of applied mathematics. In this section some mathematical methods are presented that may be applied for multi-component analysis in odour sensing. Categorisation of classifiers can be made depending on certain aspects as shown in figure 2.4. For example, discriminant function analysis is a parametric and supervised learning classifier,

[4]Chemometrics is defined as the use of statistical techniques to extract relevant, but often hidden, information from chemical data.

which can be used for both qualitative and quantitative analysis. Internal classifier parameters are adjusted according to the error between the actual output and desired output. Principal components analysis is nonparametric and is often used to implement a linear supervised classifier, in conjunction with discriminant analysis. At this point it is important to understand the following typical chemometrics.

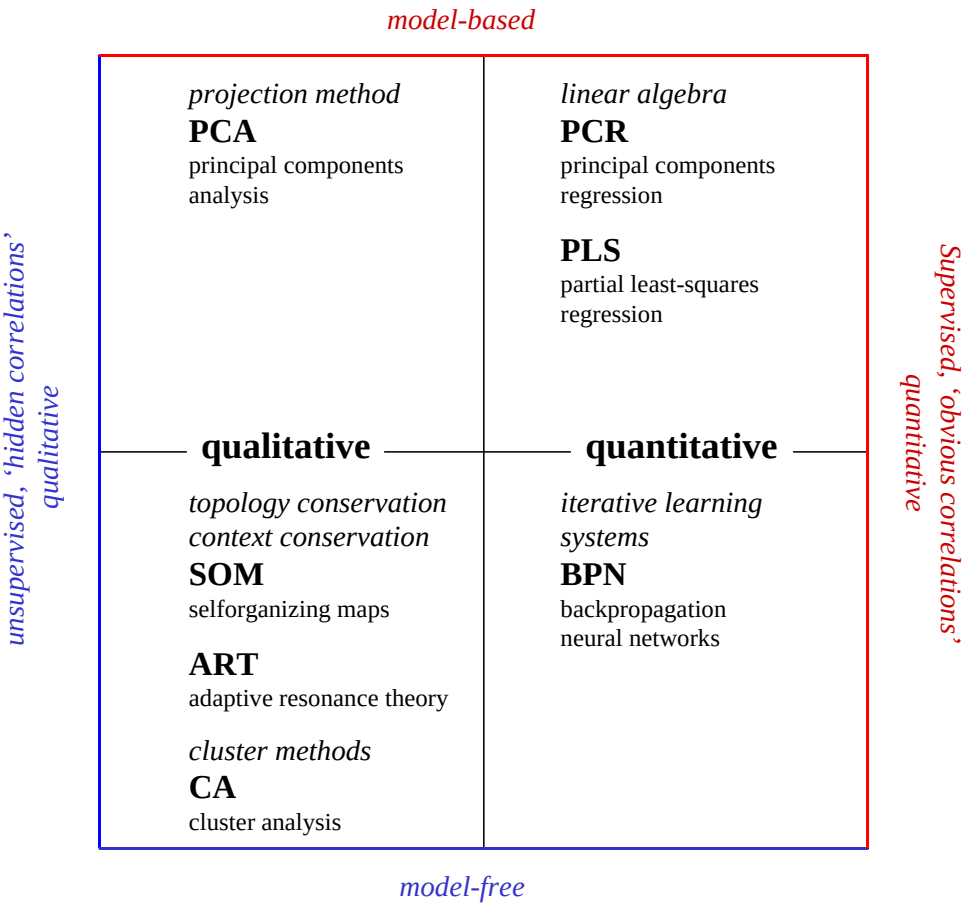

Fig. 2.4 Survey on multivariate approach. PCA = principal components analysis; CA = cluster analysis; PCR = principal components regression; PLS = partial least-squares regression; SOM = self-organizing feature map; ART = adaptive resonance theory; BPN = back-propagation neural network [26].

Principal Components Analysis (PCA)

PCA is a multivariate statistical method, based on the Karhunen-Lowve expansion, used in classification models, which produces qualitative results for pattern recognition. PCA is a linear supervised pattern recognition technique that has often been used to explore gas sensor array data in conjunction with cluster analysis. In PCA, a set of correlated variables are transformed into a set of uncorrelated variables (principal components) such that the first few components define most of the variation in the data set. It is a specific kind of orthogonal projection and its coordinate system is usually called 'feature space'. The principal component, or score, is expressed in terms of linear combinations of the variables, $X_1, X_2, ..., X_p$, and the eigenvectors, a_{ij}, which are often called the 'loadings'.

$$Z_i = \sum_{j=1}^{p} a_{ij} X_j \qquad (2.1)$$

where Z_i is the *i*th principal component and p is the number of sensors.

PCA is in essence a data reduction technique for correlated data, so that PCA has been applied to high dimensional data sets to identify their variation structure for gas sensor applications, such as the discrimination of beverages, coffees, alcohols, and tobaccos. For example, PCA was able to differentiate between several classes of odours when it was applied to electronic nose data, but if the sensor outputs have not been linearized, the results of PCA can not be guaranteed. Hexahedra of data, which are 3D matrices for a simultaneous analysis of distributed sensor arrays, have also been considered by Gemperline et al.

Cluster Analysis (CA)

Cluster analysis is a model-free qualitative analysis and generally undergoes an unsupervised learning phase. The term cluster analysis covers a class of techniques which seek to divide a set of samples or objects into several groups or clusters. The clusterings are based on the proximity of the vector in feature space and five basic types of clustering methods have been identified [36]: hierarchical, optimization-partitioning, clumping, density-seeking and other methods. The hierarchical and optimization-partitioning methods are the most popular. The hierarchical technique has been applied to electronic nose data for the discrimination of beverages, such as bitters, lagers, and spirits [27]. It is simple and rapid to compute and interpretation is straightforward and intuitive. In this study, objects are grouped first into small clusters of two or three objects; these are then grouped into larger clusters, and so on. Also, there was a comparison of CA on original and normalised responses and it was revealed that the normalisation enhanced the results of CA [27]. Although CA is very sensitive to data pre-processing methods, it is still widely used in many fields including electronic noses [4, 27, 37] with PCA to identify groups or clusters of points in feature space.

Discriminant Function Analysis (DFA)

Discriminant function analysis (DFA) is one of the parametric PARC techniques. There are many ways of computing DFA, but the classical approach, devised by the statistician Fisher [38], is called linear discriminant analysis (LDA). A direction is found to pass through the data. This direction is a straight line, and is somewhat analogous to a principal component, but a different criterion is used to find this line. LDA is not always clear, for example there is sometimes a little overlap between classes: it is not possible to guarantee that a cut-off value will exactly

separate classes. Many other sophistications have been developed, these include quadratic discrimination and logistic discrimination that require some assumptions about the original data, but provide better discrimination performance. One of the problems is that the nature of the resultant function is dependent on the algorithm used. LDA has been applied to the discrimination of commercial coffee flavours [28] and alcohol vapours [27] with almost 100% success rate.

Partial Least Squares (PLS)

Partial least squares is one of the latest regression procedures, based on the properties of multiple linear regression, to be developed for concentration prediction. PLS was first described in the mid-1960s by Wold [39]. The groups of Wold and Martens have been refining and specialising the method for chemical applications. In contrast to principal component regression (PCR), this approach takes into account the concentrations already in the model building. One of the main advantages of PLS and its applicability to sensor arrays is that it can separate noise from useful information.

A nonlinear PLS for correcting nonlinearities after calculations has been applied to evaluate signals of gas sensor arrays and used for quantitative multicomponent analysis [40]. Without any linearisation the prediction using PCR and PLS showed clearly the nonlinearity of the sensor but linearisation improved the results of this analysis. However, in most situations the electronic nose is not used to solve multi-component problems and so PLS is less important.

2.3.4.2 Artificial Neural Networks (ANNs)

Since the 1990, Artificial Neural Networks (ANNs) have been widely used in the artificial olfactory system. Aleksander and Morton (1990) described the definition of a neural network as follows.

"A neural network is a massively parallel distributed processor that has a natural propensity for storing experimental knowledge and making it available for use. It resembles the brain in two respects [41]*:*

1. *Knowledge is acquired by the network through a learning process.*
2. *Interneuron connection strengths known as synaptic weights are used to store the knowledge."*

Neural networks are also referred to in the literature as neurocomputers, connectionist networks, parallel distributed processors, etc. The history of neural networks is said to have begun by McCulloch and Pitts [42] who described a logical calculus of neural networks. Since then, the number of research and the pioneering works has been performed. An historical review on neural networks has been given by many researchers [24]. This section gives a brief review of ANNs related to the electronic nose systems.

The recognition ability of ANNs is higher in comparison with the classical PARC methods described previously, due to parallel signal processing. ANNs have many advantages in that they can handle nonlinear data sets, and have greater tolerance to sensor noise and drift. Also ANNs give high speed results, are efficient with information processing and learn by themselves. However ANNs have several disadvantages, for example, it is often difficult to decide the optimal network parameters and training procedures. If the patterns have a great difference in shape,

volume and density or they are overlapped with each other, then the ANNs often have some problems to get a good recognition. Recently, ANNs have been widely used in odour recognition and many different ANN paradigms have been developed.

Back Propagation (BP)

Back propagation (BP) is a effective learning algorithm for training a perceptron[5] network which has more than one layer of adaptive weights. It was formalised first by Werbos in 1974 [43] and is now the most widely used algorithm in multilayer feedforward networks. The BP consists of a forward phase and a backward phase. In the forward phase the input pattern has been applied as a stimulus to the first layer of the network and it propagates through the network layer by layer until an output is generated. The output is then compared to the desired output and an error signal is computed for each output unit. In the backward phase the undefined parameters weights of the network are adjusted in order to minimise the sum of squared errors. Based on the error signal received, weight values are updated by each unit until some convergence criterion is met. However the learning procedure of BP is often slow and sometimes fails to converge to a global minimum solution.

A three-layer back propagation network has been widely used for pattern recognition using an electronic nose system. Shin et al. [44] used the BP as the supervised learning rule to identify 4 different gases with different concentrations and the recognition probability was 100 % for each of five-trials of twelve gas samples. At the University of Warwick, a multi-layer perceptron (MLP) with a BP

[5]The perceptron was invented by psychologist Frank Rosenblatt in the late 1950s. It is the simplest form of a neural network which consists of a single neuron with adjustable synaptic weights and threshold.

learning algorithm has been applied to the prediction of bacteria type and culture growth phase [45]. Results show that the type of bacteria can be correctly predicted for 96% of all samples taken during a 12 h incubation period.

Multi-Layer Perceptron (MLP)

A multi-layer perceptron (MLP) is the most popular arrangement of neurones within an ANNs and it represents a generalisation of the single-layer perceptron. A MLP with a BP training algorithm described previously was the first ANN to be applied to an electronic nose system. Typically, the MLP consists of a set of sensory units that constitute the input layer, one or more hidden layers, and an output layer. The input values are linked by weights and each neurone computes a weighted sum of the input. In the hidden layers, these values are correlated by other weights with the output layer. Each of the weighted sums is transformed by a nonlinear function, respectively, and by a threshold value. The output of the neurone is then into the last layer and compares the outputs with the desired output to generate an error signal for back propagation (see chapter 4.2.2 for further details including equations). MLPs generally show a better performance than more established classical PARC methods but there are many empirical parameters to be considered, such as network architecture, training parameters, recognition estimation etc.

Self-Organising Map (SOM)

A self-organising map algorithm was developed by Kohonen in 1982 [46] to transform an incoming signal pattern of arbitrary dimension into a one- or two-dimensional discrete map. A SOM is more closely related to the neural structures of the human olfactory cortex than other ANNs because it emulates part of the brain.

Furthermore, a SOM has benefits in an electronic nose system because of its inherent features such as a reduction in dimensionality and invariance to drift and transitory noise [47]. Therefore a SOM is a very promising ANN for the optimal transformation of multidimensional nonlinear sensor characteristics without any assumptions.

Kohonen developed a supervised learning technique from SOM, which is called Learning Vector Quantisation (LVQ). LVQ is an improved supervised learning technique with a self-organising feature map. The hidden layer in this network is a Kohonen layer, which does the learning and classifying. The LVQ scheme has phases, LVQ1 and LVQ2. LVQ1 is the basic LVQ learning algorithm that helps all processing elements (PEs) to take an active part in the learning. LVQ2 is a fine tuning mechanism, which refines class boundaries. Therefore the output from LVQ2 is the final encoded version of the original input signal applied to LVQ1.

SOM has been applied to a wide variety of applications including the classification of odours in the electronic nose [47, 48]. Hines et al. used the supervised Kohonen SOM for analysing alcohol and coffee data sets and found good performance results in terms of both accuracy (over 90% within only 500) and generalisation.

Fuzzy Neural Network (FNN)

Fuzzy set theory was invented by Zadeh in 1965 [49] to provide a mathematical tool for dealing with linguistic variables. Fuzzy logic has been applied to ANNs and many attempts to use fuzzy functions to identify odours have been made [16, 50]. A fuzzy set is defined as a set whose boundary is not sharp [24]. The fuzzy neural network introduces the fuzzy concept into the neural network system, in general, and has received a great deal of attention in recent years [49, 50]. In FNN,

the signal conditioning that occurs during fuzzification and de-fuzzification translate many properties of overlapping sensor arrays into parameters which are better handled by a classifier. It suggests the potential to improve the electronic nose system for the goal of an intelligent artificial olfactory system.

Singh et al. [16] showed that the performance of FNNs was superior to that of non-fuzzy neural network analysis. Ping and Jun [50] used a combined neural network with the fuzzy clustering algorithm and could get good performance owing to its consideration of the correlation of the samples and the total characteristic of the classes. The FNNs are getting popular and produce a considerable improvement for the application field of electronic nose systems.

Carpenter et al. [51] introduced the Fuzzy ARTMAP for incremental supervised learning and nonstationary pattern recognition problems. Llobet et al. [52] used the Fuzzy ARTMAP to analyse the state of ripeness of bananas and found a good performance result in terms of 90.3% accuracy, which outperformed the MLP. The Fuzzy ARTMAP is a supervised variant of Fuzzy adaptive resonance theory (ART) which is self-organising, self-stabilising and suitable for incremental learning. Therefore it has an advantage of performing on-line learning without off-line training, unlike MLP. The details of neural network algorithms applied in this research will be discussed again in chapter 4.

2.4 Summary

In this chapter a brief history and the technology of electronic nose systems were explored, also the relationship between mammalian and artificial olfaction outlined. The architecture of the human olfactory system was compared with an

electronic system, which is composed of different kinds of sensors, transduction circuitry, and an artificial neural network.

A large variety of gas sensor technology, signal processing and PARC techniques were described and the architecture of the artificial olfactory system for this study was decided as follows.

MOS and CP were chosen as sensing materials, due to their attractive material characteristics, i.e. MOS thick-film gas sensors have very good sensitivity, stability and are relatively easy to make. CP gas sensors are readily grown by electrochemical polymerisation and operate at room temperature with fast reversible changes in conductivity. This hybrid sensor system will be employed to give a large flexibility to the general purpose of electronic nose used (chapter 5).

Several promising pre-processing techniques including a difference model and a fractional model will be used in order to improve the classification process and reduce any noise and base-line drift of sensors. In addition, autoscaling and normalisation will be employed to give equal weighting to each sensor and thus compensate for differences in the magnitudes of the signals.

PCA was chosen to assess clustering within data set. It is the most effective classical statistical method to show the visualisation of pattern recognition before neural networks. Three supervised classifiers, MLP, LVQ and Fuzzy ARTMAP neural network will be used and compared for the classification of both two strains and four different growth phases of cyanobacteria in chapter 4.

2.5 References

1. J.W. Gardner, and P.N. Bartlett, A brief history of electronic nose, Sensors and Actuators B, 18-19, (1994) 211-220.

2. F. Winquist, H. Arwin, E. Lund, R. Forster, C. Day, and I. Lundström, Screening of irradiated tomatoes by means of an electronic nose, The 8th International Conference on Solid-State Sensors and Actuators, and Eurosensors IX, Stockholm, Sweden, June (1995) 691-694.
3. K. C. Persaud, and G. H. Dodd, Analysis of discrimination mechanisms of the mammalian olfactory system using a model nose, Nature, 299 (1982) 352-355.
4. K. C. Persaud, and P. Pelosi, An approach to an electronic nose, Artificial Internal Organs, 31 (1985) 297-300.
5. J.W. Gardner, and P.N. Bartlett (eds.), Sensors and Sensory Systems for an Electronic Nose, Kluwer Academic Publishers, Dordrecht, (1991).
6. J. W. Gardner, Pattern recognition in the Warwick Electronic Nose, 8th Int. Congress of European Chemoreception Research Organisation, University of Warwick, UK, July (1987).
7. J. D. Hartman, A possible objective method for the rapid estimation of flavors in vegetables, Proc. Am. Soc. Hort. Sci., 64 (1954) 335.
8. W. F. Wilkens, and J. O. Hartman, An electronic analog for the olfactory processes, Ann. NY Acad. Sci., 116 (1964) 608.
9. T. M. Buck, F. G. Allen, and M. Dalton, Detection of chemical species by surface effects on metals and semiconductors, Spartan Books Inc., (1965).
10. A. Dravnieks, and P. J. Trotter, Polar vapour detection based on thermal modulation of contact potentials, J. Sci. Instru., 42 (1965) 624.
11. S. Zaromb, and J. R. Stetter, Theoretical basis for identification and measurement of air contaminants using an array of sensors having partially overlapping sensitivities, Sensors and Actuators, 6 (1984) 225-243.

12. A. Ikegami, and M. Kaneyasu, Olfactory detection using integrated sensors, Proc. 3rd Int. Conf. Solid-State Sensors and Actuators (Transducers '85), Philadelphia, PA, USA, June 7-11 (1985) 136-139.
13. T. Nakamoto, K. Fukunishi, and T. Moriizumi, Identification Capability of Odor Sensing Using Quartz Resonator Array and Neural-Network Pattern Recognition, Sensors and Actuators B, 1 (1989) 473-476.
14. H. Sundgren, I. Lundstrom, F. Winquist, I. Lukkari, R. Carlsson, and S. Wold, Evaluation of a Multiple Gas Mixture with a Simple MOSFET Gas Sensor Array and Pattern Recognition, Sensors and Actuators B, 2 (1990) 115-123.
15. T. Aishima, Aroma discrimination by pattern recognition analysis of responses from semiconductor gas sensor array, J. Agric. Food Chem., 39 (1991) 752-756
16. S. Singh, E. L. Hines, and J. W. Gardner, Fuzzy neural computing of coffee and tainted water data from electronic nose, Sensors and Actuators B, 30 (1996) 185-190.
17. H. Ulmer, J. Mitrovics, G. Noetzel, U. Weimer, and W. Göpel, Odours and flavours identified with hybrid modular sensor systems, Sensors and Actuators B, 43 (1997) 24-33.
18. P. N. Bartlett, J. M. Elliott, and J.W. Gardner, Electronic Noses and Their application in the Food Industry, Food Technology, Vol. 51, No.12, December (1997).
19. F. A. Geldard, The Human Senses, John Wiley & Sons Inc. (1972).
20. J. L. Davis, and H. Eichenbaum, Olfaction, The MIT Press (1991).
21. S. Firestein, and G. M. Shepherd, Olfactory receptors share antagonist homology with other g-protein coupled receptors, J. Physiol., 430 (1991) 135-158.
22. H. B. Barlow, and J. D. Mollon, The senses, Cambridge University Press (1982).

23. L. B. Haberly, Neuronal circuitry in olfactory cortex: Anatomy and functional implications, Chem. Senses, 10 (1985) 219-238.
24. S. Haykin, Neural Networks: A comprehensive foundation, Macmillam Publishing Company, (1994).
25. W. Göpel, J. Hesse, and J. N. Zemel, Sensors: A comprehensive survey, VCH, Vol. 2 (1991).
26. H. Baltes, W. Göpel, and J. Hesse, Sensors Update, VCH, Vol. 2 (1996).
27. J.W. Gardner, Detection of vapours and odours from a multisensor array using pattern recognition. Part 1: Principal components and cluster analysis, Sensors and Actuators B, 4 (1991) 109-116.
28. J.W. Gardner, H. V. Shurmer, and T. T. Tan, Application of an electronic nose to the discrimination of coffee, Sensors and Actuators B, 6 (1992) 71-75.
29. S. Morrison, Semiconductor gas sensors, Sensors and Actuators, 2 (1982) 329-341.
30. G. Horner, and C. Hierold, Gas analysis by partial model building, Sensors and Actuators B, 2 (1990) 173-184.
31. M. Egashira, Y. Shimizu, and Y. Takao, Trimethylamine sensor based on semiconductive metal oxides for detection of fish freshness, Sensors and Actuators B, 1 (1990) 108-112.
32. H. Abe, T. Yoshimura, S. Kanaya, Y. Takahashi, and S. Sasaki, Extended studies of the automated odor-sensing system based on plural semiconductor gas sensors with computerised pattern recognition techniques, Anal. Chem. Acta, 215 (1988) 155-168.

33. D. M. Wilson, and S. P. DeWeerth, Odour discrimination using steady-state and transient characteristics of tin-oxide sensors, Sensors and Actuators B, (1995) 123-128.
34. P.N. Bartlett, J. M. Elliot, and J.W. Gardner, Integrated sensor arrays for the dynamic measurement of food flavour release, Measurement + Control, 30 (1997) 273-279.
35. C. Di Natale, F. Davide, and A. D'Amico, Pattern recognition in gas sensing: well-stated techniques and advances, Sensors and Actuators B, 23 (1995) 111-118.
36. B. S. Everitt, Cluster Analysis, Heineman, London, (1981).
37. M. Holmberg, F. Winquist, I. Lundstrom, J. W. Gardner, and E. L. Hines, Identification of paper quality using a hybrid electronic nose, Sensors and Actuators B, 26-27 (1995) 246-249.
38. R. A. Fisher, The use of multiple measurements in taxonomic problems, Annals. Of Eugenics, 7 (1936) 179-188.
39. H. Wold, Festschrift Jersy Neyman, New York, Wiley, (1966).
40. J. Mitrovics, U. Weimar, and W. Göpel, Linearisation in multicomponet analysis based on hybrid sensor-array with 19 sensor elements, The 8th International Conference on Solid-State Sensors and Actuators and Eurosensors IX, Stockholm, Vol. 1 (1995) 707-710.
41. I. Aleksander, and H. Morton, An introduction to neural computing, London, Chapman & Hall, (1990).
42. W. S. McCulloch, and W. Pitts, A logical calculus of the ideas immanent in nervous activity, Bulletin of Mathematical Biophysics, 5 (1943) 115-133.

43. P. Werbos, Beyond Regression: New tools for prediction and analysis in the behavioral sciences, PhD thesis, Harvard, Cambridge, MA, (1974).

44. H. W. Shin, H-K. Hong, H. S. Park, D. H. Yun, C. H. Kwon, K. Lee, S-T. Kim, and T. Moriizumi, The 8th International Conference on Solid-State Sensors and Actuators and Eurosensors IX, Stockholm, Vol. 1 (1995) 687-690.

45. J. W. Gardner, M. Craven, C. Dow, and E. L. Hines, Prediction of bacteria type and growth phase by an electronic nose with a multi-layer perceptron network, Meas. Sci. Technol., 9 (1998) 120-127.

46. T. Kohonen, Self-organised formation of topologically correct feature maps, Biological Cybernetics, 43 (1982) 59-69.

47. E. L. Hines, J. W. Gardner, and C. E. R. Potter, Olfactory feature maps from an electronic nose, Measurement + Control, 30 (1997) 262-268.

48. R. A. Lemos, M. Hakamura, I. Sugimoto, and H. Kuwano, A self-organising map for chemical vapour classification, In Technical Digest, Transducers ’93, Yokohama, Japan (1993).

49. L. A. Zadeh, Fuzzy sets, Information and control, 8 (1965) 338-353.

50. W. Ping, and X. Jun, A novel recognition method for electronic nose using artificial neural network and fuzzy recognition, Sensors and Actuators B, 37 (1996) 169-174.

51. G. Carpenter, S. Grossberg, N. Markuzon, J. Reynolds, and D. Rosen, Fuzzy ARTMAP: A neural network architecture for incremental supervised learning of multidimentional maps, IEEE Trans. Neural Networks, 3 (1992) 698-713.

52. E. Llobet, E. Hines, J. W. Gardner, and S. Franco, Non-destructive banana ripeness determination using a neural network-based electronic nose, Meas. Sci. Technol. 10 (1999) 538-548.

Chapter 3

Experimental Procedure: Analysis of Blue Green Algae in Water

This chapter describes the development of an electronic nose system for water analysis; the procedures for testing and characterisation of the modified system, the methods of data collection, and the characterisation of prototype thin film sensors as well as commercial thick film sensors.

3.1 Environmental Water Monitoring

The release of chemical pollutants from industries, automobiles and homes into the environment has caused global environmental problems, such as acid rain, the greenhouse effect, ozone layer depletion, and water enrichment [1].

The enrichment of water by inorganic plant nutrients is fast becoming a severe problem in the quality of water and a common source of odour pollution into the environment [2, 3]. In 1989, widespread toxic cyanobacterial (blue-green algae) blooms occurred in lakes within the United Kingdom, causing animal poisoning and human health problems. In 1990, a wide programme of research on cyanobacteria was commissioned. Figure 3.1 shows the shoreline scum of the cyanobacteria *Microcystis aeruginosa* [4].

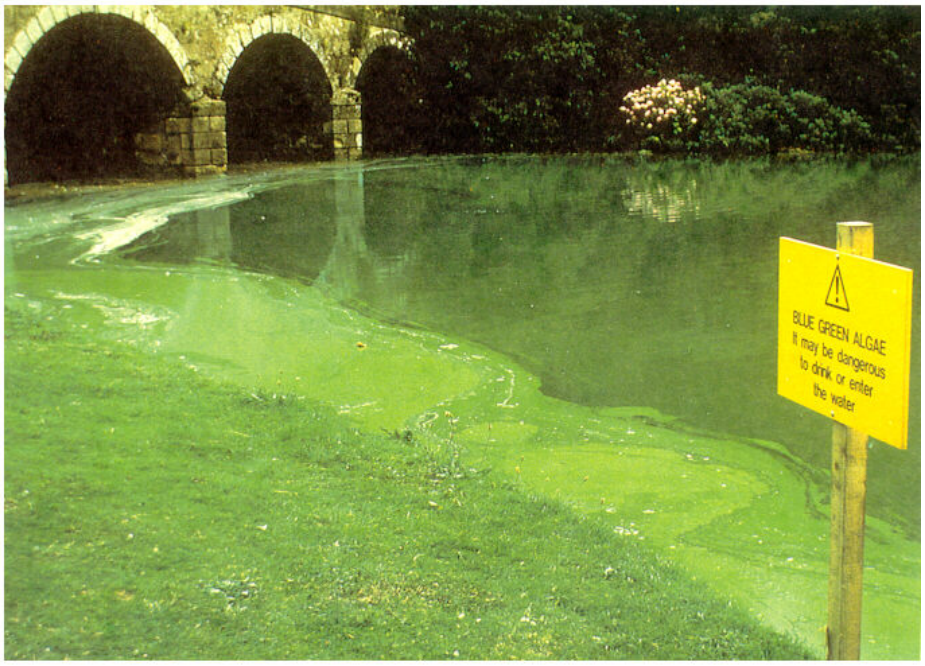

Fig. 3.1 The shoreline scum of the cyanobacteria *Microcystis aeruginosa*.

So far water analysis has been carried out mostly by analytical instruments that are based on liquid chromatography or optical microscopy. These instruments may give precise analytical data, but in most cases they require long data acquisition times and can not determine which algae is toxic. Such a disadvantage highlights the importance of the electronic nose approach, as another tool in the detection of toxic algae. Commercial electronic nose companies such as Osmetec plc. and EEV Ltd are trying to expand the possible applications of their electronic nose system into the biomedical and environmental field and are revealing the potential uses to the water industry.

3.1.1 Cyanobacteria

Cyanobacteria (blue-green algae) are the largest group of photosynthetic prokaryotes and contain chlorophyll that differs from the bacteriochlorophylls of the photosynthetic eubacteria. The name, cyanobacteria came to replace the term blue-green algae as a means of distinguishing them from the eukaryotic algae. It is derived from the Greek for blue (Kyanos) because of its characteristic blue-green colour.

Cyanobacteria are found to be of some benefit to humans and other living organisms. These are the primary producers of organic matter and oxygen in the natural environment because of their photosynthetic activity. Moreover, some of them are a primary food source, which also includes secretion of substrates to organisms associated with them. However there are many negative aspects associated with cyanobacteria. When present in large concentrations in lakes and reservoirs, the cyanobacteria blooms cause serious nuisance. They clog up water treatment filters, impart unpleasant tastes to drinking water, and produce offensive smells resulting from bloom decay. More importantly, a major problem associated with some cyanobacteria is that they may produce toxins that are effective against cattle, wildfowl, fish, and humans. Many species of cyanobacteria have been observed to produce these toxins, which can be divided into three groups; peptide hepatotoxins, neurotoxins and lipopolysaccharides. Thus finding appropriate methods to detect and quantify these toxins in natural waters is essential for pollution control.

3.1.2 Preparation of Blue-Green Algae

For the measurement of cyanobacteria samples, it is necessary to grow blue-green algae. The growth medium used was BG-11 (table 3.1) that is able to allow the growth of blue-green algae commonly found in rivers. This medium was made using

analytical grade chemicals and double distilled water, sterilised by autoclaving at 15 lb $inch^{-2}$ for 30 minutes. Table 3.1 shows the composition of the BG-11 medium.

Table 3.1 Composition of the BG-11 medium.

Chemicals	$g\ l^{-1}$
$NaNO_3$	1.5
$K_2HPO_4 \cdot 3H_2O$	0.04
$MgSO_4 \cdot 7H_2O$	0.075
$CaCl_2 \cdot 2H_2O$	0.036
Citric acid	0.006
$FeNH_4$ citrate	0.006
$Na_2Mg \cdot EDTA$	0.001
Na_2CO_3	0.02
Trace metal mix A_5+Co*	1 ($ml\ l^{-1}$)
Trace metal mix A_5+Co	
H_3BO_3	2.86
$MnCl_2 \cdot 4H_2O$	1.81
$ZnSO_4 \cdot 7H_2O$	0.222
$Na_2Mo \cdot O_4 \cdot 2H_2O$	0.390
$CuSO_4 \cdot 5H_2O$	0.079
$Co(NO_3)_2 \cdot 6H_2O$	0.049

The maintenance of a particular cyanobacteria culture is very important, because a bacteria culture will be useless if all the cells die, do not grow well, or if the culture is contaminated with different micro-organisms.

Cyanobacteria produce toxic substances when the cyanobaterial population forms a bloom. There are many physical factors leading to blooms of cyanobacteria such as, the temperature, light and the nutrient. Planktonic cyanobateria are very

similar to most photosynthetic plankton in that they require a certain minimum average light intensity for growth. Light is usually provided in the laboratory by a bank of fluorescent lamps (cool white, daylight, or warm white). The intensity for stock culture maintenance can vary enormously, through it has been shown that an intensity lower than 500 lux is appropriate [5]. The optimum temperature for cyanobactera is generally suggested between 15-30 °C. Rates of nutrient supply may be of more importance than actual nutrient concentrations. Actually, the requirement of nutrient substances is variable depending on the cyanobacteria species. In this experiment, 3.5 *l* of medium (1.5 *l* head-space) was placed in a standard 5 *l* glass jar and small number of cells (contained in 100 ml of inoculum) from the reference storage (master culture[1]) were inoculated into the medium.

3.1.3 Measurement of Growth Phase in Bacteria Cultures

The number of cells and cell size are sensitive indicators of the physiological status of cells. They change as the cells go through different stages of growth. Thus the cell size and cell numbers can be used to evaluate culture conditions and growth phase.

3.1.3.1 CellFacts Instrument

Small samples of liquid were extracted and analysed using a commercial CellFacts instrument (Microbial System Ltd), from which it is possible to measure the size and distribution of the bacteria (Figure 3.2). The CellFacts instrument uses electrical flow impedance determination to count and size particles and cells in a

[1]Master cultures were kept in a refrigerator in order to slow the metabolism of the bacteria cells and thus lengthen their useful life.

water sample. This is done quickly and easily by employing a real-time, on-line sampling technique. Cyanobacteria cells are passed through a 30 μm orifice in an electrolytic fluid, the displacement creating voltage pulses, which can be measured and counted. The range of cell size is 0.1 to 450 μm^3 and information about individual cells in a population can be gathered and automatically downloaded to a computer.

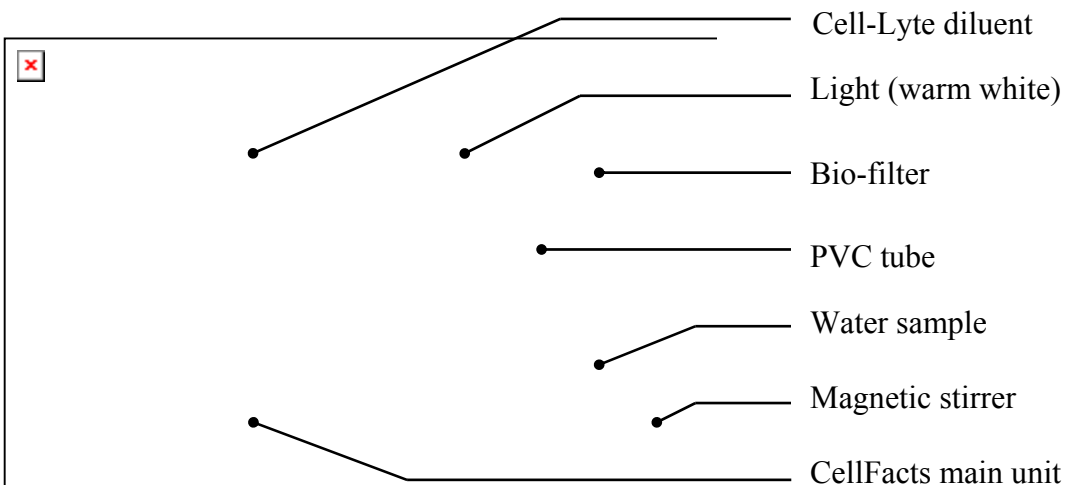

Fig. 3.2 Photograph of CellFacts instrument main unit connected with water samples in the Biological Sciences Department at the University of Warwick.

3.1.4 Measurement System Set-up with the Electronic Nose

The whole measurement apparatus used for data collection was set-up in the Microbiology Laboratory in the Biological Sciences Department at the University of Warwick. Figure 3.3 shows a construction of the measurement system for the testing of the cyanobacteria (blue-green algae) in water.

The system consisted of three main parts: the odour sampling unit, the Warwick Fox 2,000 unit and the Cellfacts instrument. The sampling system and the Warwick Fox 2,000 were controlled through custom designed software written in

LabView (National Instruments, Inc.) within an IBM PC compatible computer. It was also possible to achieve automated data gathering, using software that interfaced directly to the sensor array within the Warwick Fox 2,000 and the sampling system.

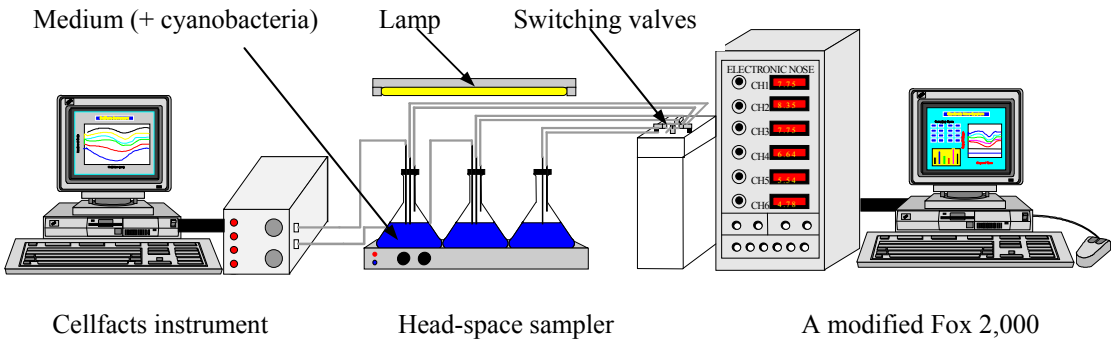

Fig. 3.3 Schematic diagram of the complete measurement system, to collect data from water samples.

Liquid samples were extracted and analysed by the commercial CellFacts instrument and gas samples from each headspace were introduced to the electronic nose system. Gas flow was directed through one of three routes by the action of three precision solenoid valves (Lee Company LFAA1200118H). Fittings were easily assembled onto Teflon tubing, and then connected to Lee miniature three-way solenoid valves. Each vessel had a solenoid valve associated with it. When power was applied to a valve the associated sample vessel was connected to the rest of the sub-system and gas flowed through this route. At any one time, only one valve was powered (i.e. open). Software run on the PC ultimately controlled the gas flow by solenoid valves, through a digital I/O from a data acquisition card (National Instruments manuf. No. PC-LPM-16). Thus the sub-system had three channels for gas to flow through from the input to the output, with one channel per vessel. The gas

pathways for all channels were designed to be of equal length and it was important to preserve identical gas flow characteristics across all channels in order to reduce any inter-channel variation. The sampling system was operated in a cyclic fashion, whereby a set sequence of timed valve actuation was repeated for a pre-determined number of times. The system consists of sampling the head-space of three identical vessels that contain reference (medium) and odour samples. The reference vessel, when selected, allowed the sensor array to stabilise its response to a known odour. Next, one of the sample vessels was selected and the change in sensor response was observed and recorded. It was possible to set up the sampling system to activate any channel at a specific time using a custom LabVIEW program. The sequence of channel activation that was adopted in the LabVIEW program for each cycle was; channel 1/channel 2/channel 1/channel 3. The connection between the valves and the vessels was made using PVC piping, except where brass pipe connectors were used. This had an approximate outer diameter of 1.5 mm and an approximate inner diameter of 1.2 mm. The rest of the piping was PVC (Lee Company TUVA4220900A), which fitted tightly over the brass pipes, the inner diameter was approximately 1.37 mm (when unstretched). The small diameter of the pipe-work allowed a small 'dead-volume' and therefore a fast response. The time delay (T_d) could be calculated with the dead volume (V_d) and the gas flow rate (Q), see equation 3.1:

$$T_d = \frac{V_d}{Q} \tag{3.1}$$

The total length of pipe-work was 700mm, therefore the volume of the pipe-work was 1031mm^3. The flow rate was 100ml/min.. Using equation 3.1, the time delay, T_d, was calculated to be 0.618 s.

3.2 Electronic Nose System Overview

The photograph shown in Figure 3.4 shows the Warwick Fox 2,000, which was used for data collection, in Biological Sciences, at the University of Warwick. The Fox 2,000 was designed and built by the University of Warwick and is sold by Alpha M.O.S. There are now several newer electronic noses of Alpha M.O.S., Fox 3,000/4,000[2]/5,000[2], commercially available with several more arrays, which can be consisted of MOS, conducting polymers, or SAW devices. There have been many electronic nose studies performed at the University of Warwick. Originally, Craven [6] modified the Fox 2,000 system and improved upon the performance of its subsequent pattern recognition. There were four major modifications to the Fox 2,000; an automated odour delivery system was added to the input, the volume contained within all the gas fittings was reduced, the gas sensor chamber was re-designed and an odour temperature controller was installed. This work is detailed in his PhD thesis [6].

Figure 3.5 shows a schematic diagram of the modified Fox 2,000. The main sensor chamber contained six metal oxide gas sensors and a temperature sensor

[2]These model were designed and built by Alpha MOS without additional input by the University of Warwick.

Fig. 3.4 Photograph of the Warwick Fox 2,000 electronic nose system.

(LM35CZ). The pre-sensor chamber contained a temperature sensor (LM35CZ) and a relative humidity sensor (MiniCap 2) that measured the temperature and humidity of the gas exiting from the pre-heater chamber. The pre-heater chamber was designed to reduce the fluctuation of temperature of the gas input to the main chamber. For these modifications, an extra circuit was built and connected to a spare analogue channel on the ADC (analogue to digital convertor) in the LPM-16 card. As a sub-system an autosampler [6], which controls the delivery of target gases to the sensor chamber, was built and added to the electronic nose system.

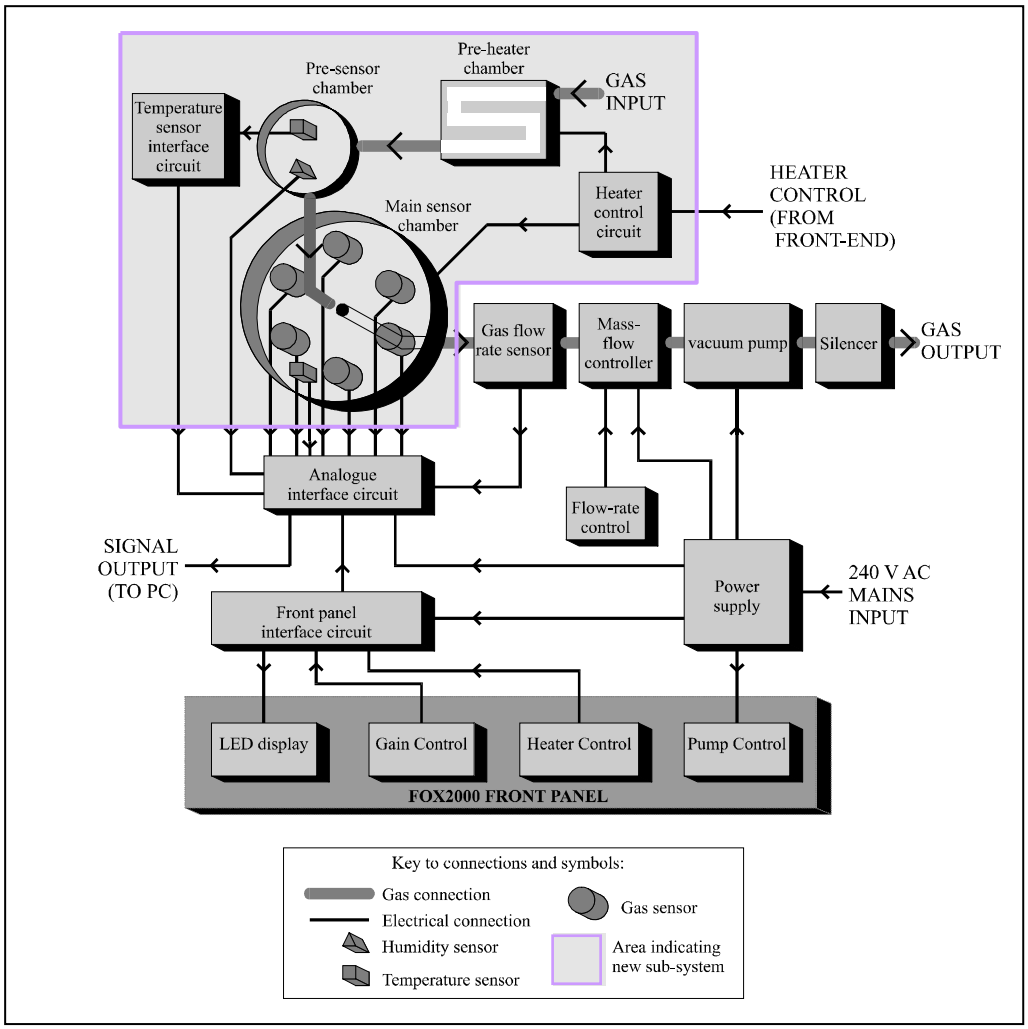

Fig. 3.5 The Warwick electronic nose showing the new main sensor chamber, pre-sensor chamber, pre-heater chamber, heater control circuit and the temperature sensor interface circuit [6].

The Warwick Fox 2,000 also has a gas flow sensor, a diaphragm vacuum pump (KNF Neuberger manuf. No. NMP30KNDC) and analogue op-amp interfacing circuitry, that converts the resistance of the gas sensors into a DC voltage (0 to 10 V) for input to a computer. The results of these modifications were that the new main chamber improved gas flow characteristics, because of its radial design [6], and a improved ambient temperature control, to an accuracy of ±0.1 °C using closed-loop feedback control via the heaters.

3.3 Gas Sensors

Many kinds of gas sensors have been employed within an electronic nose system, e.g. metal oxide chemoresistors, conducting polymer chemoresistors, SAW devices, and MOSFETs. In this research, two sensing materials, namely MOS (metal oxide semiconductor) and conducting polymer have been studied, for applications in water quality.

3.3.1 Thick Film Tin Oxide Gas Sensor

The gas sensors employed in the first stage of the research were thick-film tin oxide gas sensors, which were supplied by Alpha M.O.S. Figure 3.6 shows a diagram of the sensor structure and target gases of each sensor (FIS, Japan) employed in the Warwick Fox 2,000. Metal oxide semiconductor materials have been extensively studied and commonly employed in chemoresistor gas sensors, especially SnO_2 and the oxides of transition metals. These are the most commercially used materials in thick or thin films because they offer relatively high sensitivity and a wide range of sensitivity by adding different catalytic materials such as Pd, Pt, Ir and Au [7]. Figure 3.7 shows the simplified circuit diagram for the measurement of sensor voltage in the Warwick Fox 2,000. In this section, the gas sensing mechanism of SnO_2 and the operation of thick film gas sensors are briefly described.

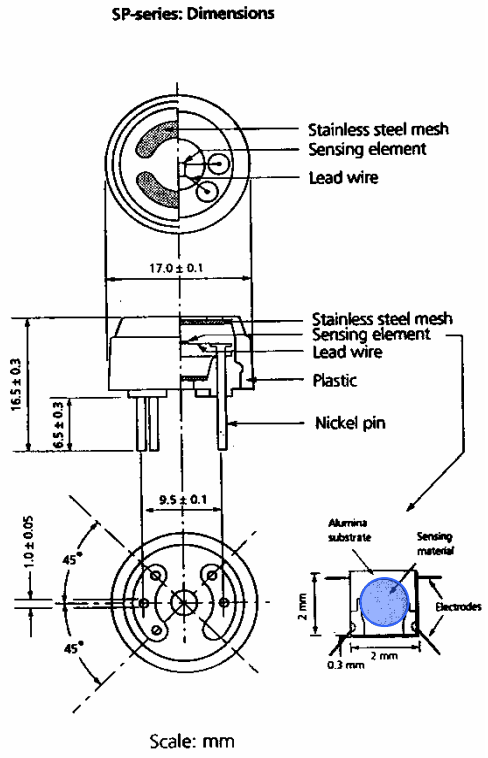

No.	Sensor model numbers (Target gases)
1	FIS SP12 (non-polar compounds)
2	FIS SP11 (Hydrocarbons)
3	FIS SP31 (Polar compounds)
4	FIS SP AQ 2 (Polar compounds)
5	FIS ST MW2 (Alcoholic compounds)
6	FIS ST41 (Heteroatom/chloride/aldehyds)

Fig. 3.6 Dimensions of the SP-series FIS gas sensor and the types employed in the Warwick Fox 2,000.

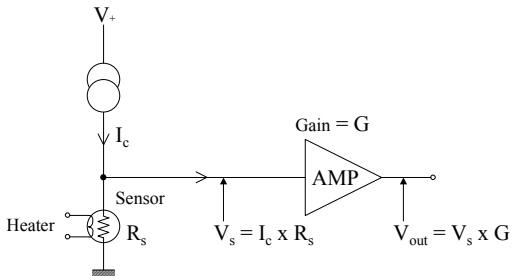

Fig. 3.7 Simplified MOS interface circuit diagram. The sensor voltage, V_s, is amplified by an op-amp, providing the voltage output, V_{out} (0 –10 V).

SnO_2 is an n-type semiconductor and the intrinsic donors are connected with a stoichiometric excess of metal (Sn), generating oxygen vacancies. When exposed to air, the oxygen is chemisorbed onto the oxygen vacancy sites in the non-stoichiometric semiconductor [8]. This chemisorption process produces a number of surface acceptors that bind free electrons from semiconductor and so create a surface

depletion layer. Subsequently, the chemisorbed oxygen reacts with the reducing gases, which release electrons to the SnO_2, so causing a change in the conductivity of the tin oxide. These reactions are very dependent on operating temperature. Generally SnO_2 sensors operate at elevated temperatures (300 –500 °C) to avoid interference from water, to aid rapid response and recovery times, and to enhance selectivity to the target gas. The kinetic reaction scheme on the surface of SnO_2 is shown in figure 3.8.

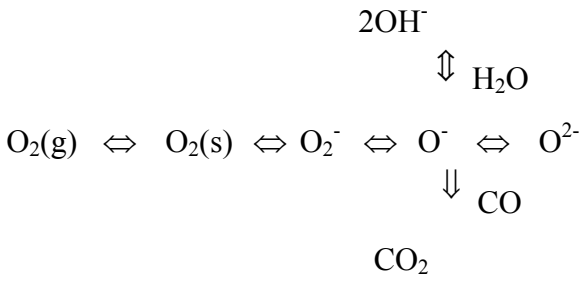

Fig. 3.8 Kinetic reaction scheme on the surface of a SnO_2 sensor where $O_2(g)$ and $O_2(s)$ denote oxygen gas and adsorbed oxygen, respectively.

FIS gas sensors employed in the Warwick Fox 2000 are porous polycrystalline, thick-film sensors, which follow the most accepted model [9, 10] for adsorbate-dorminated n-type semiconductors as shown in Figure 3.9. The adsorbed oxygen has extracted the conduction electrons from the surface of SnO_2 grains leading to a depletion layer, which forms a barrier at the grain boundary. Therefore, when it is exposed to reducing gases, the potential barrier decreases, which corresponds to higher conductance. The properties of SnO_2 films are highly dependent on the choice of sintering temperature, grain size and catalyst. For selectivity to different gases, four popular ways are used: the addition of a catalyst, selection of operating temperature, the use of a specific surface additive, and the use of a filter. In

particular, a catalyst is supposed to impart speed of response and selectivity in gas sensors because of "spillover" and control of the Fermi energy [11].

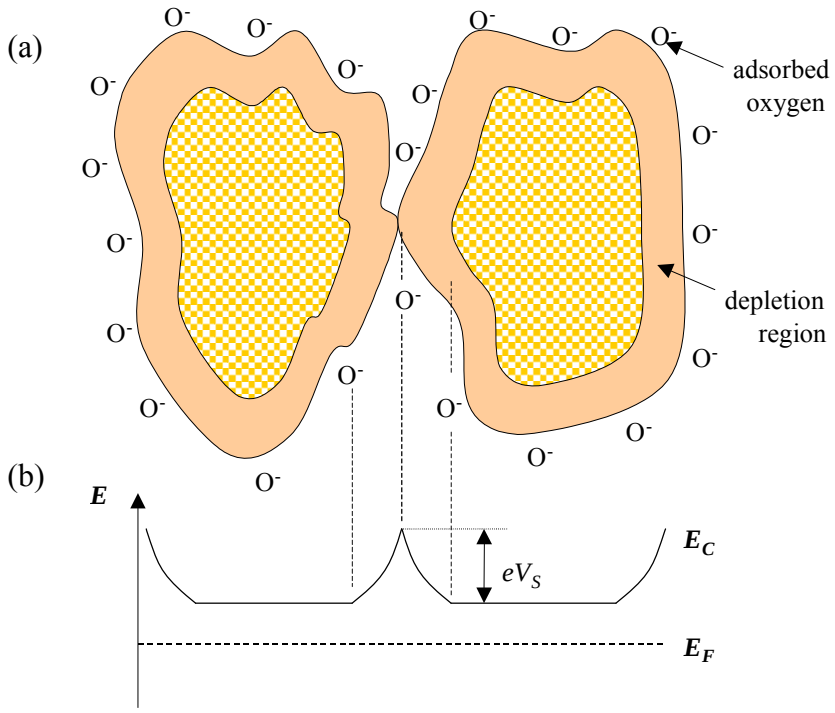

Fig. 3.9 General grain boundary model for adsorbate-dorminated n-type semiconductor powder in gas sensing. (a) Schematic of model generating depletion layer, (b) band model showing the potential barrier (eV_s) at the grain boundary.

3.3.2 Metal Oxide Semiconductor (MOS) Thin Film Gas Sensor

3.3.2.1 SRL125/MOS thin film sensor

The SRL125/MOS thin film sensor was designed in the Sensors Research Laboratory (SRL) at the University of Warwick [12] and fabricated at the University of Neuchâtel in Switzerland. This silicon micromachined device was used as a dual sensor that can be simultaneously operated as a microcalorimeter and a resistive gas sensor.

Conventional semiconducting oxide gas sensors (e.g. Taguchi gas sensor) require considerable labour effort to manufacture and have high power consumption.

Similarly, conventional calorimetric gas sensors (i.e. pellistors) require considerable manual labour to manufacture and possess a high power consumption (*ca*. 500 mW). Consequently, there is a general demand to mass-produce small, cheap, low-power calorimeters and resistive gas sensors, e.g. for the automotive market, and in particular battery-powered hand-held instruments (including electronic noses).

Generally calorimetric sensors are based upon the measurement of reaction heat fluxes resulting from the catalytic oxidation of combustible gas species in air at the surface of the heated device. They are usually operated in a Wheatstone bridge arrangement with an inactive reference sensor. The sensor response may be chosen as the change in temperature ΔT monitored by the changed resistance of a platinum heater. If, under the conditions of measurement, the rate of reaction is dependent on the presence of the gas, then determination of the heat evolved is a measure of gas concentration. A catalyst is usually required to increase the rate at which a thermodynamically feasible chemical reaction approaches equilibrium and achieves this without itself becoming altered by the reaction. For example, the enthalpy changes ΔH (heats of combustion) during these reactions lead to a change in the electrical power ΔP required to keep the sensor temperature at a constant value. The oxidation of reducing gas species leads to a decrease in the electrical power consumption. The value ΔP is given by the reaction rate *dr/dt* (moles of the reducing gas oxidised per second), by the catalytically active area A_{eff} of the calorimetric sensor, and by ΔH.

$$\Delta P \approx A_{eff}\, dr/dt \;\; \Delta H \qquad (3.1)$$

Figure 3.10 shows the wafer processing steps required to make the SRL125/MOS thin film sensor. A five mask process is used for the fabrication of the device, and the initial substrate was a 3", 280 μm thick, p-type (100) oriented silicon wafer.

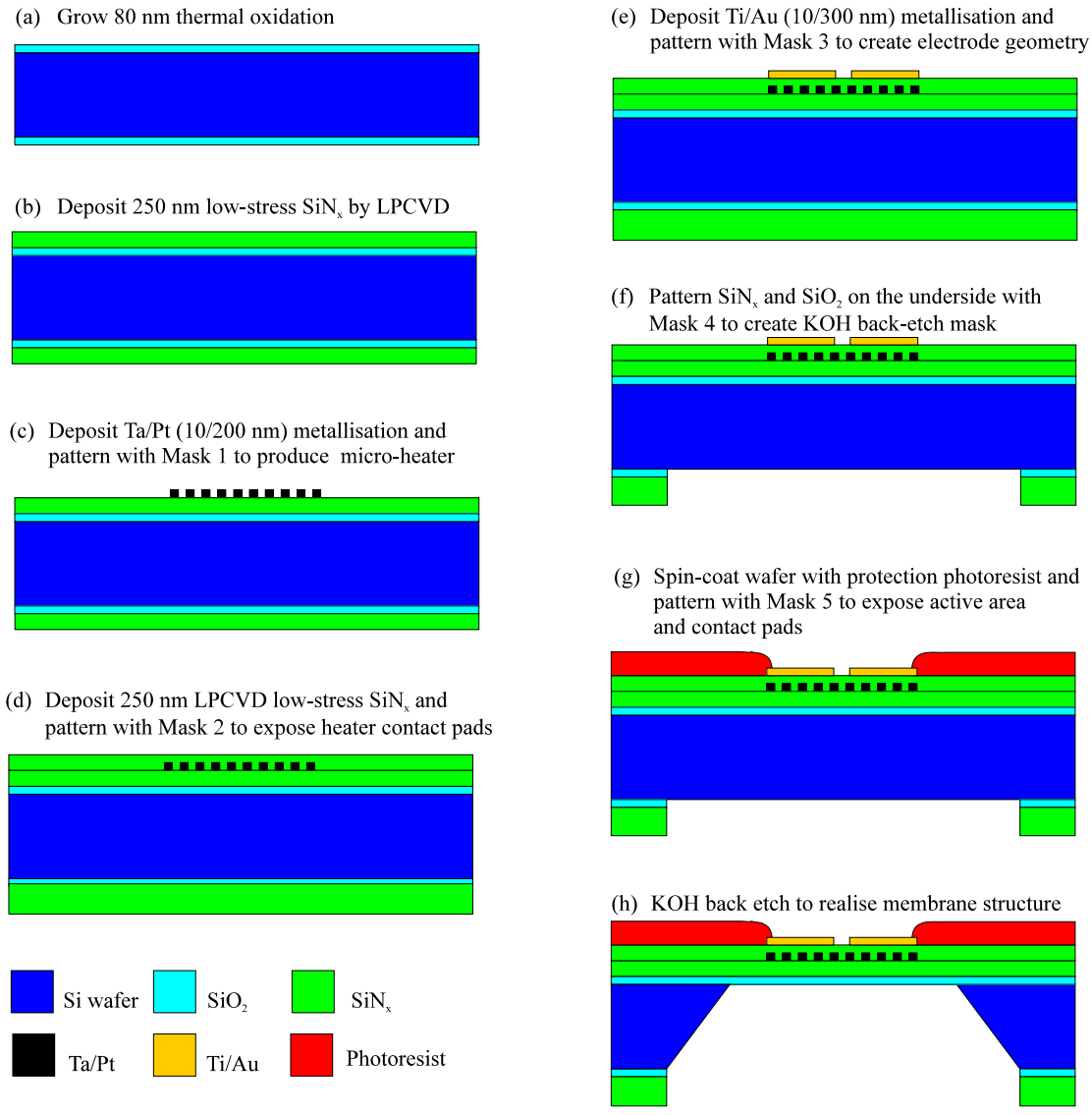

Fig. 3.10 Schematic of the wafer processing steps required for the SRL125/MOS.

The fabrication process of the membrane consisted of the thermal oxidation (80 nm) of Si, followed by LPCVD of 250 nm low stress SiN_X. The heater was made of

platinum (200 nm) deposited on a tantalum layer (10 nm), by d.c. sputtering under standard conditions. The metallisation layer was patterned using a positive photo resist (Shipley 1813) and conventional UV lithography. A second 250 nm LPCVD low stress SiN_x was then deposited, which electrically insulates the microheater from the electrodes deposited in a later stage. The wafer was subsequently subjected to a photolithography process to define contact holes which were etched out by the plasma etching. The electrodes and bonding pads were made of an Au/Ti (300/10 nm) double layer, deposited on the insulating layer by sputtering.

After the deposition of the electrodes, the windows for the backside etching were made by plasma etching. Another protective layer was then photolithographically patterned with the last mask to expose the active areas and the contact pads. The resist did not cover the hot active areas and permited on-chip annealing. The wafer was then backside-etched anisotropically in KOH, thereby leaving behind the thin membrane. The chips were mounted onto a custom-designed PCB header (or metal d.i.l package) using a special epoxy resin and the pads were ultrasonically wire-bonded to the gold-plated PCB. The gas sensitive material selected was Pd-doped SnO_2, deposited by dropping of paste [13]. Figure 3.11 shows a photograph of the sensor mounted in a custom-designed PCB.

The final stage of fabrication involved on-chip annealing of the SnO_2 at 600 °C. This device has an ultra-fast thermal response time of *ca*. 3 ms from 20 to 300°C, a low d.c. power consumption of 75 mW at 300°C, and potential low-cost due to the use of silicon microtechnology [14]. The fast thermal response permits pulsed-mode of operation and hence lower average power of *ca*. 1 mW.

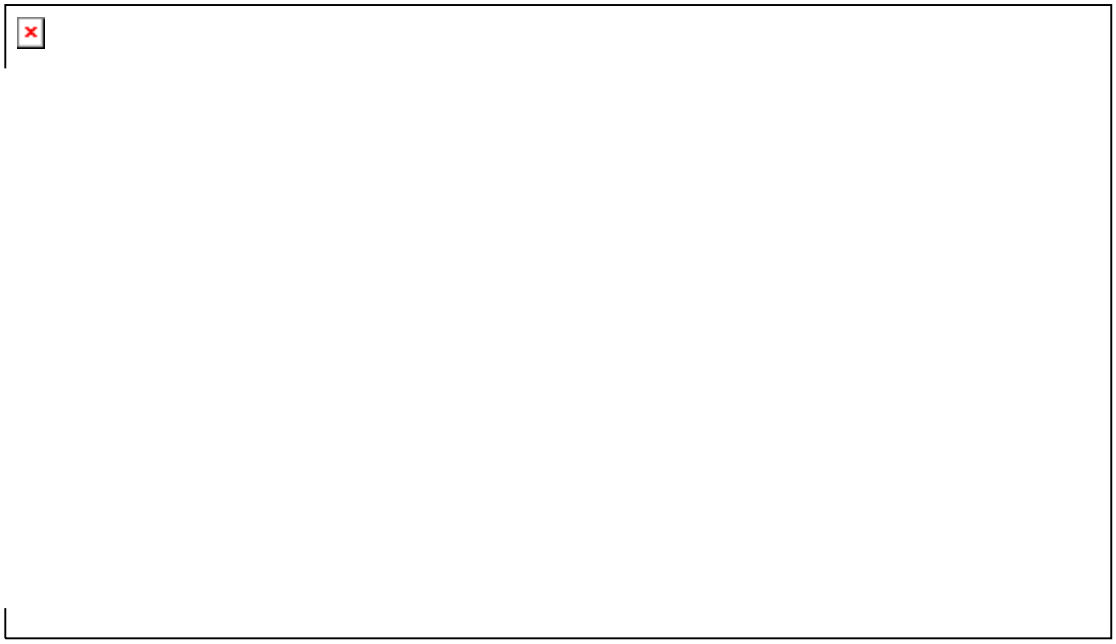

Fig. 3.11 Photograph of SRL125/MOS device

In order to measure the output of the calorimeter and chemoresistor, a programmable, low noise, high sensitivity Wheatstone-bridge based amplifier circuit was used. The use of National Instruments LabVIEW based PC user-interface simplified the testing, characterisation and comparison procedures for a range of gas sensitive devices including both chemoresistors and microcalorimeters [14].

1 wt% Pd-doped SnO_2 was selected as the sensing material because tin dioxide is widely used in resistive gas sensors but not in calorimetric sensors and was, thus, of research interest. An automated gas flow system was used to supply pulses of the sample gas (here ppm levels of CO) and control the temperature and water vapour pressure of the zero gas. The typical responses of the resistive and calorimetric sensors was acquired to a range of 100 to 500 ppm of CO in 100 ppm steps (Figure 3.12). The response times are set by the dynamics of the mass flow system. As expected the resistance ($\propto V$) falls with the introduction of CO, however, unexpectedly, the temperature ($\propto V$) of the tin oxide layer also fell. This is believed to be associated with a

reduction in film resistance causing a corresponding fall in its thermal resistance. This in turn resulted in an increase in the heat loss to the silicon substrate and so a fall in temperature when driving the heating element at constant voltage.

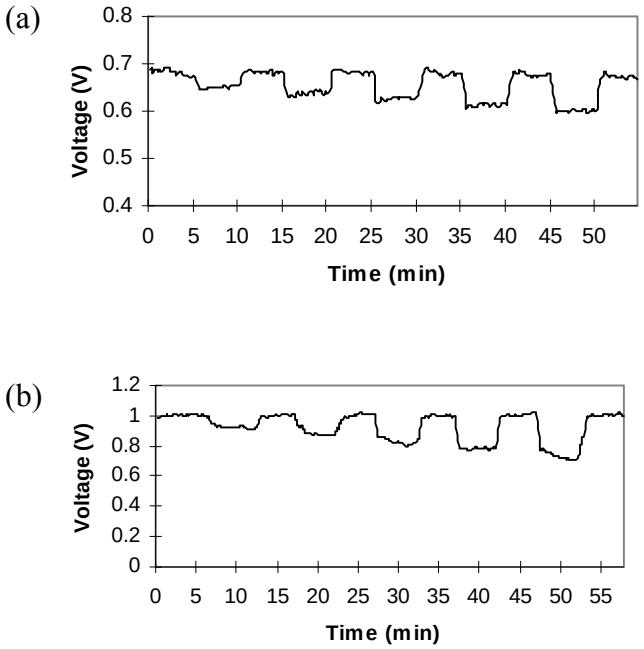

Fig. 3.12 (a) Resistive and (b) calorimetric response of the dual silicon microsensor.

3.3.2.2 Inter-digital capacitive (IDC 10) thin film sensor

The IDC 10 device, fabricated at the University of Neuchâtel in Switzerland on a Brite-EURAM project, was also used for the detection of CO and NO_2. The fabrication steps required for the IDC 10 device were similar to the ones of the SRL125 device. A low-stress LPCVD nitride passivation layer on top of the CVD films improved the robustness of these micro-hotplate membranes. The heater was made of the platinum (500 nm) deposited on a tantalum layer (10 nm) by d.c. sputtering under standard conditions. A second 500 nm LPCVD low stress SiN_x insulates electrically the microheater from the electrodes deposited in a later stage. The wafer was subsequently

subjected to a photolithography process to define contact holes which were etched out by the plasma etching. The electrodes and bonding pads made of the Pt/Ta (150 nm) double layer were formed on the insulating layer by sputtering. Figure 3.13 shows the schematic and photograph of IDC 10 device without a sensing layer.

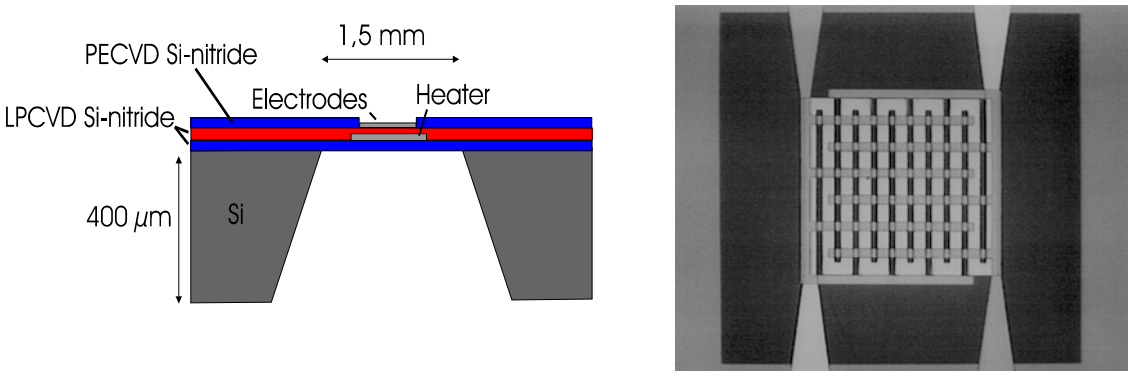

(a) (b)

Fig. 3.13 (a) Schematic diagram of a IDC 10 device, (b) top side view.

Three MOS sensing materials, $CrTiO_3$, WO_3 (Capteur Sensors & Analysers Ltd) and SnO_2 paste (University of Neuchâtel) were investigated as sensing materials for the IDC thin film sensor.

The paste was mixed up and inserted into a syringe for deposition onto the surface of the active area of the devices using a precision liquid dispenser (RS Components, No. 552-179) under pneumatic control (Figure 3.14). The film thickness was less than 50 μm and the area was about 1 mm X 1 mm. From previous experience, $CrTiO_3$, WO_3 pastes were fired at 600 ºC in a tube furnace for 30 mins and Pd-doped SnO_2 paste was fired at 700 ºC to evaporate the solvents and obtain stable characteristics. It was found that the $CrTiO_3$ and WO_3 layers were not stable enough to use and the resistance values were too high. Therefore further studies into

these problems are required. The following results are from the IDC device with SnO_2 as a sensing material.

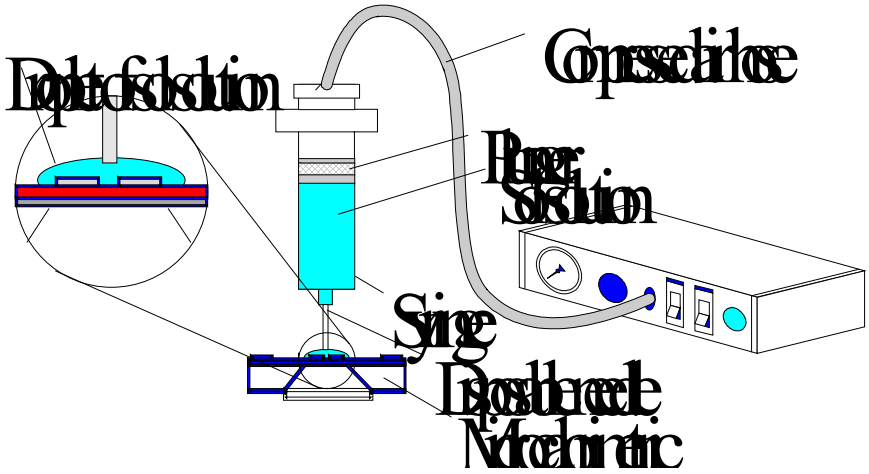

Fig. 3.14 Deposition of ceramic materials using a precision liquid dispenser.

The resistance of the platinum heater was measured as a function of temperature in the oven in order to calibrate the temperature scale. Figure 3.15 shows

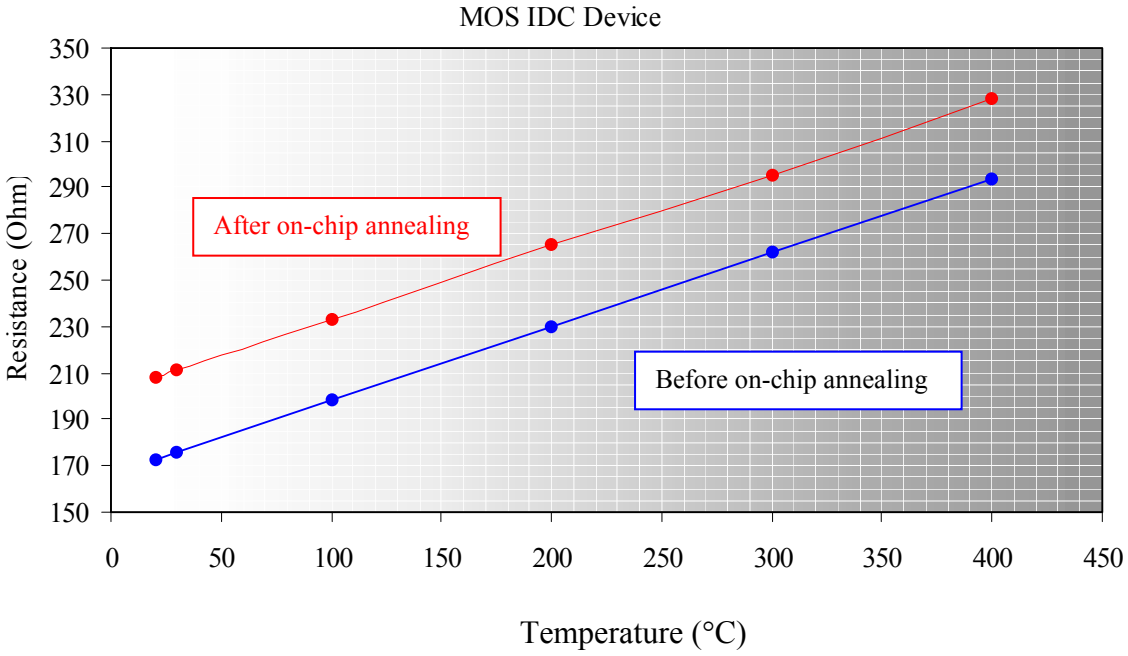

Fig. 3.15 Heating characteristics of micro-heater in a IDC 10 device.

the heating characteristics of the micro-heater in an IDC 10 device before and after on-chip annealing, at 6 V for 48 hrs. The resistance of the Pt heater, after on-chip annealing, was about 35 Ω higher than before on-chip annealing. The real temperature of the active area, of the IDC sensor, was measured as a function of heater temperature using Figure 3.15. The power consumption was obtained by measuring the voltage and corresponding current across the heating resistance (Figure 3.16).

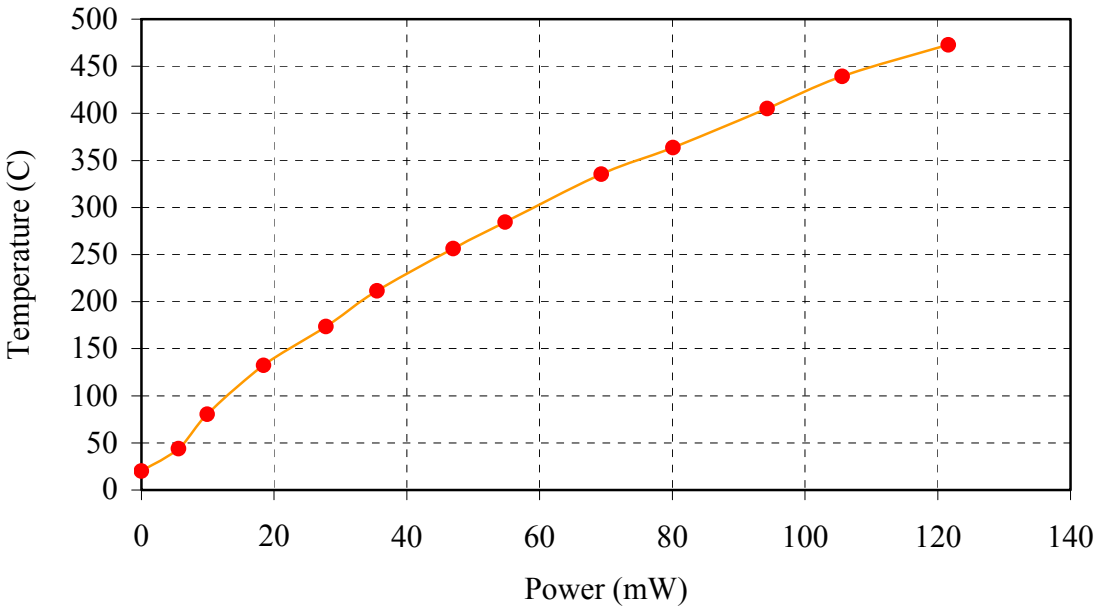

Fig. 3.16 Power consumption characteristics for an IDC 10 device.

Fig. 3.17 shows the sensitivity associated with CO concentrations (20, 40, 80, 130 ppm) at constant voltage mode (5 V). Alternating periods of CO and air were used after an initialisation period in air (200 ml/min) for 1 hour. The resistivity of the SnO_2 falls in the presence of CO. The dopant palladium principally determines the height of the potential barrier of SnO_2 by the withdrawing of electrons from the SnO_2. Palladium, on receiving electrons from the CO, would be less electronegative,

withdrawing fewer carriers from SnO_2 and decreasing the Schottky barrier height, and consequently the resistivity. There was a linear trend between the CO concentration (20, 40, 80, 130 ppm) and voltage change in the heating element. This resulted in an increase in the heat loss to the silicon substrate and so to a fall in temperature when driving the heating element at constant voltage. The sensitivity of the micro-heater was 38.92 mV/Ω.

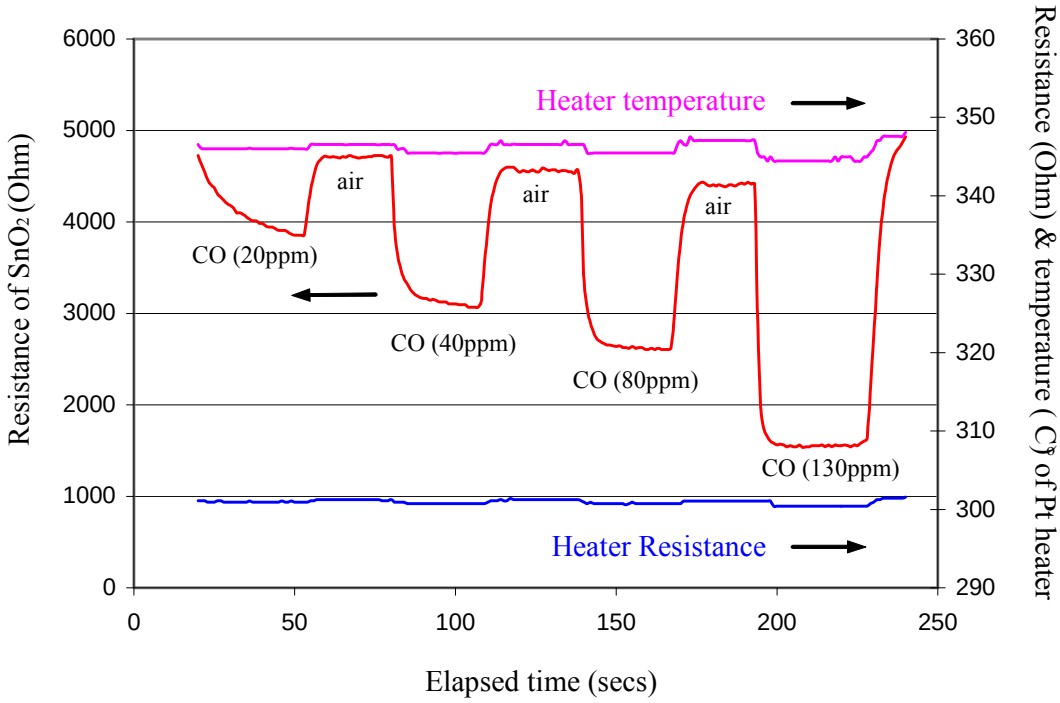

Fig. 3.17 Characteristics of Pd doped thin film SnO_2 sensor (IDC 10) to different CO concentrations (20 ppm, 40 ppm, 80 ppm, 130 ppm) at 5 V (heater voltage).

3.3.3 Conducting Polymers (CPs)

Conducting polymers have attracted considerable interest since their discovery in the late 1960s [16]. Although there has been much interest shown in the use of conducting polymers as electronic devices, e.g. organic diodes or transistors, there has been less interest, until recently, in exploiting their possible use as the active material

in gas sensors. A large number of CPs have been used for chemoresistive gas sensors. CP sensing materials have three main advantages when used as gas sensors [16]:

- A wide variety of polymers are available, including substituted polypyrrole, polythiophenes, polyindoles and polyanilines.
- CPs are readily grown by electrochemical polymerization of the monomer or deposited under controlled conditions.
- CP gas sensors operate at room temperature.

Conducting polymer sensors have been fabricated by electro-polymerisation of a thin film of polymer across the gap between gold-plated electrodes. Deposition of the conducting polymer gas sensor was carried out under the direction of Prof. Bartlett at Southampton University. Figure 3.18 and Figure 3.19 show the microdeposition apparatus designed for CP deposition.

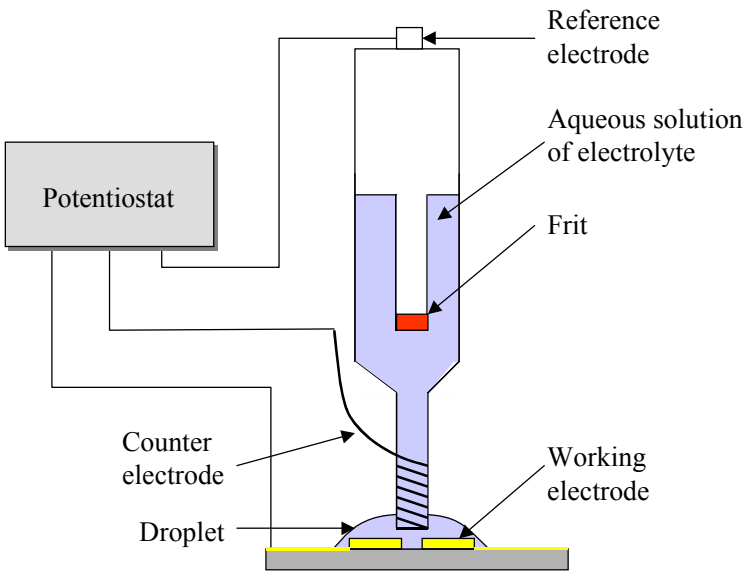

Fig. 3.18 The schematic diagram of the microdeposition apparatus for conducting polymer deposition.

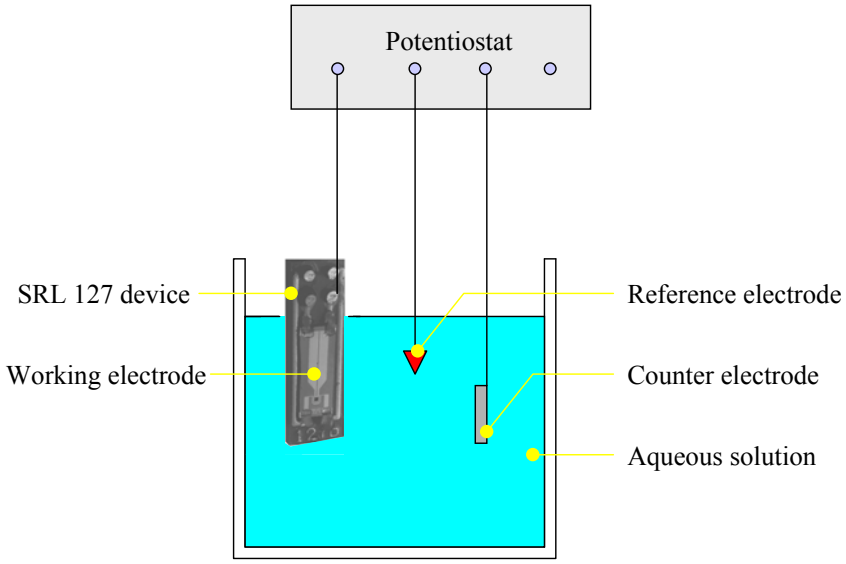

Fig. 3.19 The schematic diagram of the microdeposition apparatus for conducting polymer deposition.

The three-electrode configuration is established by dipping the apparatus into the droplet and aqueous solution, respectively. These methods were designed by Bartlett and Gardner for the deposition of different CPs on the same sensor array device [15]. In Figure 3.19, the calomel reference electrode and gold counter electrode are held directly above the working electrodes of the sensor device. A frit is used to separate the electrolyte and the electrolyte from the droplet when microdeposition is processed. The polymers deposited were a series of poly(aniline) pentane sulfonate. Aqueous solutions of 0.5 mol dm^{-3} aniline and 0.5 mol dm^{-3} pentane sulfonic acid sodium salt were used. The polymers were deposited potentiostatically by applying 0.9 V for 5 s, followed by +0.78 V for a variable time.

The details of the gas sensing mechanism in conducting polymers are poorly understood and several empirical models have been suggested. Bartlett et al. [16] have suggested five possible mechanisms of the gas sensitivity of CP chemoresistor which are likely to have dominant effects in most cases: (1) direct carrier generation

or removal by oxidation or reduction, (2) change in the interchain carrier mobility, (3) interaction with the counter ion, (4) change in interchain hopping, and (5) change in interfacial charge transfer. G. Wegner et al. [17] have considered the charge-carrier motion in conducting polymers which explains the hopping of charge-carrier between localised states of adjacent chain segment or different chains. It explains that the temperature dependence of the film conductance can be described by a variable range-hopping model of the Mott type. At present, the adsorption model by Bartlett et al. [18] has empirically shown good explanation for chemoresistive CP gas sensors.

3.4 System Control Software

Initially, the Warwick Fox 2,000 system was provided with dedicated software to perform data collection but the software was unable to control the new valve system and the work involved in the new application. It was thus modified for applying the electronic nose to the testing of blue-green algae in water.

LabVIEW is a language which allows the user to generate virtual instruments (VI's) quickly and efficiently from a series of building blocks and macro units. In this section, the modified software design approach is described for the real-time data acquisition/control system.

3.4.1 Software Design

LabVIEW is a hierarchical, object oriented language and lends itself to the design of highly structured, modular programs. Therefore, the software is structured with a main Virtual Instrument (VI) capable of calling and dismissing the sub VIs. The LabVIEW hierarchy for the modified system control is shown in Figure 3.20.

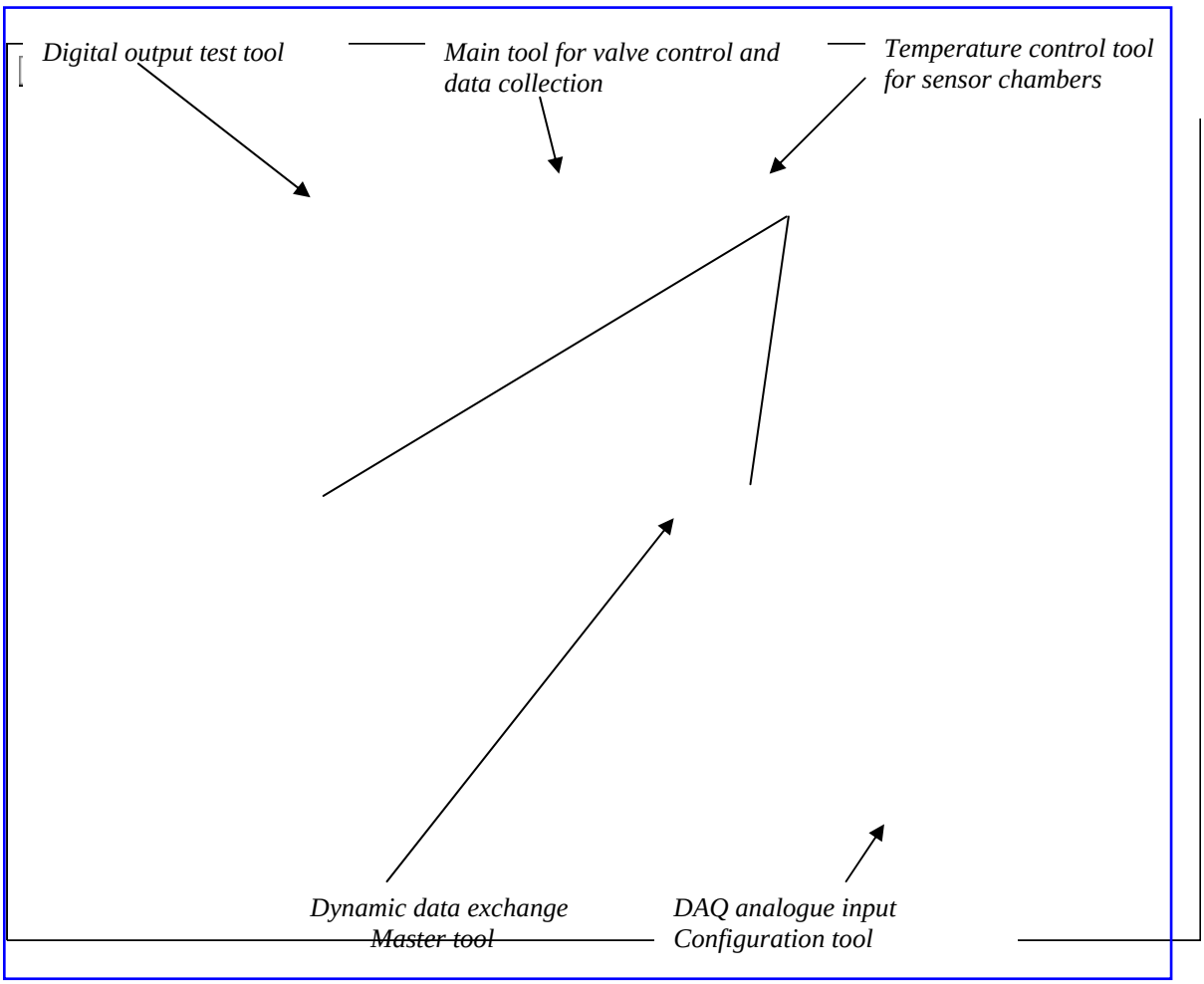

Fig. 3.20 The structure of LabVIEW hierarchy for the new Warwick Fox 2,000 system.

The program is divided into a hierarchy of objects, the main VI tool for valve control and data collection, the temperature control VI tool for sensor chambers and the digital output test VI tool for diagnosis.

The following section shows program details for each VI following the procedures developed.

1. To check the digital output lines from the LPM-16 I/O card, it is necessary to run LPM port test VI and open solenoid valve 1, before running the whole experiment.

2. Use the temperature control VI to maintain a constant temperature. Set to proper temperature and run by clicking on the running button. This program runs as a background task all the time. Figure 3.21 shows the parts of the temperature control program, the values of offset and the ratio for the conversion of temperature sensor output voltage into degrees centigrade.

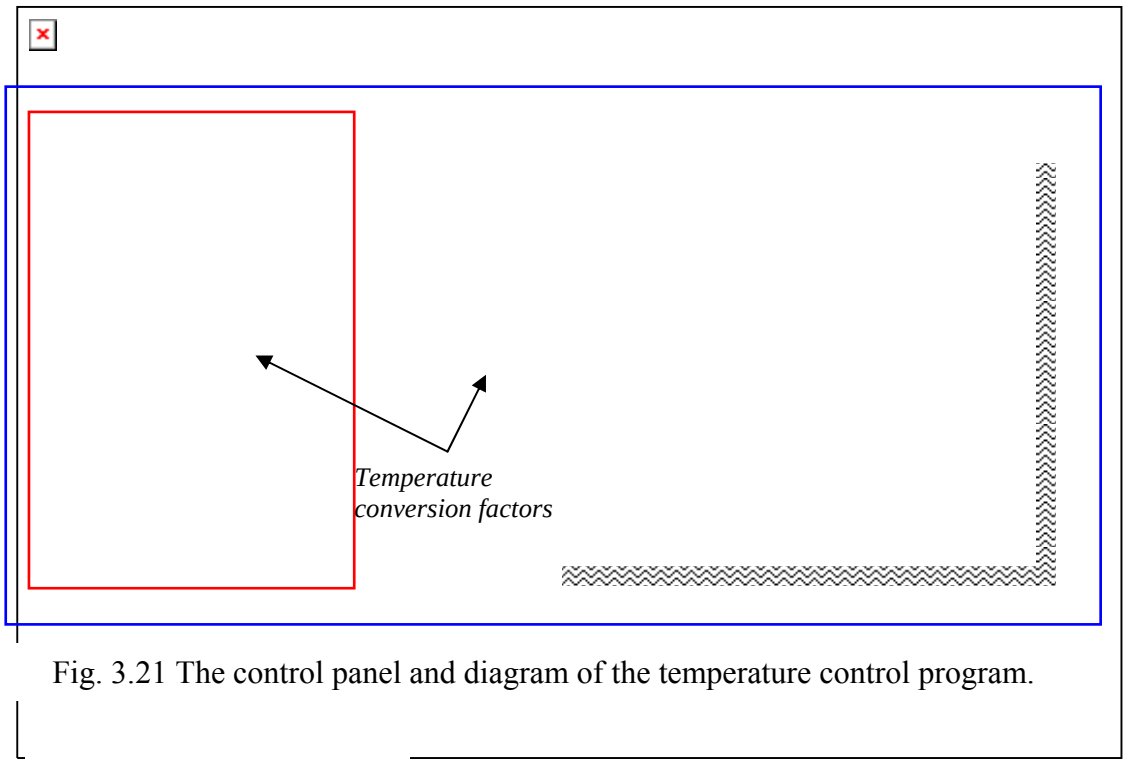

Fig. 3.21 The control panel and diagram of the temperature control program.

3. Select the main VI for the valve control and data collection. If it is activated, then a dialogue box is opened and asks for a configuration file. It simply creates a new file or overwrites the old file and changes the configuration within the program. Figure 3.22 shows the sampling cycle example for a configuration. For flexibility of data collection, the sampling rate is changeable using a cycle division mode.

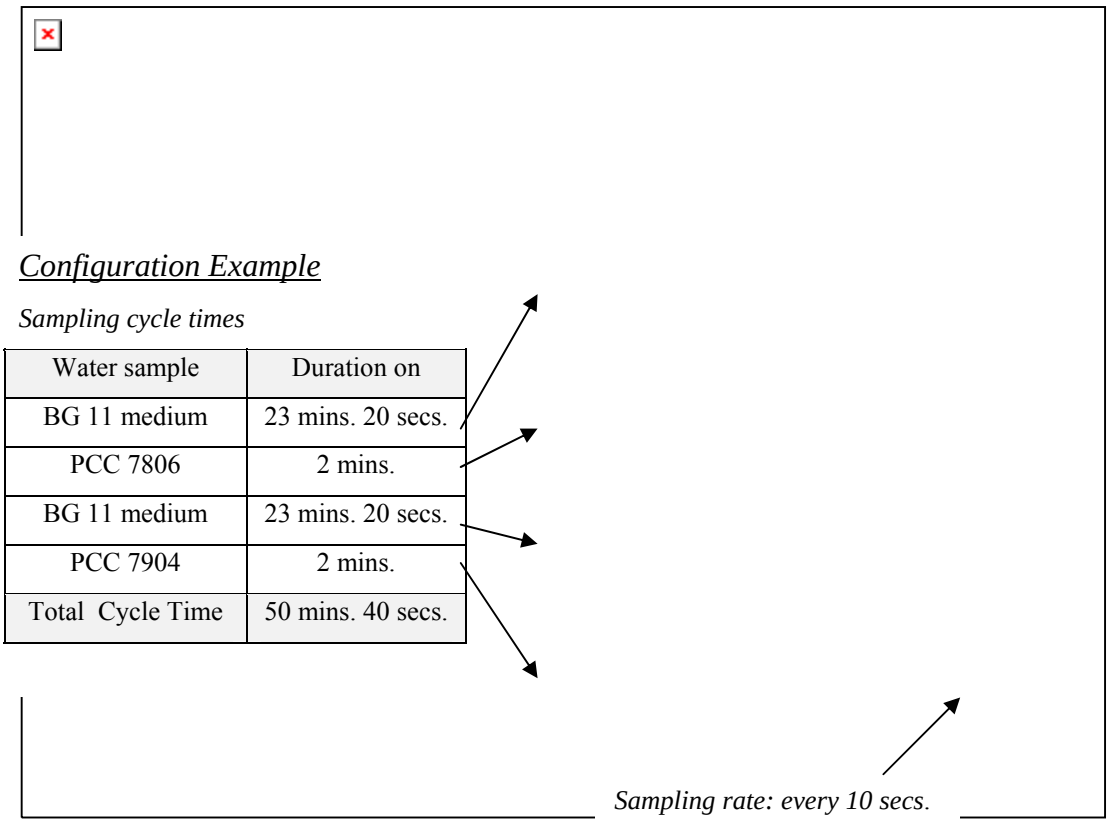

Fig. 3.22 Diagram of main VI for valve control and data collection.

4. Start the system control program and leave it for a duration time. If there is an error or problem, then simply activate the exit button to stop running the program.

3.5 Initial System Test and Characterisation

Before the bacteria experiments commenced, the electronic nose system was left in a standby condition for several days to stabilise it in its new environment. This helped to reduce start-up drift. During the initial test stage, air leaks, diaphragm pump condition, solenoid valve and temperature of sensor chambers were checked by the LabVIEW system program. The plot in Figure 3.23 shows an example of output results from six gas sensor arrays, the temperature sensor and humidity sensor according to the elapsed time.

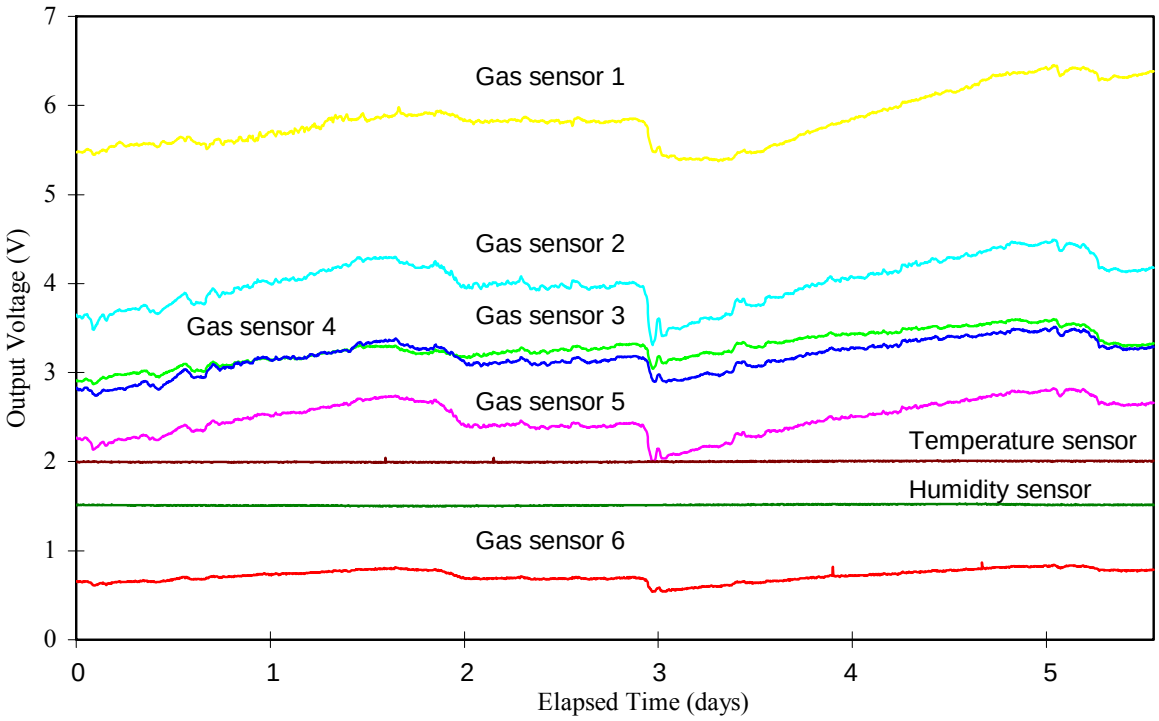

Fig. 3.23 Plot of gas sensor outputs, temperature sensor output and humidity sensor output according to the elapsed time (days). All outputs were expressed by an arbitrary voltage (V).

The temperature control program was run, with a target temperature within the sensor chamber of 45 °C. This allowed the gas sensor array to be in a stable condition before the experiment began. The output of the temperature sensor and relative humidity sensor were very stable, but the output from the gas sensors showed relatively long-term signal drift because of spurious odours in the laboratory. This was an undesirable occurrence because it introduced unwanted variance into subsequent data. It does reflect more closely the field situation but may be less than diurnal variation of growth rates. The temperature fluctuation of main chamber was around ±0.1 °C during the test and it seemed to have negligible effect when performing the biological experiment. The temperature sensor ouputs a linear voltage

of 10 mV per °C and was interfaced with a simple circuit consisting of a simple op-amp based amplifier with an adjustable offset as shown in equation (3.2).

$$Ts = a\,(V_T + V_o) \qquad (3.2)$$

V_T : voltage ouput of temperature sensor Ts : temperature of sensor (°C)

a: coefficient (= 20.1 °C/V) V_o : voltage offset

3.6 Initial Experiments with Chemical Samples

Before the experiment using real cyanobacteria cultures began, validation experiments with standard chemical samples were performed in the Biological Sciences Department. All data were taken from each sensor every second but it was also possible to control sampling rate using a cycle division function in the LabVIEW operating program. Each test was based on 4 elements, reference sample-target sample 1-reference sample-target sample 2, which are tested during several cycles, where one cycle was programmed to be 40 min in length. Figure 3.24 shows the responses from standard chemicals, glycerol, citral and β-cyclocitral.

This validation experiment was for the discrimination between standard chemicals and the results are described in chapter 4. The main reason for using these standard chemicals was that they are readily available c like the medium sample in cyanobateria cultures. The system bling the headspace of three identical vessels containing glycerol, c itral. The headspace was sampled by the modified Warwick Fox 2,000 with a set of six commercial metal oxide sensors, a temperature sensor and a humidity sensor as explained in the previous section. One cycle was programmed to be 40 min as follows.

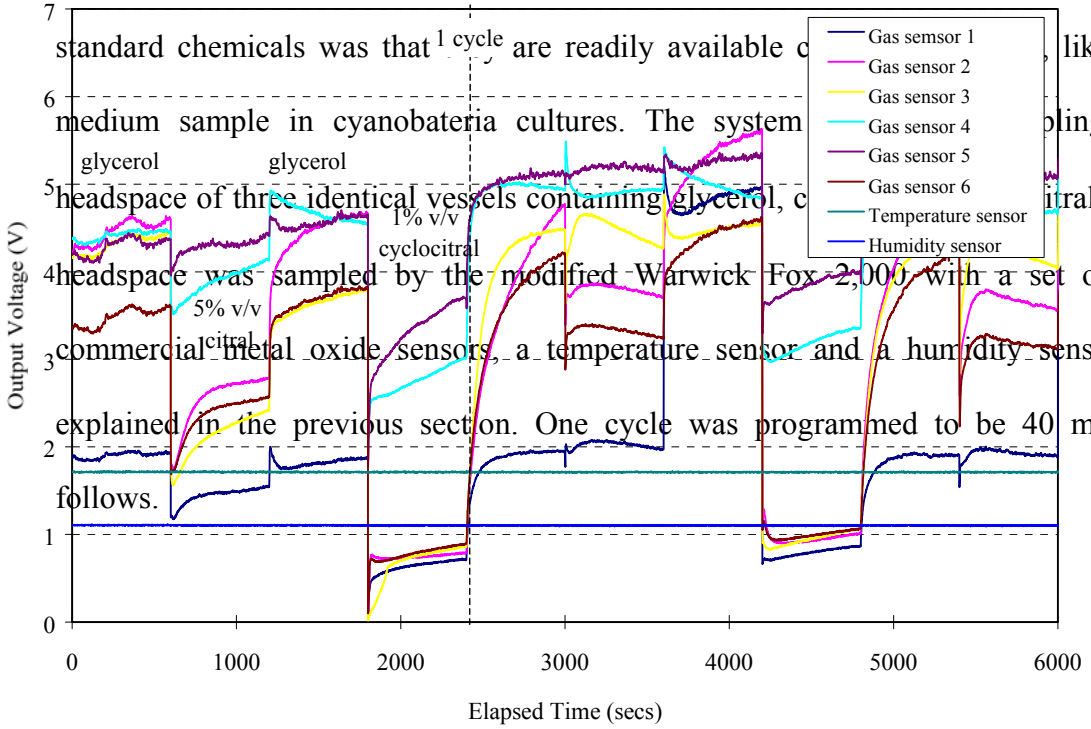

Fig. 3.24 Plot of the responses from standard chemicals, glycerol, citral, glycerol and β-cyclocitral with cycles.

One cycle (40 min) = glycerol (10 min)
5% v/v citral solution in glycerol (10 min)
glycerol (10 min)
1% v/v β-cyclocitral solution in glycerol (10 min)

Another series of experiments was carried out to discriminate the nature of two similar chemical standard samples, 1% v/v gerianol solution in glycerol and 1% v/v nerol solution in glycerol (Figure 3.25).

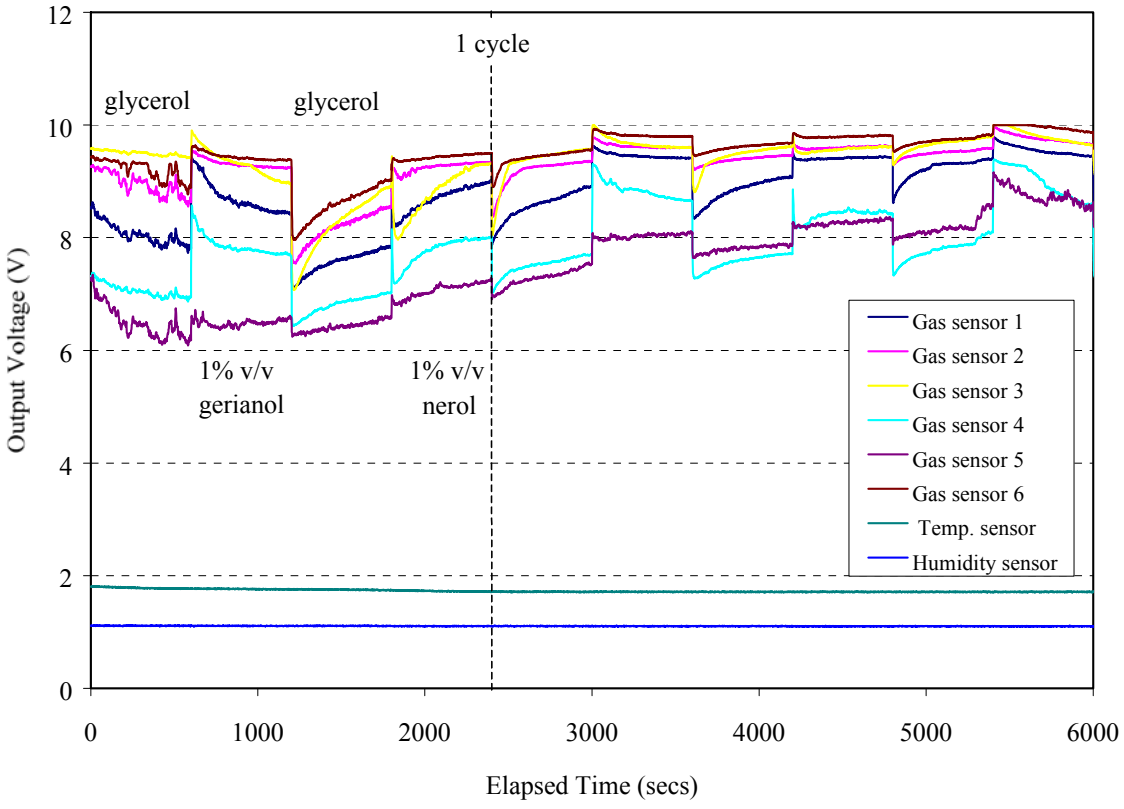

Fig. 3.25 Plot of the responses from standard chemicals, glycerol, gerianol, glycerol and nerol with cycles.

One cycle (40 min) = glycerol (10 min)
1% v/v gerianol solution in glycerol (10 min)
glycerol (10 min)
1% v/v nerol solution in glycerol (10 min)

Analysing the two plots, Figure 3.24 and Figure 3.25, shows that the variance in the signals between the gas sensors was significant. The temperature fluctuation of the main chamber was around ±0.1 °C during the test. The output of the humidity sensor was affected by the ambient temperature, and thus was not as significant a source of noise as temperature. There was significant fluctuation of reference sample, glycerol, through two previous experiments. The output voltages in Figure 3.24 are lower than those in Figure 3.25, even using the same reference chemical, glycerol. Therefore a base-line correction would be required for the discrimination processing. Hence the activity difference between the reference and the standard chemical can be used to make a base-line correction. PCA analysis of the standard chemicals is summarised in section 4.1.1.

3.7 Conclusion

A measurement system has been developed for the testing of cyanobacteria in water and consists of three main stages: the odour sampling system, an electronic nose and a Cellfacts instrument that analyses liquid samples. The software was structured with a main Virtual Instrument (VI) capable of calling and dismissing the sub VIs. During the initial test stage, air leaks, pump condition, solenoid valve and temperature control were checked with the LabVIEW system program. The

temperature fluctuation of the main chamber was around ±0.1 °C during the test and it seemed satisfactory for performing the biological experiment.

Several sensing materials based on MOS (metal oxide semiconductor) and conducting polymer have been focused on for use in an application of the electronic nose. Thick film tin oxide sensors (Alpha MOS), SRL125/MOS thin film sensor, micromachined IDC device, and CP sensors were explored for the application of water samples. Two prototype silicon devices, SRL 125/MOS and IDC 10 sensors, were characterised and tested for the detection of CO. Each device showed low-power consumptions, 75 mW and 60 mW at 300 °C, respectively.

Finally a set of data gathering experiments was performed on standard chemicals before the cyanobacteria experiments commenced. Experimental methods for data collection were developed under the LabVIEW environment. The variance in the signals from six thick film sensors were significant and required some pre-processing such as a base-line correction for the classification of samples.

References

1. N. Yamazoe, and N. Miura, Environmental gas sensing, Sensors and Actuators B, 20 (1994) 95-102.
2. W. W. Carmichael, The toxins of Cynanobacteria, Scientific American, January (1994) 64-72.
3. W. W. Carmichael, Cyanobacteria secondary metabolites-the cyanotoxins, Journal of Applied Bacteriology, 72 (1992) 445-459.
4. G. A. Codd, and S. G. Bell, The occurrence and fate of blue-green algal toxins in freshwater, University of Dundee, R&D report 29 (1996).

5. R. W. Castenholz, Culturing methods for cyanobateria, Methods in Enzymology, Academic, 167 (1988) 68-92.
6. M. Craven, Bacteria Classification with an electronic nose employing artificial neural networks, PhD thesis, University of Warwick, UK (1997).
7. P. T. Moseley, and B. C. Tofield, Solid State Gas Sensors, Adam Hilger, Bristol and Philadelphia, (1987).
8. K. Ihokura, and J. Watson, The stannic oxide gas sensor: principles and applications, CRC Press, Inc., (1994).
9. S. R. Morrison, Semiconductor gas sensors, Sensor and Actuators, 2 (1982) 329-341.
10. G. Heiland, Homogeneous semiconducting gas sensors, Sensors and Actuators, 2 (1982) 343-361.
11. S. R. Morrison, Selectivity in semiconductor gas sensor, Sensors and Actuators, 12 (1987) 425-440.
12. A. C. Pike, Design of chemoresistive silicon sensors for application in gas monitoring, PhD thesis, University of Warwick, UK (1996).
13. H. W. Shin, Design of microcalorimeter gas sensor, MRes thesis, University of Warwick, UK (1996).
14. H. W. Shin, C. Lloyd, and J. W. Gardner, Combined resistive and calorimetric sensing of gases using a single micromachined device, Transducers '97, Chicago, 16-19 June (1997) 935-938.
15. J. W. Gardner, and P. N. Bartlett, Microsensor deposition device, British Patent Application No. 9400855.4.

16. P. N. Bartlett, and J. W. Gardner, Odour sensors for an electronic nose, In sensors and Sensory Systems for an Electronic Nose, J. W. Gardner, and P. N. Bartlett, (eds.), Kluwer Academic Publishers, Dordrecht, (1992).
17. G. Wegner, and J. Ruhe, The structure background of charge-carrier motion in conducting polymers, Faraday Discuss, Chem. Soc., 88 (1989) 1-17.
18. P. N. Bartlett, and S. K. Ling-Chung, Conducting polymer gas sensor part II: Response of polypyrrol to methanol vapour, Sensors and Actuators, 19 (1989) 141-150.

Chapter 4

Data Processing and Classification

The objectives of this chapter are to describe the results from data processing and classification using a MATLAB toolbox and the NeuralWorks Professional II/Plus (NeuralWare Inc., USA) software. MATLAB is an interactive mathematical analysis program to help with scientific and engineering problems. Its basic data element is a matrix. NeuralWorks is a complete and comprehensive multi-paradigm prototyping and development system. It can be applied to design, build, train, test and deploy neural networks to solve complex, real-world problems.

Various pre-processing and pattern recognition techniques have been used in the field of electronic nose systems (Chapter 2). Here, principal components analysis (PCA) was chosen to explore models using difference, fractional difference and normalisation algorithms, for the classification of standard chemicals and cyanobacteria by neural networks. Also nonlinear PARC techniques called Artificial Neural Networks (ANNs) have been applied for feature classification. Three supervised classifiers, MLP, LVQ and the Fuzzy ARTMAP were applied to the cyanobacteria data.

4.1 Principal Components Analysis (PCA)

PCA is a useful classical pattern recognition technique showing clearly the visualisation of data-sets on a dimensionless PCA plot. In PCA, a set of linearly correlated variables ($X_1, X_2,..., X_p$) is transformed into a set of uncorrelated variables (principal components, $Z_1, Z_2,..., Z_p$) whereby the first few components explain most of the variance in the data-set. If a principal components analysis starts with data on *p* variables for *n* individuals, as indicated in equation (2.1), then the *i*th principal component is,

$$Z_i = a_{i1}X_1 + a_{i2}X_2 + ... + a_{ip}X_p \tag{4.1}$$

The variances of the principal components are the eigenvalues ($\lambda_1 \geq \lambda_2 \geq ... \geq \lambda_p \geq 0$) of the covariance matrix. Var(Z_i) = λ_i and the constants $a_{i1}, a_{i2},..., a_{ip}$ [1] are the elements of the corresponding eigenvector, scaled so that:

$$a_{i1}^2 + a_{i2}^2 + ... + a_{ip}^2 = 1 \tag{4.2}$$

The data-set is autoscaled to avoid one or more variable having an undue influence on the PCA result, then it sets the means of variables to zero and variances to one. The first principal component Z_1 has a set of coefficients that maximises the variance which is as large as possible given the constraint ($a_{11}^2 + a_{12}^2 + ... + a_{1p}^2 = 1$) on the constants a_{1j}. The second principal component Z_2 is such that the variance is as

[1] The constants are called the loadings which determine the correlations and prevalence of data.

large as possible subject to the constraint ($a_{21}^2 + a_{22}^2 + ... + a_{2p}^2 = 1$). Therefore PCA produces *p* PCs which are uncorrelated. The PCs are plots on two dimensional PCA coordinates which represent a proportion of the variance within the data-set. With a correlated set of odour sensors, it is not uncommon to observe over 90% of the variance in the first two components.

4.1.1 PCA Analysis of the Standard Chemicals

PCA, one of the widely used classical statistical methods, was employed for the classification of the standard chemicals analysed, i.e. glycerol, 5% v/v citral solution in glycerol, 1% v/v β-cyclocitral solution in glycerol, 1% v/v gerianol solution in glycerol and 1% v/v nerol solution in glycerol. Before PCA can be applied, preprocessing, as described in Chapter 2, was carried out in order to improve the classification process. In this case, the difference model, fractional difference model, and normalisation were employed. Each test was based on 4 stages (reference sample, target sample 1, reference sample, target sample 2) which are tested during several cycles where one cycle was programmed to be 40 min in length. In order to reduce the number of values, average values per cycle and per stage were created using a MATLAB program. Data from each experiment were combined to form one large feature-set on which PCA was applied. Sensor chamber temperature, humidity and gas flow-rate were not considered in the PCA because these parameters were practically constant over each experiment.

The PCA, of the difference signal algorithm and the fractional difference algorithm (Chapter 2), were applied to the data-set, after normalisation was used to remove experimental error in the odour concentrations. Figure 4.1 shows the results of a PCA on the first two ranked PCs, on five chemical samples based on glycerol, taken from the electronic nose.

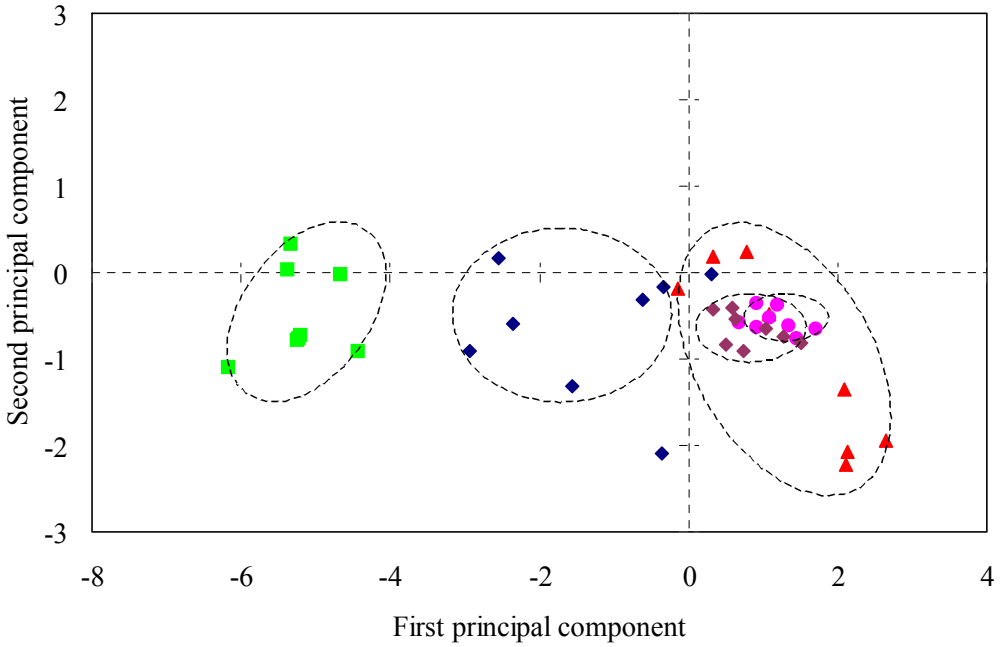

Fig. 4.1 PCA plot of the difference model on a data-set of standard chemicals, υ: 5% v/v citral solution in glycerol, σ: glycerol, ν:1% v/v β-cyclocitral solution in glycerol, λ: 1% v/v gerianol solution in glycerol, υ: 1% v/v nerol solution in glycerol. (For six-element metal oxide nose)

Different captions indicate each chemical class. In this PCA plot several clusterings can be observed and there is overlap between 1% v/v β-cyclocitral solution in glycerol, 1% v/v nerol solution in glycerol and pure glycerol. The sensor parameter was the voltage difference (voltage of reference sample – voltage of target sample) of sensor responses. Figure 4.2 also shows a PCA plot of an auto-scaled

difference model for the same chemical samples. In auto-scaling the set of scaled feature vectors is calculated such that the vector components have a mean value of zero and unity variance. The first two PCs showed 93.64% of the total variance of the feature-set. Again, in this PCA plot several clustering and overlap zones can be observed. Generally, it is expected that feature-sets exhibiting less overlap would give good classification performances.

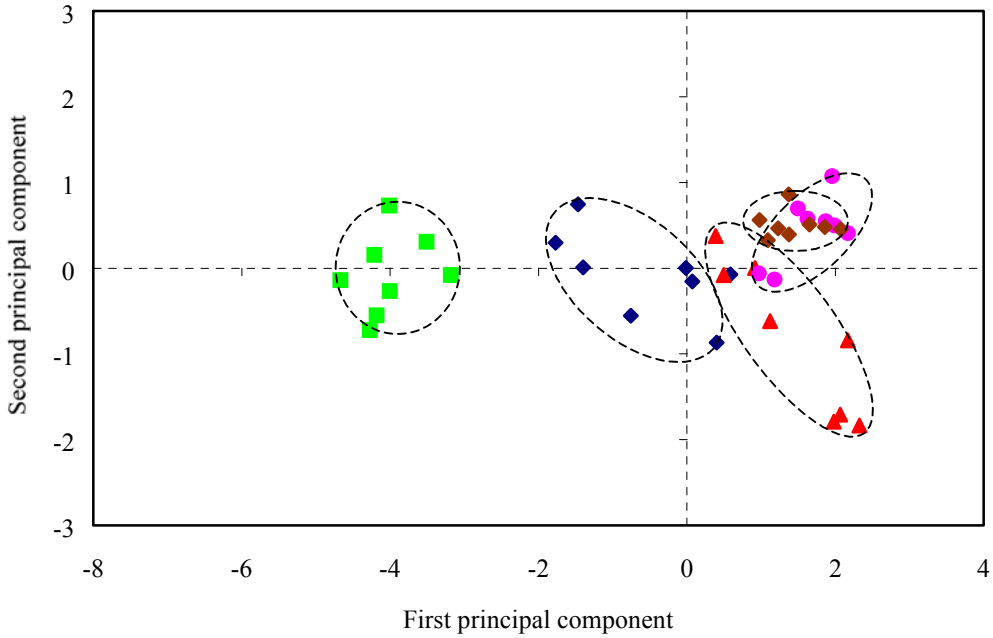

Fig. 4.2 PCA plot of the auto-scaled difference model on a data-set of standard chemicals, υ: 5% v/v citral solution in glycerol, σ: glycerol, ν: 1% v/v β-cyclocitral solution in glycerol, λ: 1% v/v gerianol solution in glycerol, υ: 1% v/v nerol solution in glycerol. (For six-element metal oxide nose)

Normalisation of the data-sets has also been used to improve the classification performance. The normalisation preprocessing algorithm used for each sensor *i* is,

$$x_i^{norm} = \frac{x_i - x_{\min}}{x_{\max} - x_{\min}}$$

(4.3)

where the normalised array parameter x_i^{norm} lies in the range of [0, +1]. It gives equal weighting to each sensor and thus compensates for differences in the magnitudes of the signals. Table 4.1 shows the eigenvalues, the variances of the principal components, and % of the total variances for a normalised difference model. The eigenvectors, the coefficients of the principal components, are important indices because values close to zero show unimportant variables and similar non-zero values indicate strong collinearity. The first principal component is

$$Z_1 = 0.3309X_1 + 0.4067X_2 + 0.4900X_3 + 0.4088X_4 + 0.4076X_5 + 0.3896X_6 \qquad (4.4)$$

where X_1 to X_6 are standardised variables (n = 6). The eigenvalue for a principal component indicates the variance that it accounts for out of the total variances. Thus the first principal component accounts for 97.6%, the second for 1.14% which shows that the first component is far more important than the others.

Table 4.1 The eigenvalues and eigenvectors of the correlation matrix for the application of PCA to the normalised difference model of standard chemicals by ranking the PCs in order of the % of total variance.

			Eigenvector, coefficient of the principal components					
PC No.	Eigenvalue	% Tot. Var	X_1	X_2	X_3	X_4	X_5	X_6
1	2.5814	97.6000	0.3309	0.4067	0.4900	0.4088	0.4076	0.3896
2	0.0303	98.7444	-0.6903	-0.1339	-0.2027	0.5322	0.4251	-0.0221
3	0.0144	99.2886	0.0287	-0.3853	0.6074	-0.1088	0.3197	-0.6064
4	0.0115	99.7233	0.5601	-0.1991	-0.5732	0.0154	0.5472	-0.1354

5	0.0052	99.9211	0.3084	-0.1738	-0.0255	0.7332	-0.4993	-0.2954
6	0.0021	100.0000	-0.0657	0.7736	-0.1435	-0.0083	0.0472	-0.61

Figure 4.3 shows the PCA plot of a normalised difference model. The classification performance was slightly improved through the use of a normalisation technique, this reduced the overlap between 1% v/v β-cyclocitral solution in glycerol and 1% v/v nerol solution in glycerol. This was an encouraging result.

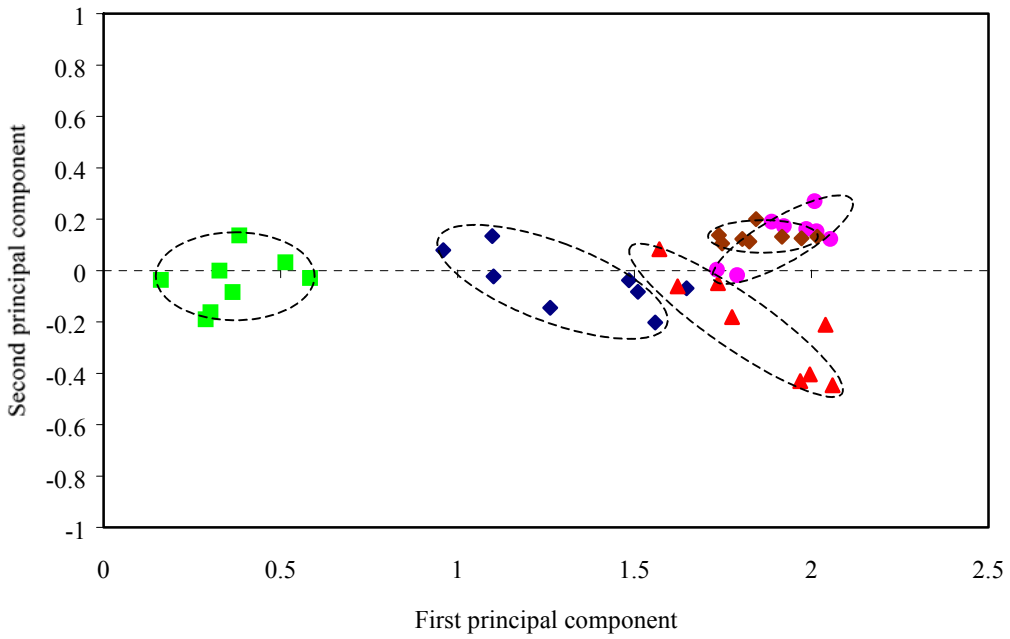

Fig. 4.3 PCA plot of the normalised difference model on a data-set of standard chemicals, υ: 5% v/v citral solution in glycerol, σ: glycerol, ν: 1% v/v β-cyclocitral solution in glycerol, λ: 1% v/v gerianol solution in glycerol, υ: 1% v/v nerol solution in glycerol. (For six-element metal oxide nose)

The performance of the fractional difference model was also evaluated when applied to the classification of five standard chemicals. The values of fractional difference are often called the "sensitivities" and widely used as indices of gas responses. The fractional difference algorithm for each sensor *i* is,

$$x_i^{fra.diff} = \frac{x_i - x_{ref}}{x_{ref}} \quad (4.5)$$

where x_{ref} is sensor signal output from a reference sample such as room air.

Table 4.2 and figure 4.4 represent the PCA result of the normalised fractional difference model, which shows an unclear boundary between β-cyclocitral and nerol.

Table 4.2 The eigenvalues and eigenvectors of the correlation matrix for the application of PCA to the normalised fractional difference model of standard chemicals by ranking the PCs in order of the % of total variance.

			Eigenvector, coefficient of the principal components					
PC No.	Eigenvalue	% Tot. Var	X_1	X_2	X_3	X_4	X_5	X_6
1	2.6467	97.8224	0.2232	0.3721	0.4770	0.4460	0.4444	0.4333
2	0.0370	99.1916	-0.8311	-0.1679	-0.0710	0.3756	0.3539	-0.0990
3	0.0095	99.5437	0.4014	-0.2993	-0.3059	-0.0872	0.7501	-0.2924
4	0.0082	99.8463	-0.0116	-0.3790	0.8139	-0.1575	0.0084	-0.4110
5	0.0034	99.9724	0.3106	-0.2457	-0.1068	0.7922	-0.3343	-0.3041
6	0.0007	100.0000	-0.0415	0.7347	0.0017	0.0080	0.0539	-0.6749

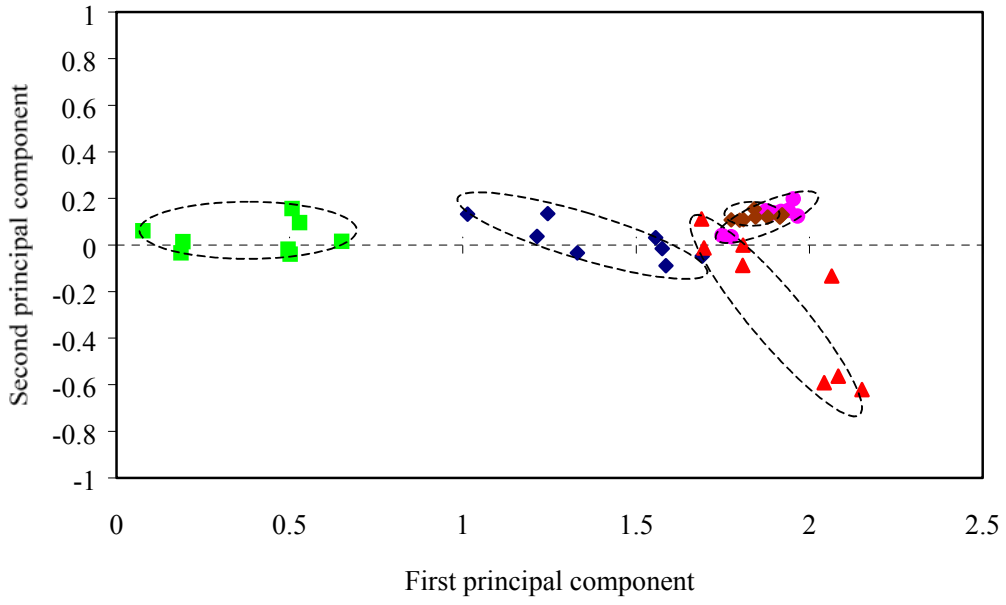

Fig. 4.4 PCA plot of the normalised fractional difference model on a data-set of standard chemicals, υ: 5% v/v citral solution in glycerol, σ: glycerol, ν: 1% v/v β-

cyclocitral solution in glycerol, λ: 1% v/v gerianol solution in glycerol, υ: 1% v/v nerol solution in glycerol. (For six-element metal oxide nose)

The first principal component accounts for 97.8%, the second for 1.8%. PCA is a linear technique and so there is no difference between the choice of a relative or fractional difference but these models are better than the difference model because they compensate for the variation of sensor responses caused by change in room air quality and temperature.

4.1.2 PCA analysis of the cyanobacteria strain

Each measurement cycle was based on four elements (medium sample - toxic cyanobacteria – medium - non-toxic cyanobacteria) as described in Chapter 3.4.1. Similar to the preprocessing of the standard chemicals, the average values per cycle and per element were created to reduce the number of data points (480 per cycle) over 400 cycles. Figure 4.5 shows the sensor responses from the initial stage of cyanobacteria samples.

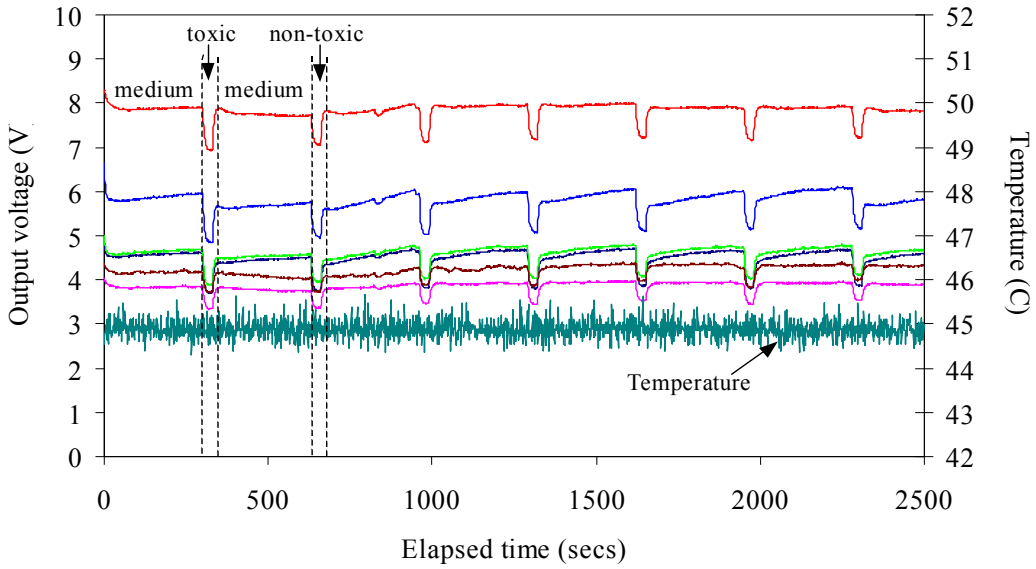

Figure 4.5 Plot of the response from BG-11 medium, toxic cyanobacteria, BG-11 medium and non-toxic cyanobacteria with cycles.

Under natural conditions, the life span of cyanobacteria is about 30 days, though these initial test were for 2 days. This was expected to give a general classification idea about the whole series of experiment. Reliable sampling is very important over the whole experimental period. Figure 4.6 shows the results of sampling test from three identical medium vessels (a) before and (b) after inoculation.

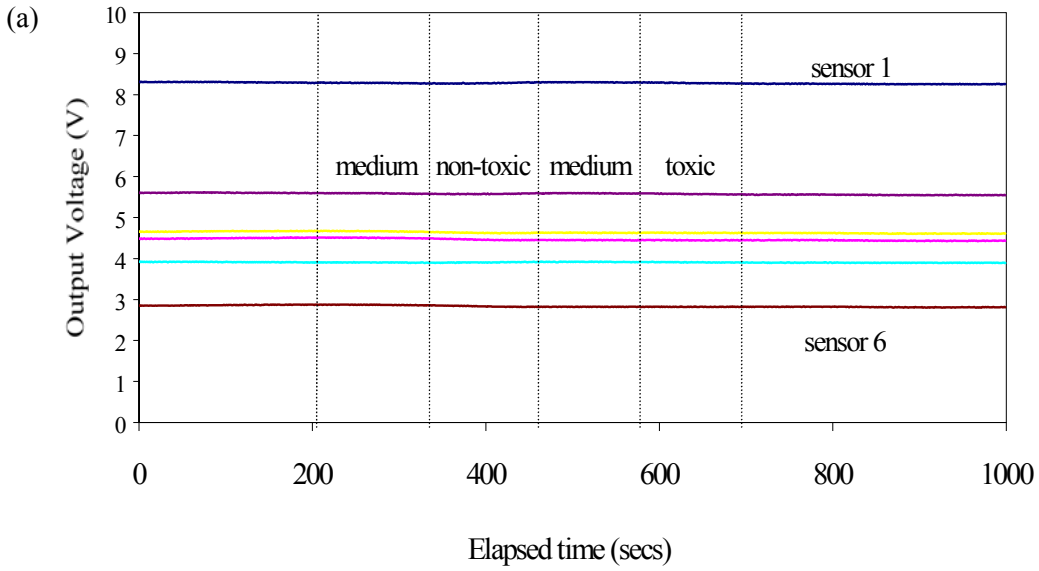

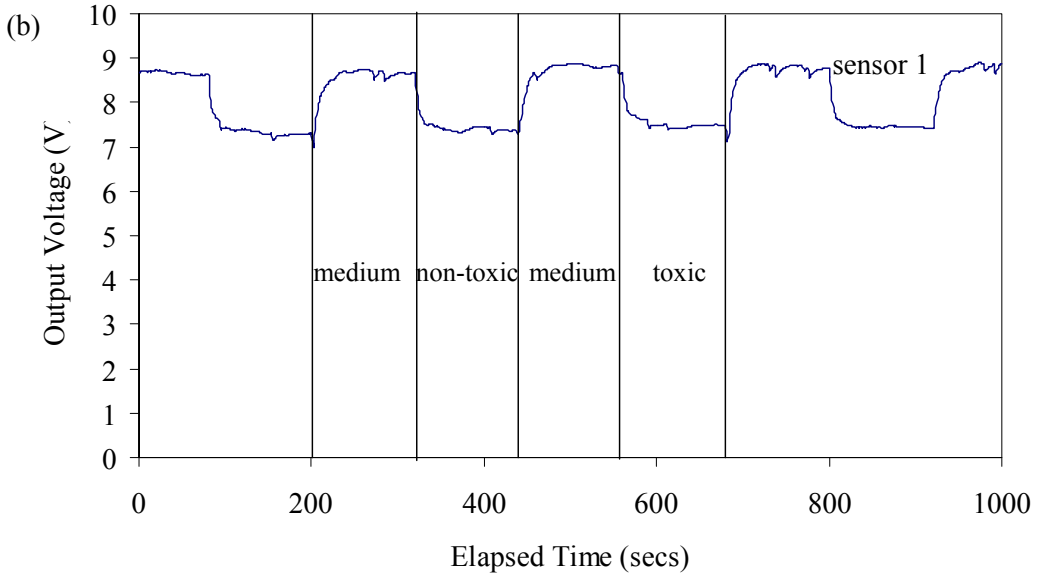

Figure 4.6 Plots of the response from medium, non-toxic cyanobacteria, medium and toxic cyanobacteria with cycles: (a) before and (b) after inoculation.

Sensor responses showed some variation with the room temperature and perhaps air humidity as shown in Figure 4.7. Temperature and humidity of the sensor chamber showed nearly constant values for every experiment, thus these values can be excluded from the data for the classification process as for the previous standard chemical experiment.

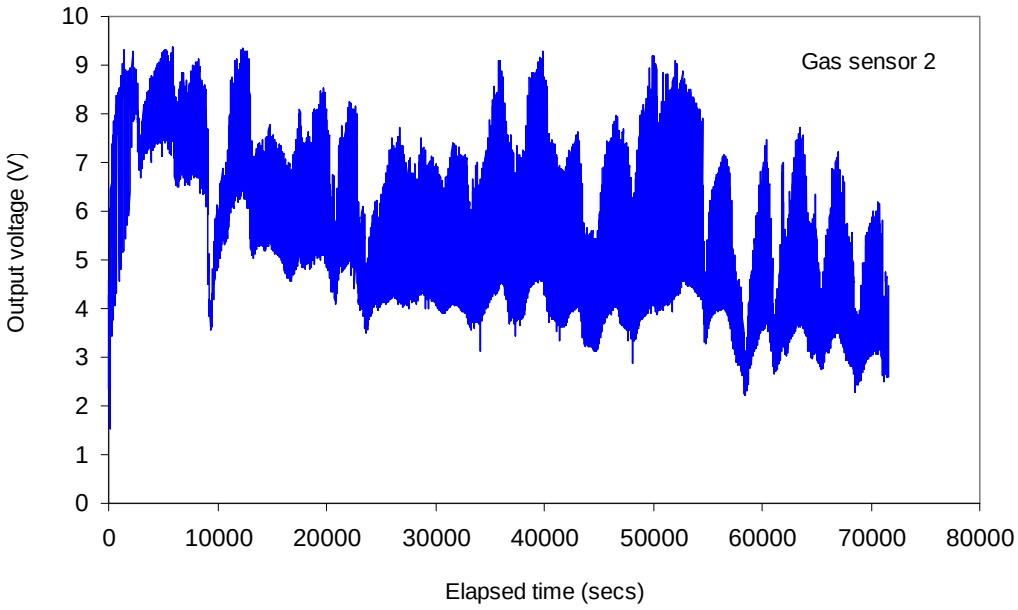

Figure 4.7 Sensor responses with significant fluctuation from medium, toxic cyanobacteria, medium and non-toxic cyanobacteria with cycles. Only the output from gas sensor 2 was used to draw this plot for the sake of clarity.

Before the PCA analysis, the correlation between gas sensors was calculated and plotted as shown in Figure 4.8, to show the sensor interdependencies about the cyanobacteria sample. If sensors are highly correlated, then the static responses from the correlated sensors can be omitted at the analysis stage. In Figure 4.8, there was correlation between sensor 2 and 6 but this was not significant. Therefore all six

sensors were used to characterise the cyanobacteria samples in water. Figure 4.9 is the first result of PCA analysis on the cyanobacteria samples.

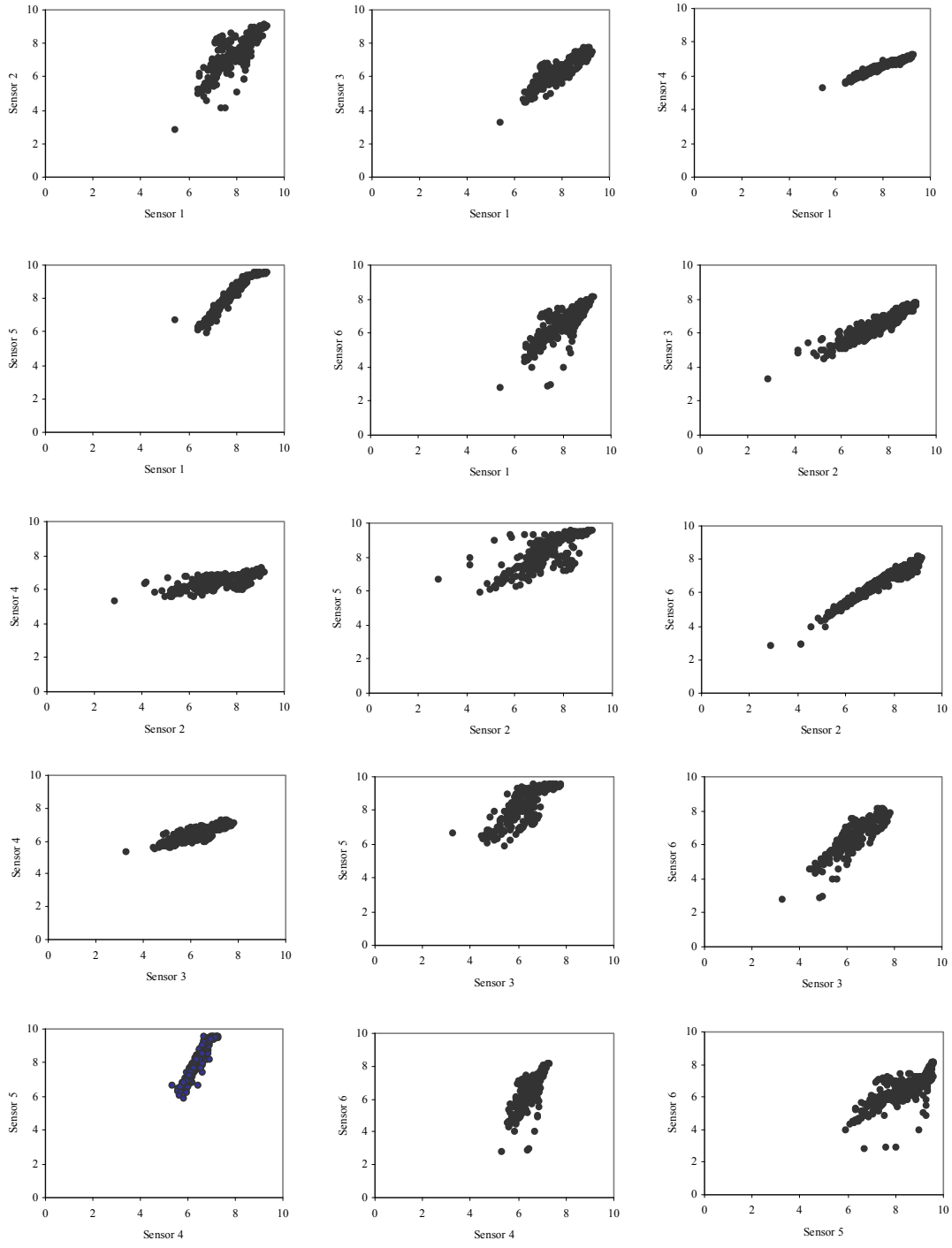

Fig. 4.8 Plots showing interdependencies of the six gas sensor array. They indicate that sensors 2 and 6 have relatively high co-linearity but might still need six gas sensor array for the characterisation of cyanobacteria samples in water.

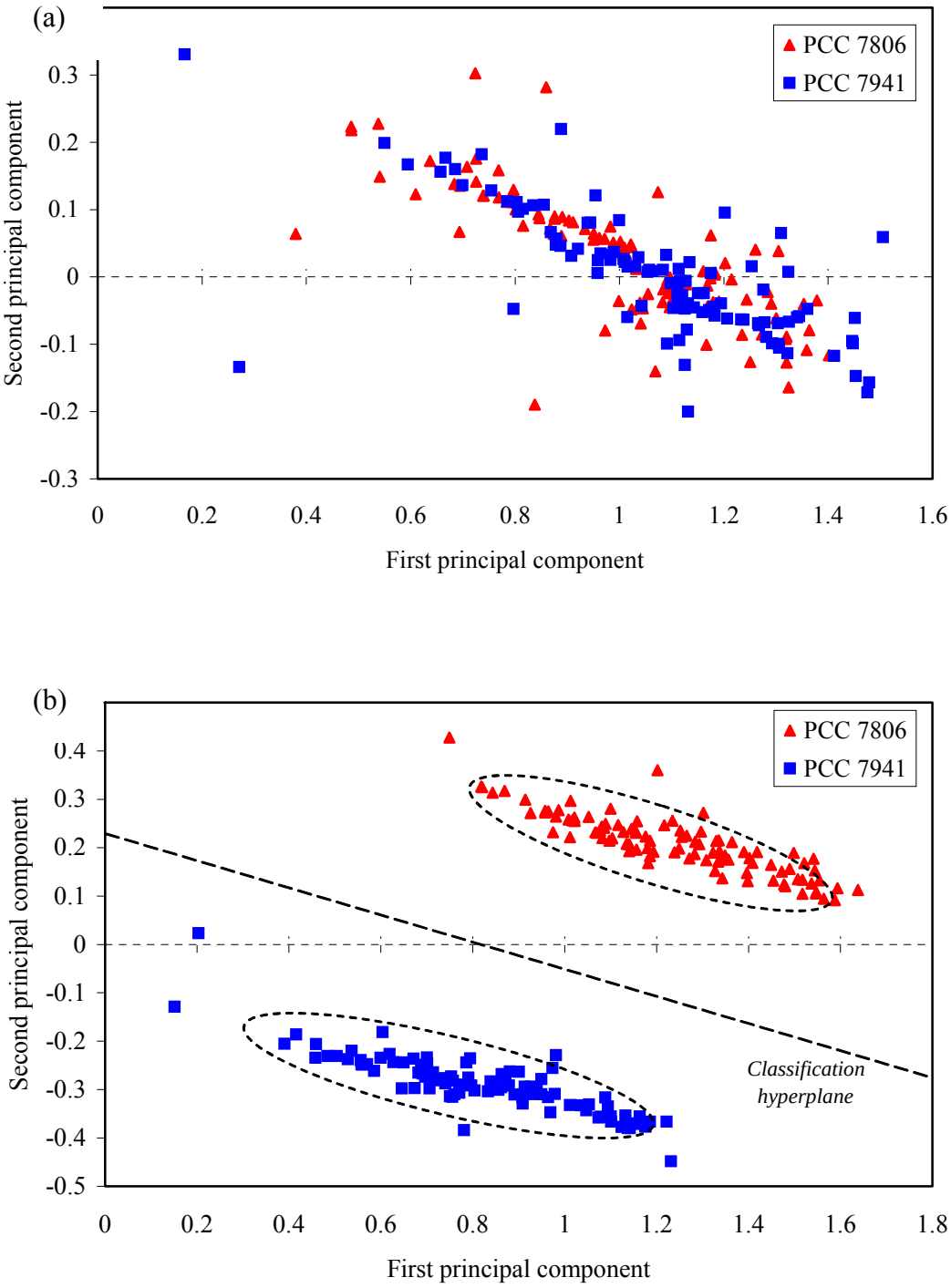

Fig. 4.9 Results of PCA on cyanobacteria samples, PCC 7806 (toxic) and PCC 7941 (non-toxic). The original data are transformed by the normalised difference model (a) and the normalised fractional difference model (b), which produced two distinct clusters of the toxic and non-toxic cyanobacteria.

The feature-set employed used the normalised difference model and the normalised fractional difference model which showed good results in the classification of the standard chemicals (Chapter 4.1.1). Similar to the former experiments, two PCAs of the normalised processing algorithms were performed to discriminate cyanobacteria types such as PCC 7806 (toxic) and PCC 7941 (non-toxic). Figure 4.9 shows PCA plots of the first 2 ranked PCs. The target classes are indicated by different captions. Figure 4.9 (a) shows that PCA was unable to separate out the two cyanobacteria types. This was dramatically improved through the use of a normalised fractional difference algorithm, which was able to produce two distinct clusters of the toxic and non-toxic cyanobacteria (Figure 4.9 (b)). The stretched clusters indicate that sensor drift occurred over time and was mainly in the

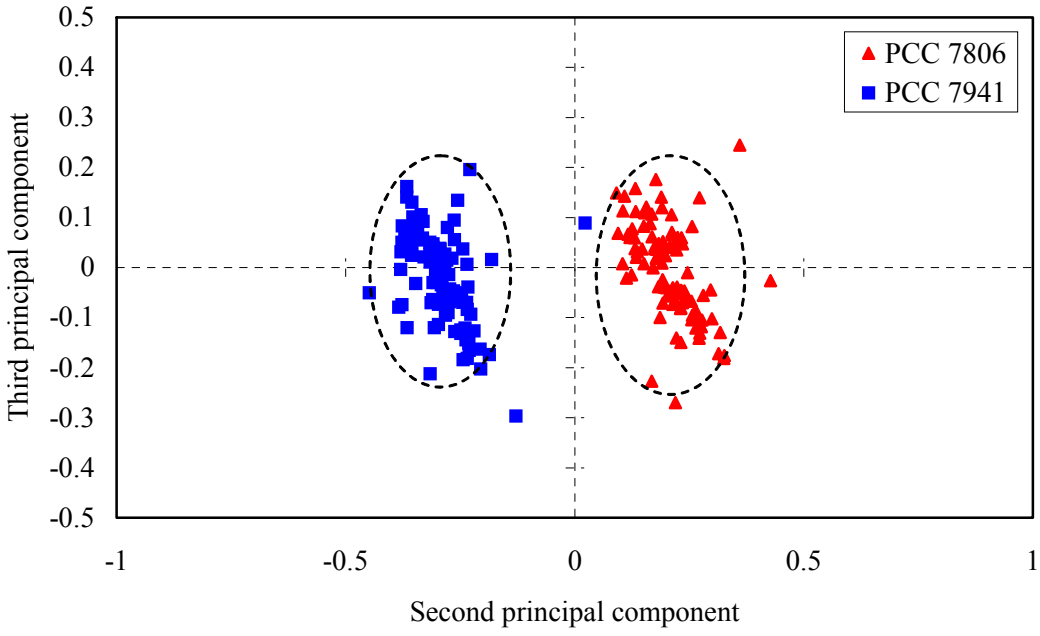

Fig. 4.10 Results of PCA plot of second and third principal components on cyanobacteria samples, PCC 7806 (toxic) and PCC 7941 (non-toxic). The original data are transformed by the normalised fractional difference model.

first component. Despite the sensor drift, the PCA of the normalised fractional difference algorithm exhibited good classification performance without any overlap between the two clusters. Figure 4.10 shows the PCA plot of second and third principal components of figure 4.9 (b), which displays two distinct groups of cyanobacteria without sensor drift. Also PCA will be used to classify cyanobacteria growth phase at the next stage of the experiment.

4.2 Artificial Neural Network

Artificial neural networks (ANNs) have been widely used in the application of electronic nose systems. This technique, applied here, especially MLP ANNs trained using back-propagation (BP) has been highlighted by many researchers in this field (see chapter 2). ANNs which mimic the architecture of the biological olfactory system do not require an explicit description of how the problem is to be solved. They learn from the data and normally configure themselves during a training period. Also, they can cope with highly nonlinear data and so, unlike PCA, can be made to cope with noisy or drifting sensor data.

4.2.1 Neurone model

Figure 4.11 shows a schematic diagram of a typical artificial neurone with R inputs. It provides a functional description of the various elements that constitutes the model of an artificial neurone. The neurone has a bias b, which is summed with the weighted inputs to form the net input n.

$$n = \sum_{i=1}^{R} w_{ki} x_i + b \qquad (4.6)$$

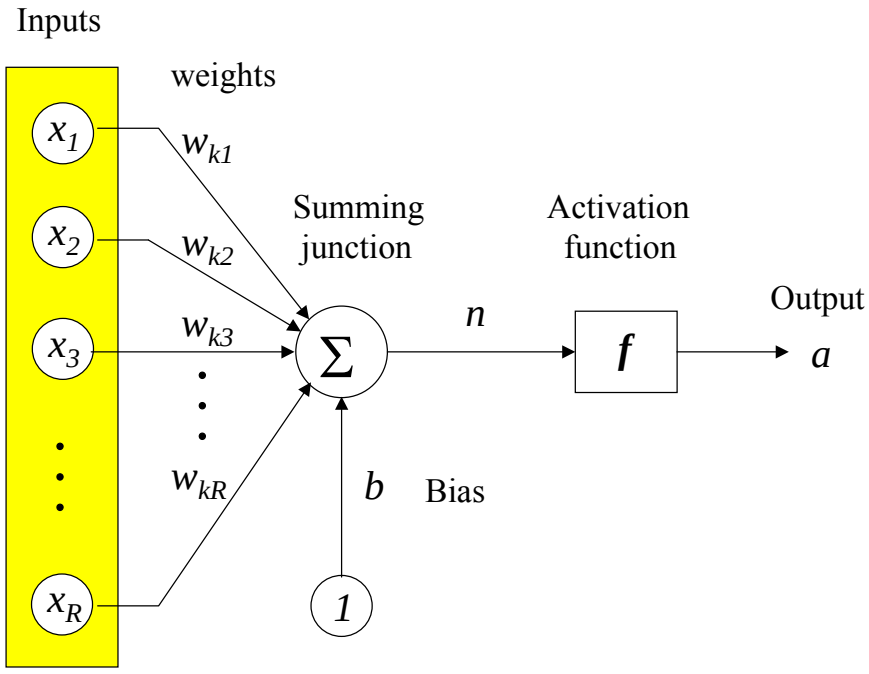

Fig. 4.11 Schematic diagram of multiple input neurone.

The neurone output can be written as

$$a = f(n) \tag{4.7}$$

Therefore the actual output depends on the particular transfer function f that is chosen. Each input has an associated adjustable coefficient called a weight w, which gives the strength of each input connected to the neurone. The bias b is much like a weight, except that it has a constant input, such as 1. The bias gives the network an extra variable, and so the network with biases would be more powerful than those without. It has the effect of lowering the net input of the transfer function[1], though the bias can be omitted in a particular neurone.

A particular transfer function is chosen to satisfy some specification of the problem that the neurone is attempting to solve. It may be a linear or a nonlinear function of the net input *n*. Different transfer functions can be used for different purposes [2]. For example, the log-sigmoid transfer function is commonly used in multilayer networks, when trained using the backpropagation algorithm. It sets the output into the range 0 to 1 and is defined as a strictly increasing function that exhibits smoothness and asymptotic properties. This can be defined by:

$$a = \frac{1}{1 + e^{-n}} \tag{4.8}$$

where *n* is the net input of the neurone. Hard limit, linear, hyperbolic tangent sigmoid and competitive transfer functions are also commonly used for particular problem. The hyperbolic tangent sigmoid function, which is similar to the log-sigmoid function, squashes the output into the range –1 to 1. The range of the output is important as it improves the training qualities of the neural network. The expression for the hyperbolic tangent sigmoid can be written as

$$a = \frac{e^{n} - e^{-n}}{e^{n} + e^{-n}} \tag{4.9}$$

[1]The bias is the negative of the threshold and the net input of the transfer function may be increased by employing a bias term rather than a threshold. The transfer function often referred to as the activation function.

A single neurone has a very limited capability, as a device for solving problems. Commonly processing elements can be combined to make a layer of node's and be interconnected. Therefore an artificial neural network is able to solve more

complicated problems, which require more intricate decision regions to group data. A single layer of neurones can be set to a different transfer function by combining neural networks in parallel.

4.2.2 Multiple layer perceptron (MLP)

Multilayer networks are more powerful than single-layer networks. The MLP network is one of the most popular neural network architectures and is suited to a wide range of applications. It consists of a set of sensory units that constitute the input layer, one, or more hidden layers, and an output layer as introduced in Chapter 2. Figure 4.12 shows one example of the fully connected three layer MLP network with 33 weights to train. For brevity the network of Figure 4.12 is referred to as a 6-4-1 network. Inputs and output were considered as layers which alternatively constitute the network architecture. All the outputs from the previous layer are input to the next layer. Each layer has its own weight, its own bias, a net input and output. By adding one or more hidden layers, the network is able to extract higher-order statistics, by virtue of the extra set of synaptic connections and the extra dimension of neural interactions. Having more than one hidden layer can cause local minima and make networks more complicated in practice.

There are many algorithms for training a neural network. One of the most powerful techniques is supervised training where for each input vector, the target output vector is known. In this process, changes in weights and biases are due to the

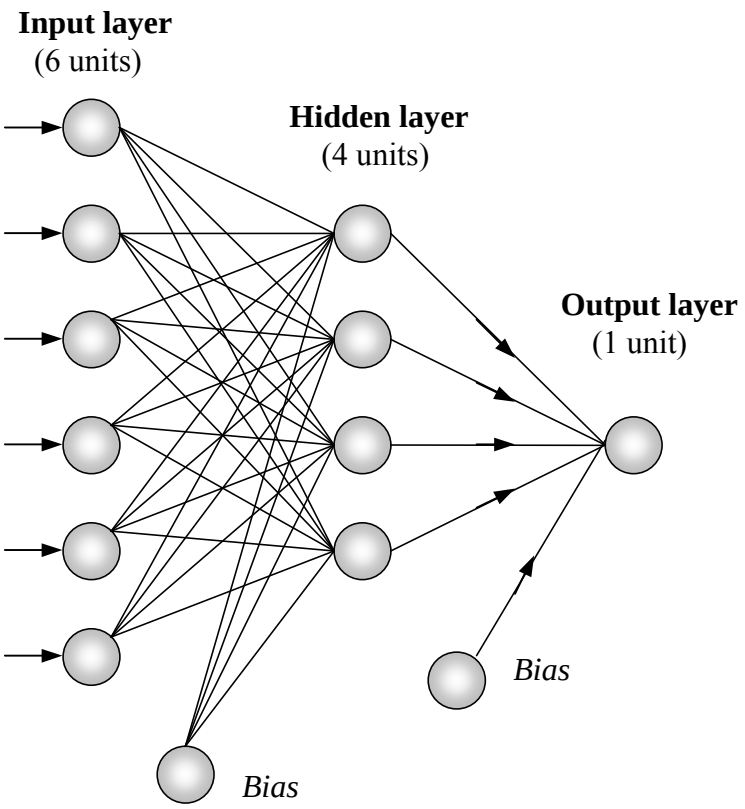

Fig. 4.12 Schematic diagram of fully connected three layer MLP network with 6 input, 4 hidden neurones and 1 output

intervention of any external assign which provides the output target. BP is a commonly used supervised training algorithm and MLPs are usually trained using BP. BP performs a gradient descent within the solution's vector space toward a global minimum along the steepest vector of the error space. The global minimum is that theoretical solution with the lowest possible error. In most problems, the solution space is quite irregular which may cause the network to settle down in a local minimum and not the best global solution. Figure 4.13 illustrates the possibility of converging to a local minimum in weight space. If a local minimum z_1 is reached, the error at the network outputs may still be unacceptably high. The BP algorithm employs a method of gradient descent, where the neural network is initialised and its

error can be visualised at a random coordinates on the error surface as shown in Figure 4.13. The error signal (δ_{pk}) at the output of *k*th at the *n*th training vector is defined by

$$\delta_{pk} = y_{pk} - o_{pk} \tag{4.10}$$

where y_{pk} is the target value and o_{pk} is the actual output from the *k*th output unit.

The sum of the squared errors for all output units can be written as:

$$E_p = \sum_{k=1}^{N} (y_{pk} - o_{pk})^2 = \sum_{k=1}^{N} \delta_{pk}^2 \tag{4.11}$$

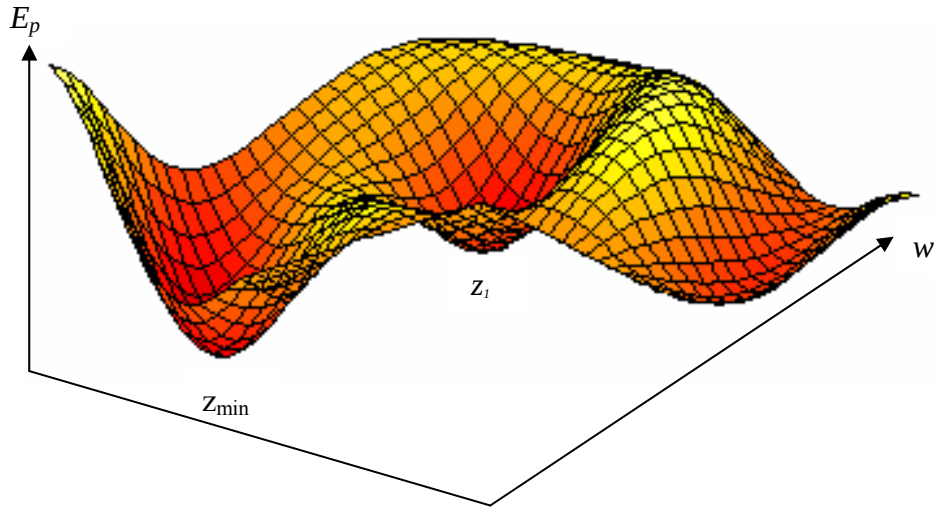

Fig. 4.13 Hypothetical surface in weight space. The point, z_{min}, is called the global minimum and the other minimum point, z_1, is called a local minimum.

The objective of BP training is to minimise the difference between the actual network output and the target output on the error space and find an appropriate set of

weights. The weights should be initialised to small, random values, often in the range of ±0.5. The gradient descent vector is calculated such that the steepest negative gradient of E_p is the path followed by the network error. Then the values of the weights are adjusted so as to reduce the total error. From the derivatives of Eq. (4.11) with respect to the weights, w_{kj}, the weights on the output layer are updated according to

$$w_{kj}(t+1) = w_{kj}(t) - \eta\Delta_p \tag{4.12}$$

where Δ_p is the gradient descent vector component for weight w_{kj} and the factor η is called the learning-rate parameter which determines the magnitude of the change in the weightings [3]. Also $w_{kj}(t)$ is the weight value between the hidden perceptron *k* and the output perceptron *j* at time *t.* The process is continually repeated for the number of iterations until the final error between the target values and actual values is acceptably low. The error that this process minimises is

$$E = \sum_{p=1}^{P} E_p \tag{4.13}$$

where *P* is the number of patterns in the training set.

4.3 The Classification of Cyanobacteria Strain

Three supervised classifiers (Chapter 2), MLP, LVQ and Fuzzy ARTMAP, were used to classify the cyanobacteria strain in water.

MLP ANNs were modelled using a software program, NeuralWorks Professional II/Plus [10], to classify cyanobacteria type. NeuralWorks Professional II/Plus software provides a comprehensive framework for rapidly implementing MLP neural networks, training methods, and flexibility of building new functions. Therefore it includes a comprehensive set of network architecture, learning rules, and training rules for the design of the network that best fits an application.

The training technique used is the back-propagation learning rule. The back-propagation command provides a dialog box with numerous choices that allow to construct thousands of variations of networks. Figure 4.14 shows the schematic representation of back propagation, especially its training phase. The training phase involves the adjustment of learning system parameters according to the learning rule adopted, until the error signal reduces to a predefined tolerance limit and the weights of the NN are trained to implement the desired classifier. The NN classifies the test samples using the static knowledge base, through the training output file created during the learning session. The architecture of the neural network used was a three-layer MLP network with 6 inputs, 4 units in the hidden layer and one output. The number of hidden units can be decided from a general rule of thumb, but the best way seems to be to vary the number of hidden processing elements (units) up or down to improve performance. There is no reliable method for estimating the optimum number of hidden units so far. The neural network was trained using an output data set from preprocessing, such as the difference model and fractional difference model. A hyperbolic tangent sigmoid function was used for the transfer function in the network because some input vector components had negative values. The target values were set to provide binary output, i.e. 1 for toxic bacteria and –1 for non-toxic bacteria.

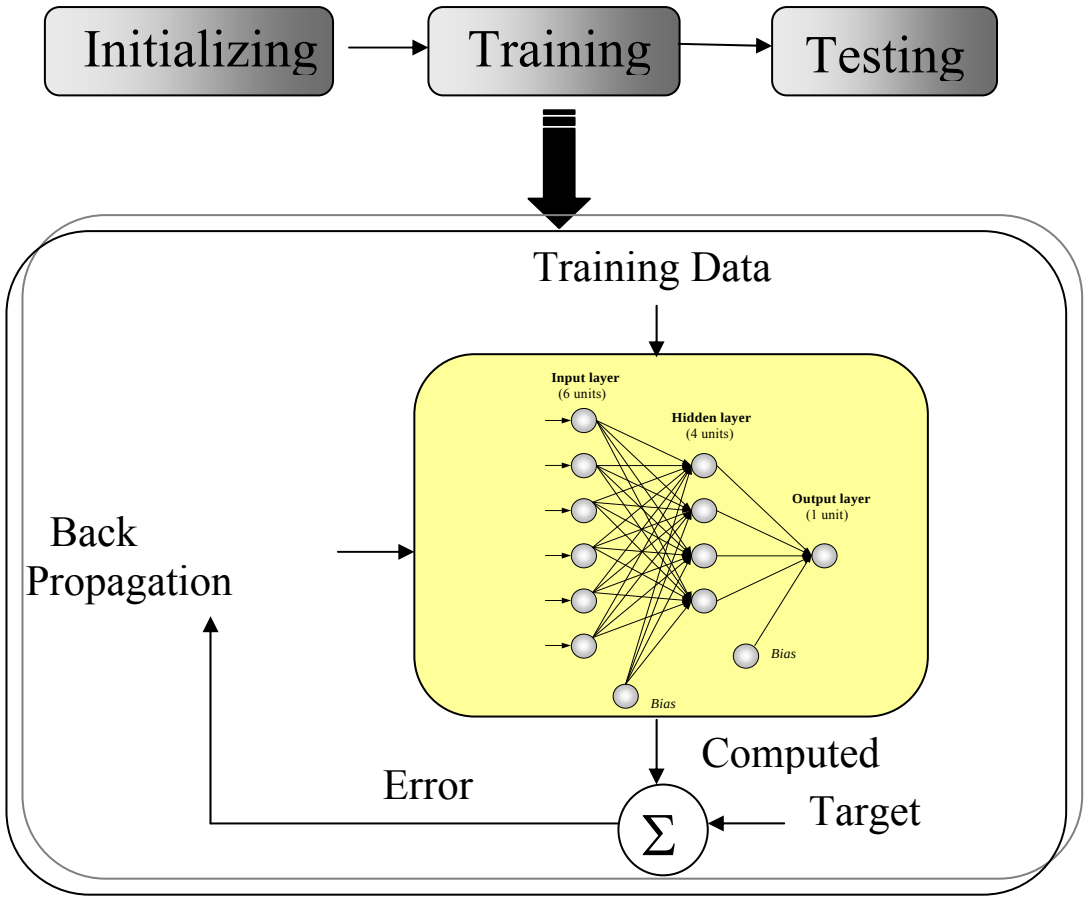

Fig. 4.14 Schematic representation of the back propagation system

The training sets were selected at random without replacement. The network training parameters were set throughout to values of learning rate $\eta = 0.3$ and the number of epochs was set to 16. An epoch is the number of sets of training data presented to the network (learning cycles) between weight updates. The best MLP set was found to classify correctly 97.1 % of the unknown non-toxic bacteria samples and 100 % of the unknown toxic bacteria samples on the basis of a set of 378 training vectors and 202 test vectors as shown in Figure 4.15.

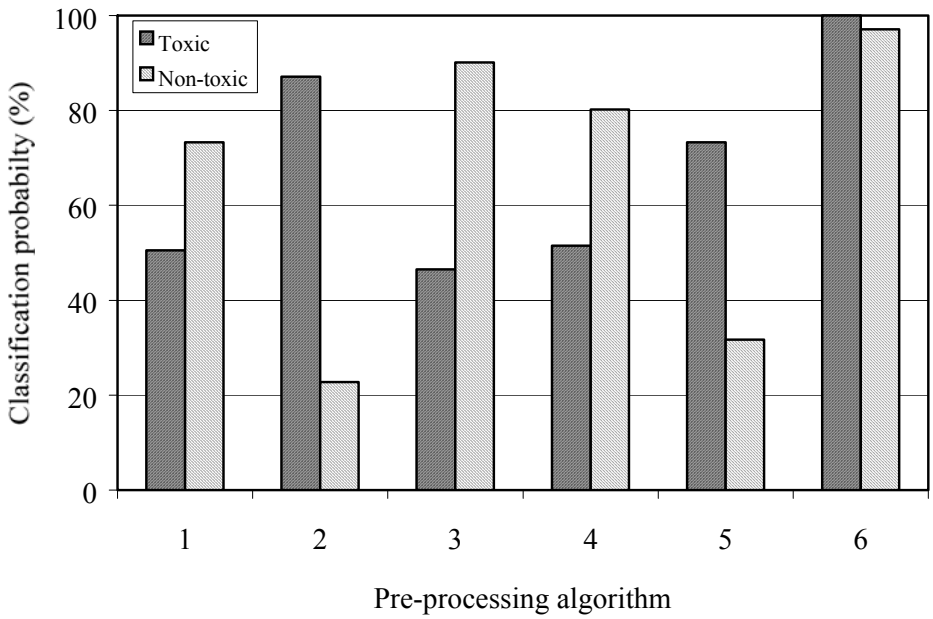

Fig. 4.15 A bar chart showing the MLP classification probabilty (%) of correctly and incorrectly classified toxic and non-toxic bacteria for 6 pre-processing algorithms; 1: Difference, 2: Difference autoscaling, 3: Difference normalisation, 4: Fractional difference, 5: Fractional difference autoscaling, 6: Fractional difference normalisation.

LVQ is an improved supervised learning technique with a self-organising feature map as discussed previously in Chapter 2. Figure 4.16 shows the schematic representation of LVQ. The hidden layer in this network is a Kohonen layer, and it carries out the learning and classifying. The LVQ scheme has three phases within its algorithm. LVQ1 is the basic LVQ learning algorithm that helps all PEs to take an active part in the learning. LVQ2 is a fine-tuning mechanism, which refines class boundaries.

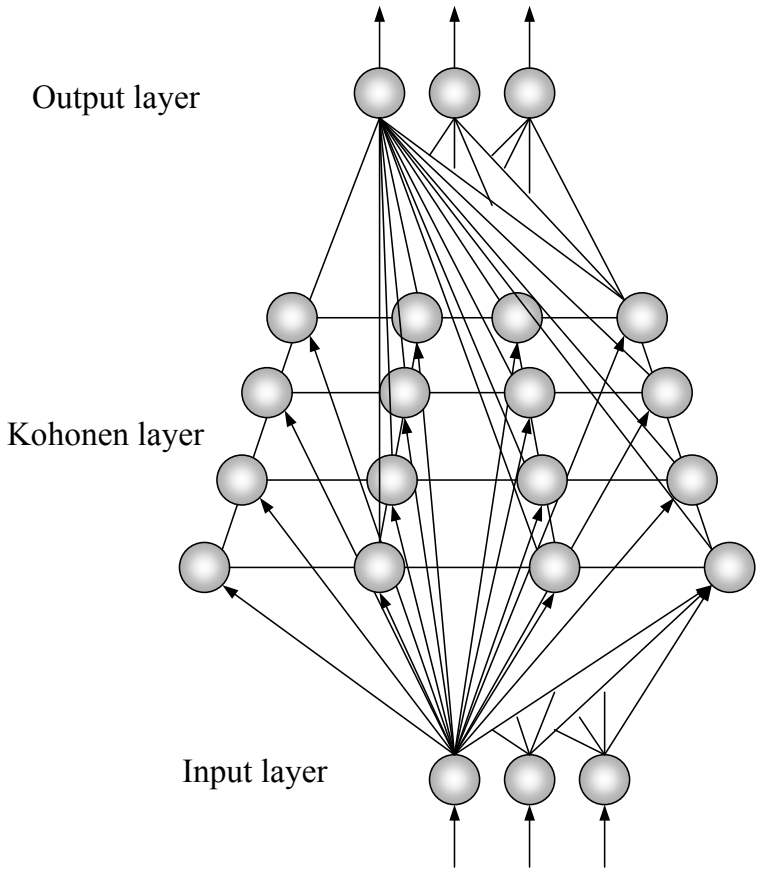

Fig. 4.16 Schematic diagram of a LVQ with a Kohonen layer.

Therefore the output from LVQ2 is the final encoded version of the original input signal applied to LVQ1. The target values were set to provide 1 for toxic bacteria and 0 for non-toxic bacteria. The same training and test sets used for the MLP were applied. The best classification results were found at the number of training iterations: 17,000 for the difference normalisation algorithm and only 100 for the fractional difference normalisation algorithm. The best LVQ set was found to classify correctly 100% of the unknown non-toxic bacteria samples and 100% of the unknown toxic bacteria samples on the basis of a set of 378 training vectors and 202 test vectors as shown in Figure 4.18.

Fuzzy ARTMAP was applied to cyanobacteria input patterns generated by a 6-MOS gas sensor array as for the MLP and LVQ algorithms. Fuzzy ARTMAP is a

supervised learning technique and also, self-organising, self-stabilising and suitable for incremental learning. Therefore it has an advantage since it can perform on-line learning without off-line training as for MLP. A Fuzzy ARTMAP network was trained with the first cyanobacteria dataset and slowly recoded during new learning without forgetting the patterns in the first one. Figure 4.17 shows the schematic architecture of a Fuzzy ARTMAP neural network. The orienting subsystem and the gain control are the two major subsystems. The orienting subsystem is responsible for generating a reset signal and the gain control sums the input signal.

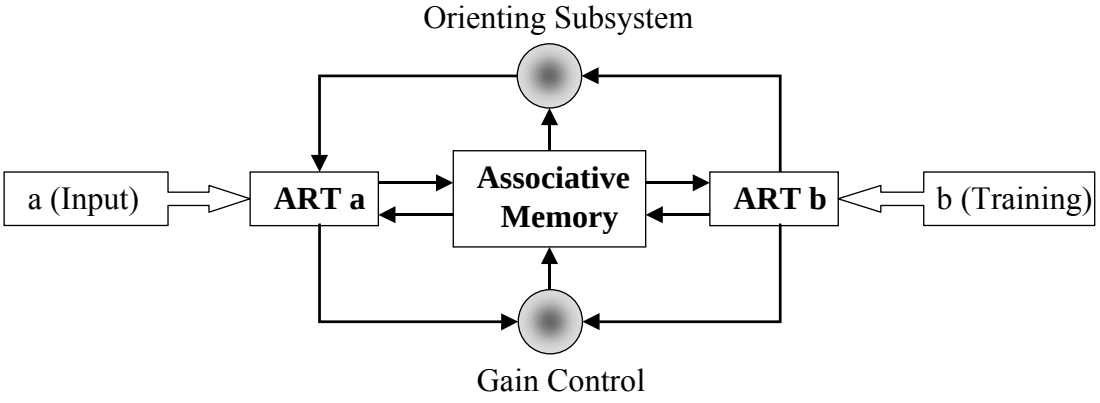

Fig. 4.17 Architecture of a Fuzzy ARTMAP neural network.

The baseline vigilance and the recode rate were set to 0 and 0.5, respectively. Fuzzy ARTMAP was able to correctly classify 100% of the cyanobacteria type. Futhermore, while the back-propagation MLP required typically 30,000 training cycles to obtain optimal results, the Fuzzy ARTMAP required only 300 training iterations. During the training process 25 nodes were committed. All results from MLP, LVQ and Fuzzy ARTMAP are summarised in Figure 4.18.

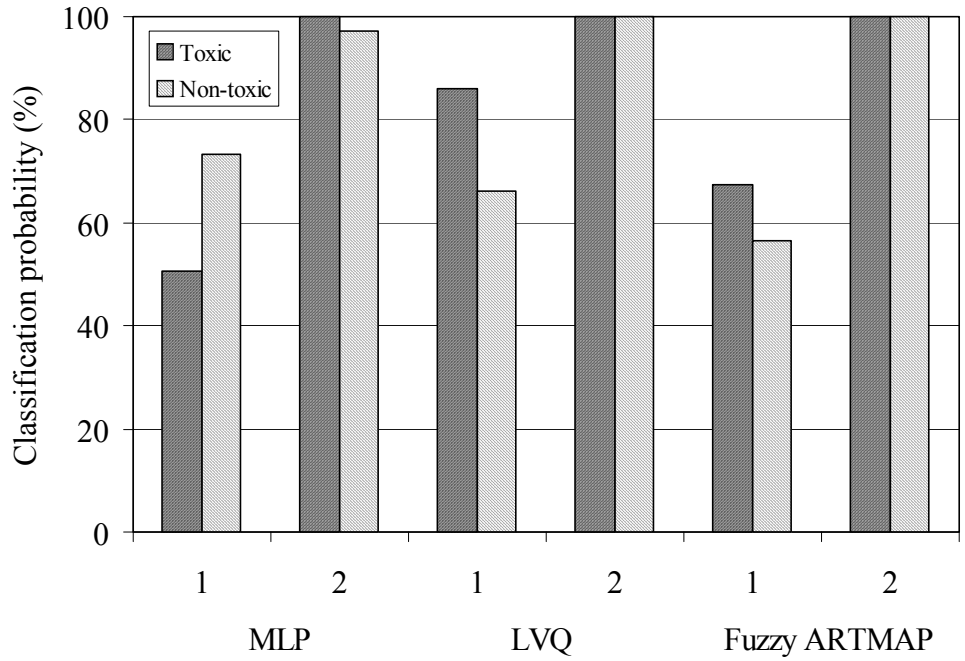

Fig. 4.18 A bar chart showing the MLP, LVQ and Fuzzy ARTMAP classification probabilty (%) of correctly and incorrectly classified toxic and non-toxic bacteria for 2 representative processing algorithms; 1: Difference normalisation, 2: Fractional difference normalisation.

4.4 The Prediction of Culture Growth Phase

CellFacts instrument (Microbial System Ltd.) was used to estimate the growth phase of the cyanobacteria cultures being measured. The CellFacts instrument uses electrical flow impedance determination to count and size particles and cells in water samples quickly and easily by using real-time on-line sampling techniques as described in Chapter 3. Every cell in a population can be gathered and automatically down-loaded to a computer at intervals of four hours. Figures 4.19 and 4.20 show the profiles of the analysis of the medium sample and the toxic cyanobacteria sample according to the number of cells and size, respectively. Each 'EXP' profile was produced every four hours.

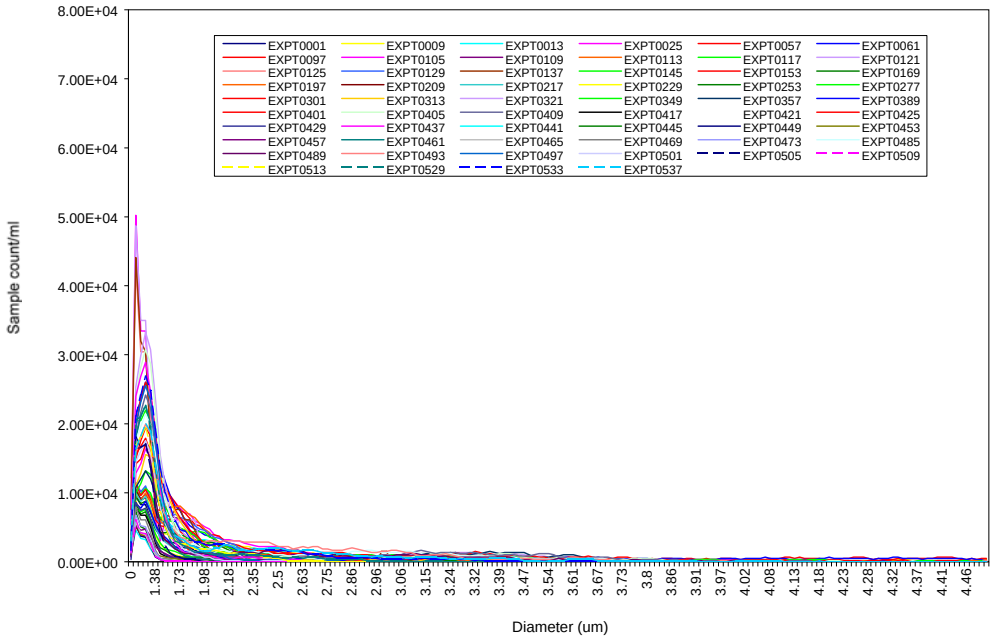

Fig. 4.19 Plot of the number of cell against cell size in 1 ml of medium sample.

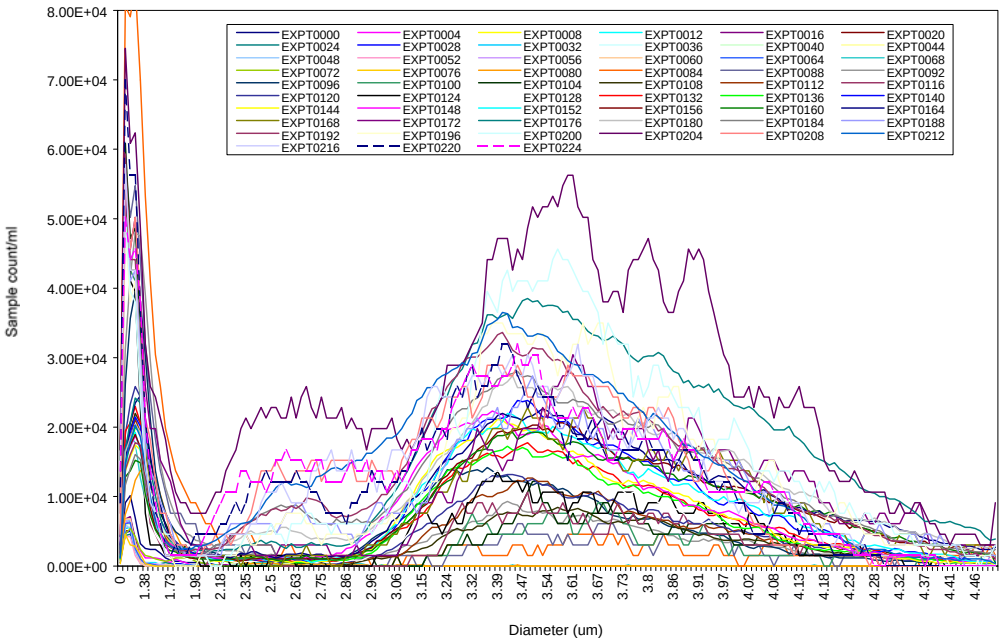

Fig. 4.20 Plot of the number cells against cell size in 1 ml of toxic cyanobacteria sample.

In order to interpret the growth phase of the cyanobacteria cultures, indicated by plots from the Cellfacts Instrument; Dr Dow in the Biological Sciences Department was

consulted to identify the boundaries between growth phases. All analysis profiles can be plotted again according to the elapsed time and analysed for growth phases. The growth boundaries are not clear cut and are only an indication of the progress of growth.

The design, topology, training methods and testing methods of each neural network employed to predict the growth phase were identical to those used for the classification of the cyanobacteria strains. The PCA and three supervised classifiers, MLP, LVQ and Fuzzy ARTMAP were used to predict the cyanobacteria in the observed four growth phases. Once again the normalised fractional difference model, which showed good results for the classification of cyanobateria strains, was used.

A series of measurements was performed on toxic cyanobacteria cultures. There were three separate experimental runs on each cyanobateria culture. Figures 4.21, 4.22 and 4.23 show the growth phase curve from the Cellfacts instrument and the corresponding PCA results from the output of the electronic nose system to four different growth phases of three cyanobacteria cultures. The growth curves show the cell counts and sizes against the elapsed time. The true phases, lag, growth, stationary and late stationary (labelled I to IV) were obtained by inspecting the growth curves and locating the changes in the slope against elapsed time. The growth curves and the PCA plots in Figure 4.22 and Figure 4.23 show very similar results compared to the results in Figure 4.21. This can be explained by the size of cells taken from the master culture because the initial cell size of cyanobacteria culture in Figure 4.21 was 2.2 μm whereas the others were 3 μm. There is some overlap of the response vectors

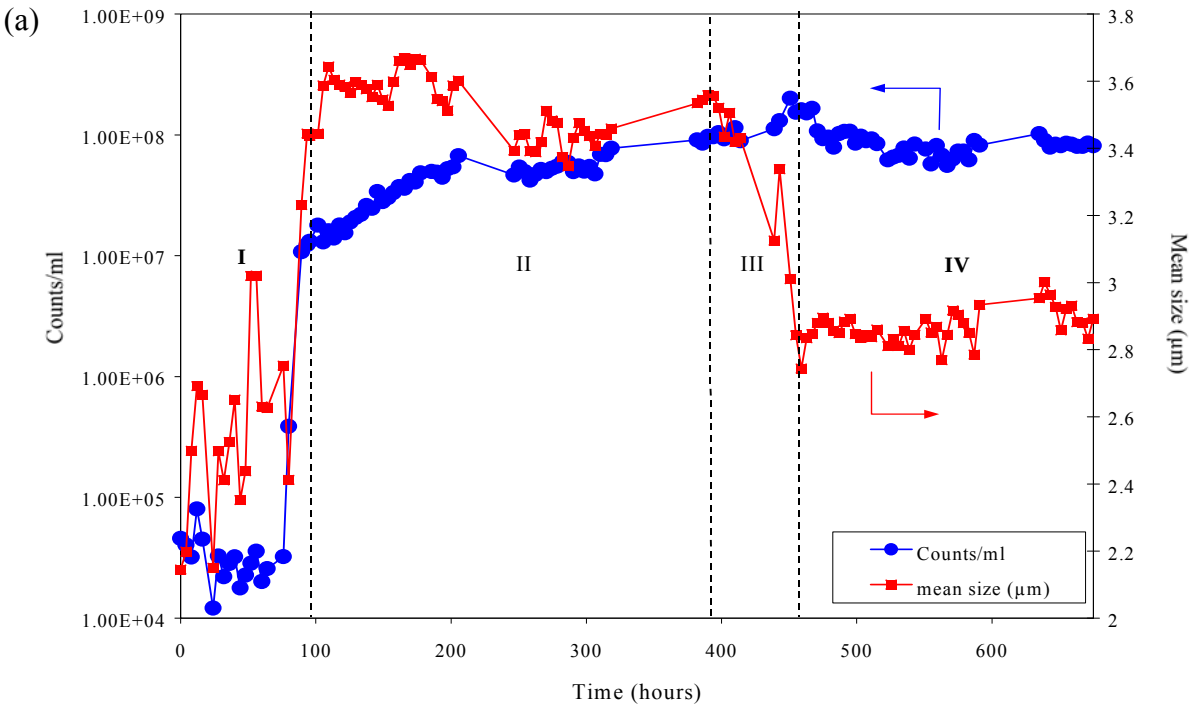
(a)
Counts/ml
Mean size (µm)
Time (hours)
I
II
III
IV
Counts/ml
mean size (µm)
1.00E+09
1.00E+08
1.00E+07
1.00E+06
1.00E+05
1.00E+04
3.8
3.6
3.4
3.2
3
2.8
2.6
2.4
2.2
2
0
100
200
300
400
500
600

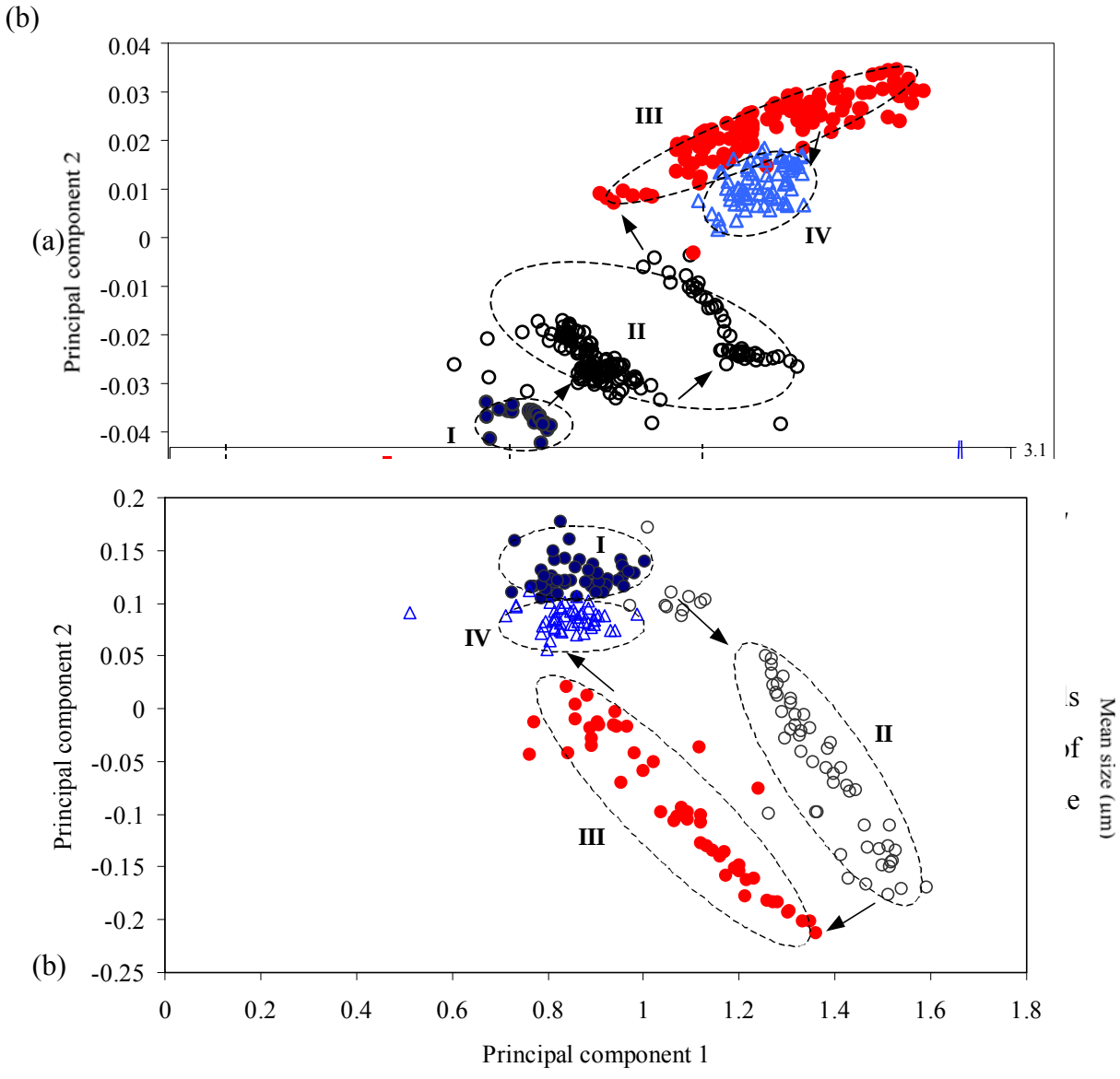
(b)
(a)
Principal component 2
I
II
III
IV
0.04
0.03
0.02
0.01
0
-0.01
-0.02
-0.03
-0.04
3.1
(b)
Principal component 2
Principal component 1
Mean size (µm)
I
II
III
IV
0.2
0.15
0.1
0.05
0
-0.05
-0.1
-0.15
-0.2
-0.25
0
0.2
0.4
0.6
0.8
1
1.2
1.4
1.6
1.8

Fig. 4.22 (a) A growth phase plot of Cellfacts instrument showing the number of cells and cell size for cyanobacteria over a 800 h period (b) PCA results of the response of a six-element gas sensor based electronic nose to the headspace of cyanobacteria. The four growth phases are lag, growth, stationary and late stationary (labelled I to IV).

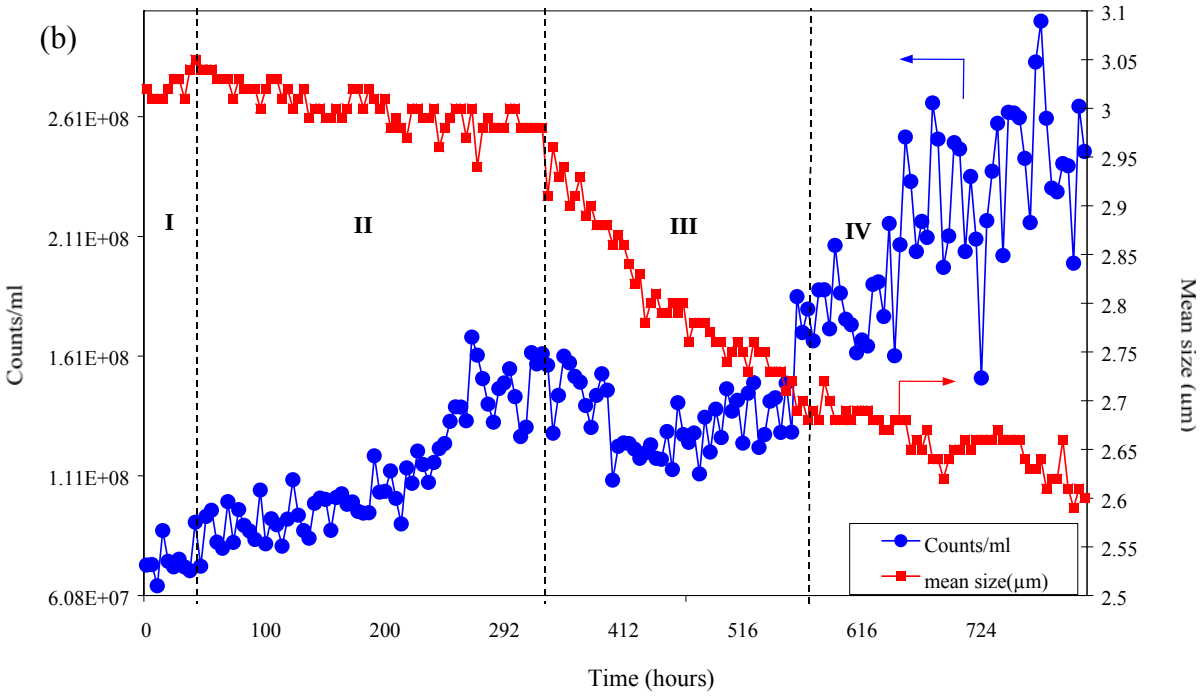

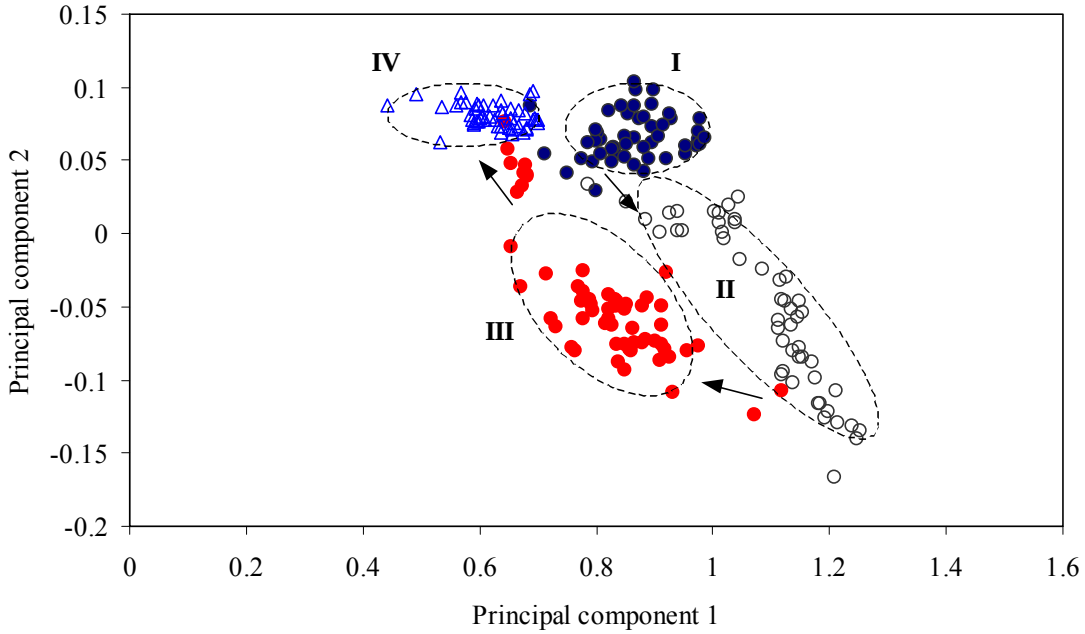

Fig. 4.23 (a) A growth phase plot of Cellfacts instrument showing the number of cells and cell size for cyanobacteria over a 800 h period (b) PCA results of the response of a six-element gas sensor based electronic nose to the headspace of cyanobacteria. The four growth phases are lag, growth, stationary and late stationary (labelled I to IV).

in each PCA plot, corresponding to the transition periods of the cyanobacteria cultures. Figure 4.24 shows the PCA plot of a six-element gas sensor based electronic nose to the headspace of cyanobacteria where point 1 and point 180 represent t = 0 and t = 9000 hours, respectively. Each point is a representation of the responses from all of the six sensor arrays after preprocessing using the normalised fractional difference, with a time interval of 50 min. The data points move from phase III into phase IV, hence result in a transition of the response pattern.

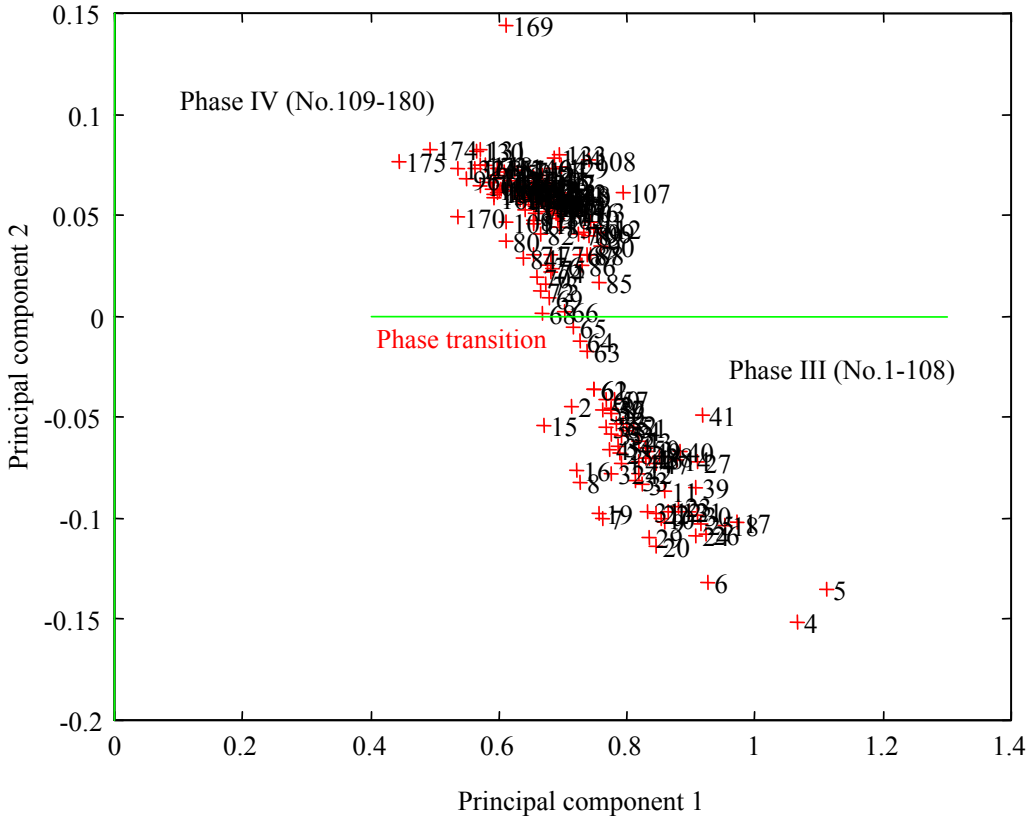

Fig. 4.24 PCA results of the response of a six-element MOS gas sensor based electronic nose to the headspace of cyanobacteria. The two growth phases are

stationary and late stationary (labelled III to IV). The response data were preprocessed by the normalised fractional difference model.

The cyanobacteria data-set was divided into 3 test folds containing 48 measurements each (12 measurements per phase category) and three neural networks were trained using 144 vectors for each fold. Test vectors were selected at random from each phase without replacement. The network has 6 inputs and 4 outputs since a 1-of-4 code was used to code the 4 different phases. The confusion matrix for the classification of the growth phases is shown in Table 4.3. The classification rates of MLP, LVQ and Fuzzy ARTMAP were similar (92.3%, 95.1% and 92.4%, respectively) but Fuzzy ARTMAP was the fastest to learn and judged to perform best because it self-organises and selects its own "hidden neurons".

Table 4.3 Confusion matrix showing the best performance of phase classification of cyanobacteria using a normalised fractional difference model with MLP, [LVQ] and (Fuzzy ARTMAP).

	Actual phase			
Predicted	Lag	Growth	Stationary	Late stationary
Lag	**140 [136] (140)**	8 [16] (20)	0	4 [4] (16)
Growth	[4]	**136 [128] (120)**	0	0
Stationary	4 [4] (4)	0	**144 [144] (144)**	0
Late stationary	0	(4)	0	**140 [140] (128)**

In order to evaluate generalisation, the MLP, LVQ and Fuzzy ARTMAP were used for the prediction of unknown growth phases. The patterns in sets 1 (Figure 4.21) and 3 (Figure 4.23) were used for training and the patterns in set 2 (Figure 4.22) were used to test the network. This led to a performance of 70% in the classification

of the test patterns for LVQ and Fuzzy ARTMAP. The MLP and LVQ network required typically 25,000 and 2,000 training cycles respectively but Fuzzy ARTMAP required only 150 training iterations, thus it was faster to learn than the others.

Table 4.4 shows the results of the generalisation tests. It was difficult to recognise the growth phase of an unknown culture which had a different trend from other cultures used for training. It was found that the majority of errors in the second generalisation test occurred in the boundaries between the different growth phases, this was due to the implementation of a hard boundary. Although a fuzzy ARTMAP provides a set for the boundary, which is not sharp, but has similar error in the phase boundaries.

Table 4.4 Results of the generalisation test of MLP, [LVQ] and (Fuzzy ARTMAP) network in growth phase classification, in terms of patterns correctly classified/numbers of patterns.

Training/tested sets	Growth phase				*Classification* rate (%)
	lag	growth	stationary	late stationary	
1, 3/2	0/50 [3/50] (20/50)	50/50 [45/50] (48/50)	2/50 [45/50] (47/50)	44/50 [45/50] (44/50)	**48** **70** **70**

4.5 Summary

This study shows the potential application of an electronic nose to potable water quality analysis. A six-element metal oxide based e-nose has been used for the continuous monitoring of the growth of cyanobacteria over a period of 40 days. Several pre-processing techniques were explored in order to remove the noise factor associated with running the electronic nose in ambient air, and the normalised fractional difference method gave the best PCA results. Three supervised neural

networks, multi-layer perceptron (MLP), learning vector quantization (LVQ) and Fuzzy ARTMAP were used and compared for the classification of both two strains and four different growth phases of cyanobacteria (lag, growth, stationary and late stationary). The best results show that the toxin strain of cyanobacteria was correctly predicted with an accuracy of 100%, and that the growth phase of the toxic cyanobacteria was correctly predicted for 70 % of all unknown samples using LVQ and Fuzzy ARTMAP. The training iterations of Fuzzy ARTMAP were found to be typically more than an order of magnitude less than those for the MLP and the LVQ network. Therefore Fuzzy ARTMAP was chosen to be the best algorithm overall.

The majority of the classification error is associated with the different growth trends of the cyanobacteria culture, and so it could be reduced significantly if the neural network was trained on-line. Even so the error occurring in the boundaries between the different growth phases is difficult to reduce, even in the case of Fuzzy ARTMAP, so further work is needed on boundary identification.

4.6 References

1. B. F. J. Manly, Multivariate statistical methods, Chapman & Hall (1994).
2. S. Haykin, Neural Networks: A comprehensive foundation, Macmillam Publishing Company, (1994).
3. J. A. Freeman, and D. M. Skapura, Neural Networks: Algorithm, Applications, and Programming Techniques, Addison-Wesley Publishing Company, (1992).
4. J.W. Gardner, and P.N. Bartlett, A brief history of electronic nose, Sensors and Actuators B, 18-19 (1994) 211-220.
5. T. D. Gibson, O. Prosser, J. N. Hulbert, R. W. Marshall, P. Corcoran, P. Lowery, E. A. Ruck-Keene, and S. Heron, Detection and simultaneous identification of

microorganisms from headspace samples using an electronic nose, Sensors and Actuators B, 44 (1997) 413-422.

6. J.W. Gardner, and P.N. Bartlett, Sensors and Sensory Systems for an Electronic Nose, Kluwer Academic Publishers (1992).
7. T. C. Pearce, J.W. Gardner, S. Friel, P. N. Bartlett, and N. Blair, Electronic nose for monitoring the flavour of beers, Analyst, 118 (1993) 371-377.
8. T. Nakamoto, A. Fukuda, and T. Moriizumi, Perfume and flavour identification by odor sensing system using quartz-resonator sensor array and neural-network pattern recognition, sensors and Actuators B, 10 (1993) 85-90.
9. J. W. Gardner, M. Craven, C. Dow, and E. L. Hines, The prediction of bacteria type and culture growth phase by an electronic nose with a multi-layer perceptron network, Meas. Sci. Technol. 9 (1998) 120-127.
10. NeuralWare Inc., NeuralWorks Professional II/Plus, Reference Guide, Pittsburgh, USA (1995).

Chapter 5

Design of New Sensor Chamber and Instrumentation

This chapter describes the design and construction of a new sensor chamber as well as other parts of the electronic nose system. The further modification of electronic nose system was performed for more useful data collection experiments. Although a mono-type sensor array based on MOS gas sensors makes for a simple electronic nose system, it may limit the resolving power of the electronic nose. Therefore there could be some advantage to making a hybrid nose out of different types of sensor, such as MOS, conducting polymers, SAW devices, and MOSFETs etc. [1]. Here, an array of conducting polymer resistive sensors has been combined with the complementary MOS sensor array to make a hybrid resistive e-nose.

5.1 Design of New Sensor Chamber

The new sensor chamber was designed to replace and improve upon a sensor chamber designed earlier by Craven [2]. It should enhance on the existing electronic nose's performance, because of the use of more sensors and better dynamic response through a reduction in dead-volume. Figure 5.1 shows the schematic design of the

thin film sensor chamber. The precise dimensions of the chamber can be seen in Appendix D.

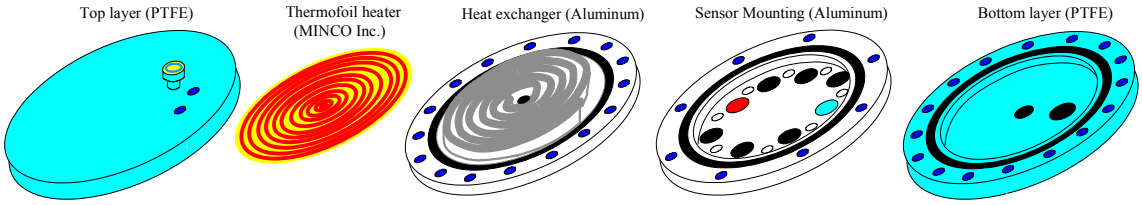

Fig. 5.1 Design of the new sensor chamber.

The combination of PTFE and aluminium was chosen for the materials for the new sensor chamber. Aluminium is cheap, easy to machine and has a lower specific heat capacity. Latter versions will be made of stainless steel. PTFE can also be easily machined and has a good thermal stability and low specific heat capacity (≈ 0.25). PTFE is inert from chemical attack by most substances and so excellent as an inner material.

The sensor chamber comprises of four layers and a thermofoil heater (MINCO Inc.). The gas enters through a hole in the top layer and passes down into the heat exchanger. The centre layer is the heat exchanger layer, on which the machined spiral channel can be seen. An efficient way of heating the gas was to feed it through the spiral channel maintained at the required temperature. The gas flows along the spiral winding before entering into a sensor mounting layer through a hole in the centre. Therefore heating of the gas is achieved by passing the gas through a heat exchanger prior to entry in the sensor mounting layer.

The main aluminium sensor chamber contains six CP gas sensors, a commercial temperature sensor (LM35CZ) and a commercial humidity sensor

(MiniCap 2). To ensure that gas sensors are exposed to the target gas simultaneously a radial sensor configuration is the best solution with the gas flow entering at the centre of the chamber. The target gas is exposed to the sensors before being drawn out of the chamber by the eight equally spaced exit holes (4 mm) around the sensor mounting. There are eight holes (8 mm) to ensure that the gas flows evenly across all of the eight sensors. The symmetry of the gas flow can give the same condition to each gas sensor. Each layer was sealed using an O-ring. The air gap around the holes in bottom layer was sealed using Araldite glue. PCBs were designed and made to link all of the sensor outputs to the computer control system and also to mount the new sensor chamber in the main electronic nose. The single-sided PCBs were designed using a software package, EasyPC, and produced within the School of Engineering at the University of Warwick.

Figure 5.2 shows the photographs of four layers of the new sensor chamber before being assembled. The top one on the left is the PTFE top layer with thermofoil heater. The other top layer on the right is the aluminium heat exchanger, on which the spiral channels can be seen. The thermofoil heater was glued on a thin (1 mm) aluminium plate for the thermal conduction to the aluminium heat exchanger. The bottom layers on the right and left are the sensor mounting layer and the PTFE bottom layer respectively.

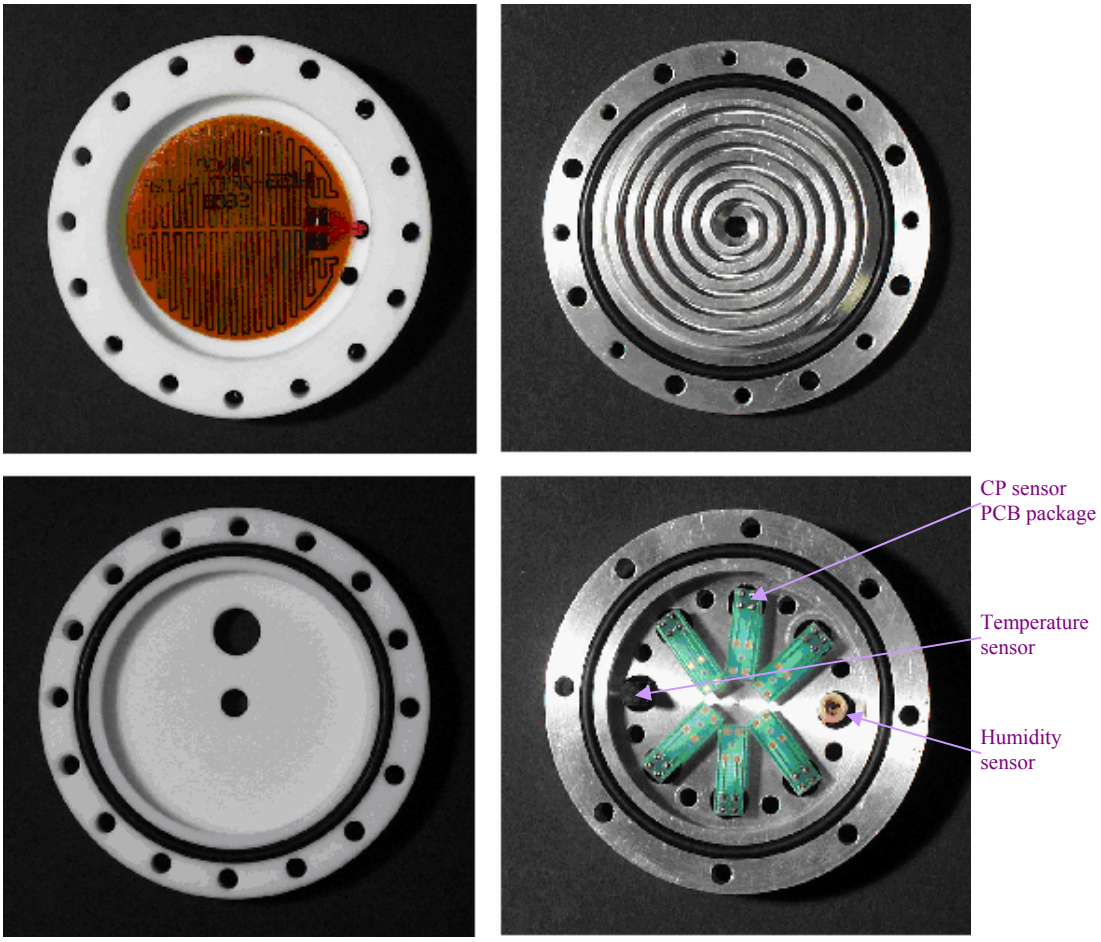

Fig. 5.2 The four layers of the new sensor chamber before assembly.

5.2 Further Development of Electronic Nose

Figure 5.3 shows the modified FOX 2000 incorporating the new sensor chamber and sub-system. A new sensor chamber is placed in parallel with the previous main chamber. The previous main chamber contained a temperature sensor (LM35CZ) and 6 thick-film MOS sensor array that was used in the original sensor array. The new sensor chamber contained the 6 thin film CP gas sensors, a temperature sensor (LM35CZ) and a relative humidity sensor (MiniCap 2). Two more gas volumetric flow-rate sensors were placed between the gas input and two sensor chambers, respectively. An additional interface circuit and a LPM-16 PnP I/O card were added to the new sensor chamber in the electronic nose system.

Figure 5.4 shows a photograph of the modified electronic nose system which has two sensor chambers, three flow-rate sensors, new interface cards and an internal power supply.

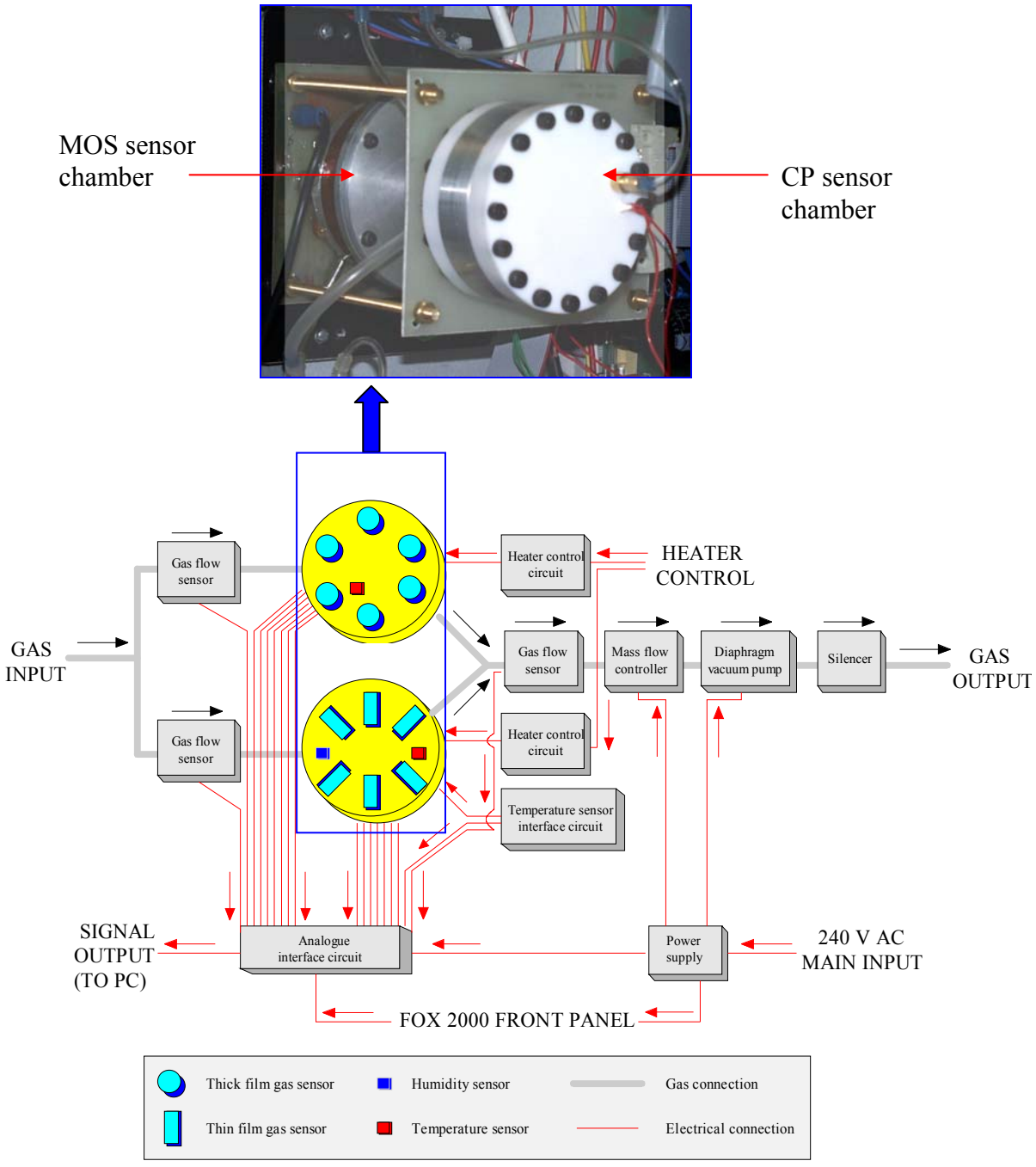

Fig. 5.3 A modified electronic nose system for the second set of measurements.

Fig. 5.4 Photograph of the final Warwick electronic nose system.

Before this modification, there were the original Fox 2,000 circuits, the analogue interface circuits modified by Craven and a LPM-16 I/O card. The LPM-16 I/O card has 8 digital outputs and 16 analogue inputs. The 8 digital outputs (6 solenoid valves + 2 heaters) and 10 analogue channels (6 gas sensor + 2 temperature sensor + 1 humidity sensor + 1 gas flow sensor) have been used. Therefore one more DAQ card, LPM-16 I/O, was required for 8 analogue inputs of the 6 CP gas sensor

array in the new sensor chamber and 2 gas flow sensors. The pre-sensor chamber and pre-heater chamber in the previous system were removed and a temperature sensor and a humidity sensor of the pre-sensor chamber were used in the new sensor chamber.

5.2.1 Computer and LPM-16 I/O cards

The computer which was central to the electronic nose system was upgraded from an Intel 80486DX33 CPU to an Intel 80486DX2/66 CPU (model: Gateway 2,000). Two LPM-16 I/O cards running 3 LabVIEW programs simultaneously were used for the control and data gathering in the whole system and these pushed the limits of the personal computer. An additional LabVIEW program was designed for the new sensor array and the flow sensors. All programs were written to run within the Microsoft Windows 95 environment. The LPM-16 PnP card and the LPM-16 card were assigned to the channels 1 and 2, respectively. If the LPM-16 base I/O address is changed, corresponding change should be followed. Therefore board configurations and switch settings were changed. The PC-LPM-16 and PC-LPM-16PnP are versatile, cost-effective boards for testing, measurement, and control. These boards contain a 12-bit, successive-approximation, self-calibrating ADC with 16 analogue inputs, 8 lines of TTL-compatible digital input, and 8 lines of digital output. The PC-LPM-16PnP was built without jumpers or switches, for use with Plug and Play operating system such as Windows 95. It also contains two 16-bit counter/timer channels for timing I/O.

5.2.2 Heater

Both sensor chambers possess a commercial thermofoil heater. These thermofoil heaters are thin, flexible heating elements consisting of an etched-foil

resistive element laminated between layers of flexible insulation. The insulation material was Kapton. The first heater (model: HK5393R8.9L12E) was attached to the external circumference of the previous main sensor chamber. It had a resistance of 8.9 Ω, therefore when supplied with 12 V, had a power rating of 16.2 W. The second thermofoil heater (model:HK5547R47.4L12A) was attached in top layer of new sensor chamber as shown in figure 5.2. It had a resistance of 47.4 Ω, therefore when supplied with 12 V, had a power rating of 3 W. The temperature was controlled by an on-off controller using LPM-16.

5.2.3 Interface Cards

The conducting polymer interface card was originally designed by Pearce [3]. It converts the DC-based resistance of each polymer film into a voltage compatible with the ADC input stage of the LPM-16 card. An Ohmic response of CP films was found at low operating voltages between ±0.15V, however at voltages greater than ± 0.5 V the polymers can become non-linear [4, 5]. Therefore a voltage range was chosen that shows a linear I-V characteristic for the interface card. The circuit consists of a constant current source with the voltage across the polymer monitored being directly proportional to the electrical resistance of the polymer film.

A simplified interface circuit diagram is shown in Figure 5.5. The sensor voltage output set to 2.5 V and the first op-amp circuit drives a constant current through the sensor because of the action of the precision reference diode (*Dz*). The magnitude of the constant current is then defined by the size of the scaling resistor and its value given by equation 5.1.

$$I_{polymer} = \frac{2.5\text{V}}{R_{scale}} \tag{5.1}$$

The resistance of the device, $R_{polymer}$ can be given by,

$$V_{polymer} = R_{polymer} \times I_{polymer}$$

$$= R_{polymer} \times \frac{2.5\text{V}}{R_{Scale}} \tag{5.2}$$

where $V_{polymer}$ is the voltage dropped across the device.

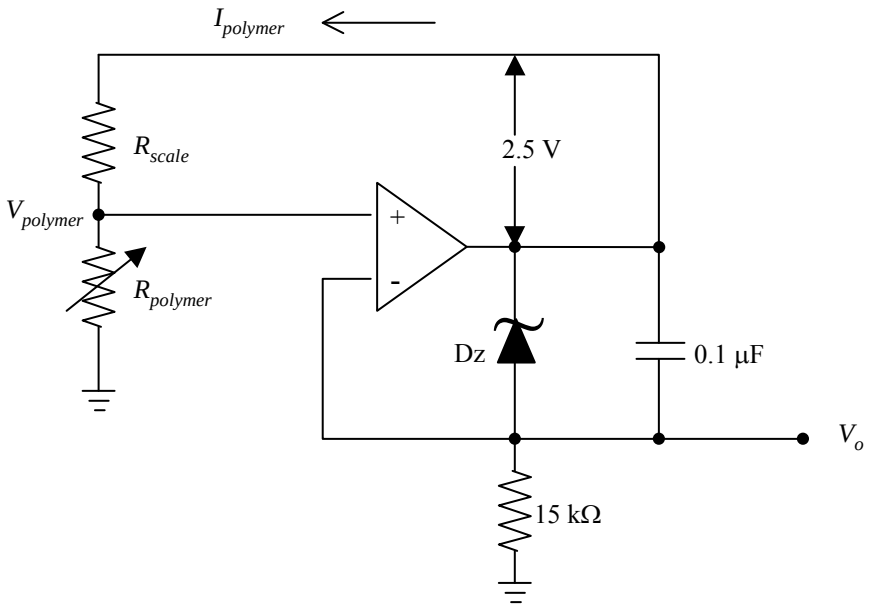

Fig. 5.5 Simplified CP interface circuit diagram. The output, V_o, is amplified by a second stage op-amp circuit, compensating offset and providing gain.

The scale settings therefore correspond to full scale readings of the CP sensor resistances up to 100 Ω, 1 kΩ, 10 kΩ and 100 kΩ, with R_{scale} being 2.5 kΩ, 25 kΩ, 250 kΩ and 2.5 MΩ, respectively. Table 5.1 shows the dip switch values depending

on polymer resistance. It was possible to change resistors if the resistance of the CP sensor is out of range. The resistor socket related to the red coloured dip switch was produced for this purpose. The second stage of the circuit amplifies the full scale sensor signal, $V_{polymer}$ to 5 V at the output V_o. The details of the circuit design are provided in [3].

Table 5.1 Dip switch values of CP interface circuit

Dip Switch	$R_{\max}(\Omega)$	$I_{polymer}$	$R_{polymer}(\Omega)$	Calibration resistor for low gain (Ω)	Calibration resistor for high gain (Ω)
Red	100	1 mA	< 100	10	1
Orange	1 k	0.1 mA	100-1 k	100	10
Yellow	10 k	10 μA	1 k-10 k	1 k	100
Brown	100 k	100 μA	10 k-100 k	10 k	1 k

The another additional interface card was produced for the interface of the flow sensors and the CP interface card with a LPM-16 card. The details of the circuit diagram and layout are as shown in Appendix B.

5.2.4 Power supply

Two external power supplies (Farnell, type E30/1) previously used to power the heaters were replaced by a high efficiency power supply made within the School of Engineering and mounted in the electronic nose system. It supplies 12 V and 3 A for two thermofoil heaters and ±15 V and 1 A for the CP interface card, and therefore has a maximum power of 66 W. It was sufficient to drive two thermofoil heaters and the interface card.

5.2.5 Valve circuit

The valve circuit was originally designed by Craven as a part of his PhD work [2] but the circuit board was relatively big and connected with an external power supply. Therefore it was replaced by a new simple sub-circuit, which was based on a design recommended by the manufacturer (Lee Components). Each valve was driven at 12 V from a internal power supply consuming 1 W maximum. Six LEDs were connected to give a visual indication of the status of the sub-circuits just like the original design [2]. The LED was lit for valve on and the LED was not lit for valve off according to digital output from the LPM-16 I/O card. It was mounted in the electronic nose system with an internal power supply.

5.2.6 CP gas sensor

CP gas sensors were fabricated at Southampton University by the electro-polymerisation (section 3.3.3) of polymer across the 10 μm gap between gold electrodes in the device SRL127/110. Six different CPs (Table 5.2) were chosen as the hybrid sensor array materials in the new sensor cell. PPy/PSA, PPy/HpSA,

PPy/DSA in H_2O and PAN/PSA, PAN/HpSA, PAN/DSA in 2M H_2SO_4 were chosen as candidate sensing materials.

Table 5.2 Electrochemical deposition conditions of conducting polymer sensors

Conducting Polymer/ Counter Ion	Deposition Conditions
PAN/PSA	0.2 M aniline, 0.5 M alkyl sulfonate, and 2 M H_2SO_4 +0.9 V vs. SCE for t_{step1} followed by +0.78 V vs. SCE for t_{step2}
PAN/HpSA	0.4 M aniline, 0.5 M alkyl sulfonate, and 2 M H_2SO_4 +0.9 V vs. SCE for t_{step1} followed by +0.78 V vs. SCE for t_{step2}
PAN/DSA	0.4 M aniline, 0.5 M alkyl sulfonate, and 2 M H_2SO_4 +0.9 V vs. SCE for t_{step1} followed by +0.78 V vs. SCE for t_{step2}
PPy/PSA	0.1 M pyrrole, 0.1 M alkyl sulfonate, and H_2O +0.85 V vs. SCE for t_{step}
PPy/HpSA	0.1 M pyrrole, 0.1 M alkyl sulfonate, and H_2O +0.85 V vs. SCE for t_{step}
PPy/DSA	0.1 M pyrrole, 0.1 M alkyl sulfonate, and H_2O +0.85 V vs. SCE for t_{step}

5.2.7 LabVIEW

A software package ‘LabVIEW (ver.4) has been used to gather data from the new CP sensor chamber and the two flow sensors. All data were simultaneously monitored on a front panel and saved in a spreadsheet file automatically. The block diagram, shown below, is the VI’s source code, constructed in LabVIEW’s graphical programing language, G. Figure 5.6 shows the CP control2.VI to create a signal array

from 8 channels. A sub-VI, AI Config, configures an analogue input operation for a specified set of channels.

Figure 5.7 shows the block diagram of the main CP control2.VI and sub-VI called output.VI. This sub-VI is concerned with the returning one scan of data

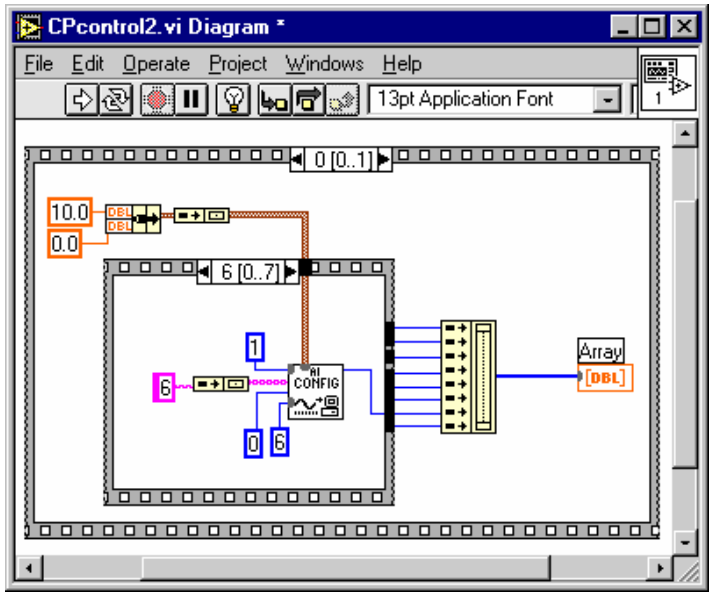

Fig. 5.6 Block diagram of CP control2.VI creating an array from 6 CP sensors and 2 flow sensors.

from a previously configured group of channels. Every voltage output from the CP sensor array is saved as a text file and the voltage outputs from flow sensors return to the real flow-rate (ml/min) through the formula node that calculates an equation inside the resizable box. Text file VI converts a 2D or 1D array of single-precision (SGL) numbers to a text string and writes the string to a new byte stream file or appends the string to an existing file. These VI were run with the valve control VI, the temperature control VI and the MOS sensor array control VI together.

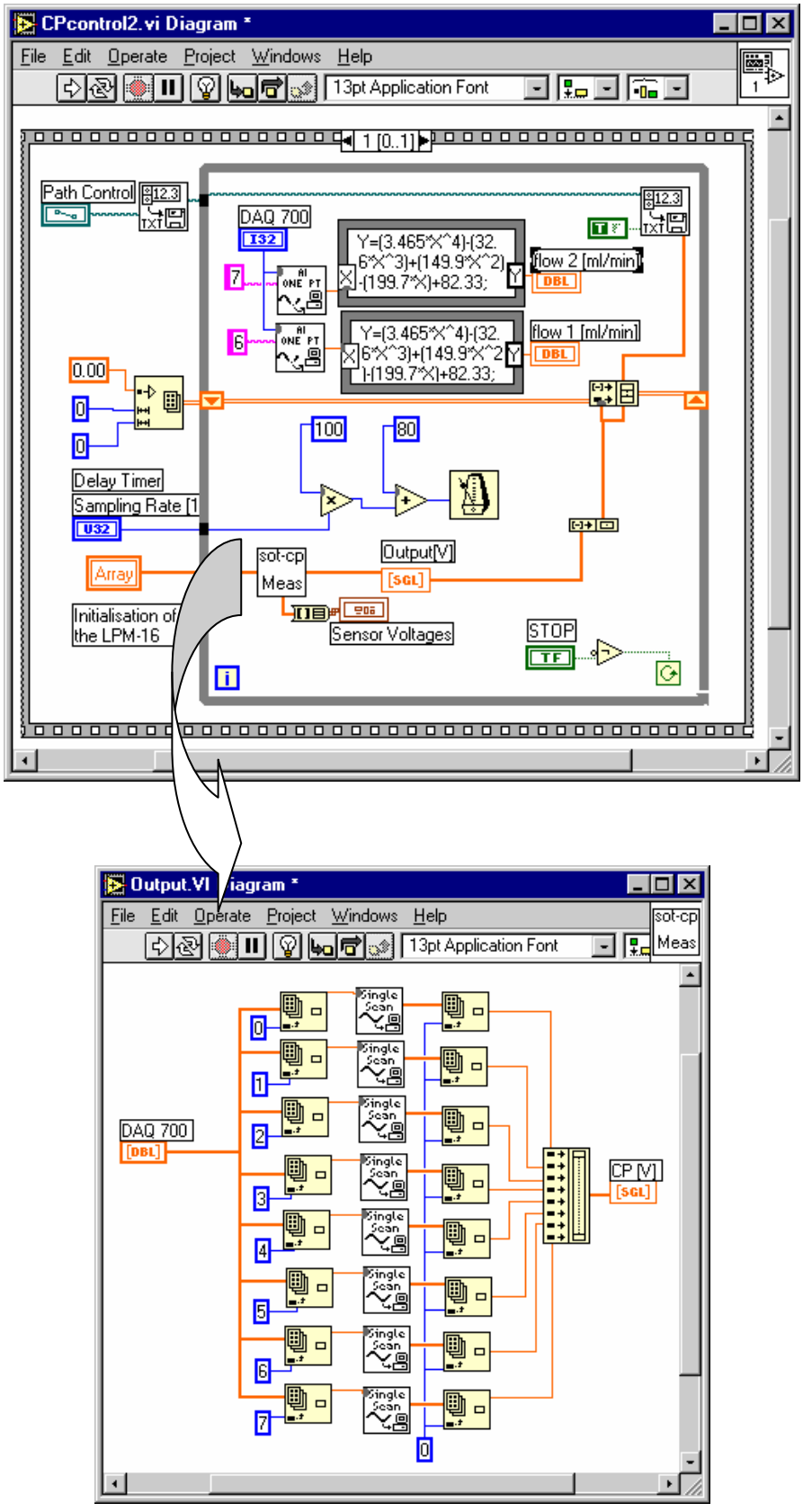

Fig. 5.7 Block diagram of main CP control2.VI and sub-VI called output.VI.

5.3 Testing of the Sensor Array Module

The pre-heater chamber was thought to reduce the temperature fluctuation of the target gas in the sensor chamber but it was possible to get certain accurate control (±0.1 °C) of the gas temperature without pre-heating (Figure 5.8). Temperatures were set to 40 ˚C for the MOS sensor chamber and 35 ˚C for the CP sensor chamber as target temperatures at first. It is essential to control accurately the temperature of gas within the sensor chambers for reliability of sensor output. The temperatures, 45 ˚C for MOS chamber and 35 ˚C for CP chamber are optimum temperatures to control, respectively. It was found [6] that the largest response of the conducting polymer sensors occurred at low humidity and low operating temperature and the temperature of the CP chamber was set to a reasonably low value, 35 ˚C.

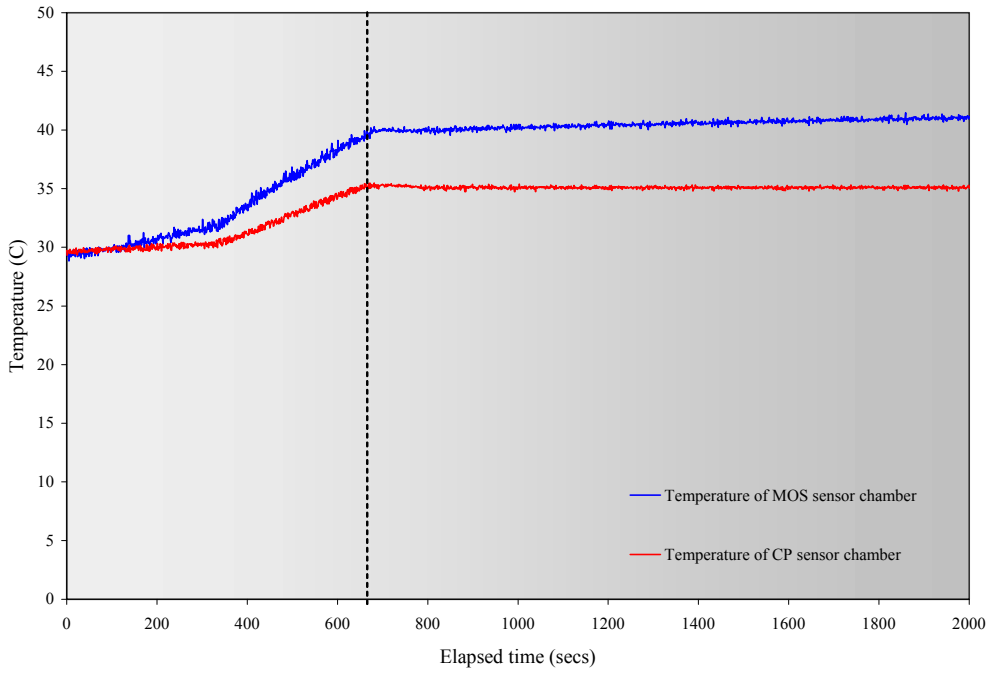

Fig. 5.8 Plot showing the temperature in the MOS and CP sensor chambers after power on. Temperatures were set to 40 ˚C for the MOS chamber and 35 ˚C for the CP chamber.

The MOS chamber contains six thick film sensors, each has about 1 W, hence the temperature, 45 ˚C, was the optimum temperature controllable in the MOS chamber. From start-up, test results have shown that thermal equilibrium was reached in approximately 650 seconds. The thermal characteristics of the two chambers were similar (temperature variation ≈ ± 0.1 ˚C) and the new CP sensor chamber showed consistent and reliable features at the operating temperature, i.e. once equilibrium was reached a steady base-line was achieved.

5.4 Cyanobacteria Experiments with Gas Sensor Array Module

A small number of cells (contained in 100 ml of inoculum) from the same reference storage (master culture) were inoculated into the medium every week. Liquid samples were extracted and analysed by the commercial CellFacts instrument and gas samples from each headspace were introduced to the electronic nose system after 5 weeks. Therefore six different growth stages of cyanobacteria cultures were prepared for the classification of growth phases. After these experiments, the same samples were used for analysis using a HP 4440 chemical sensor, which will be discussed in Chapter 6. The sampling system was operated in a cyclic fashion, whereby a set sequence of timed valve activation was repeated for a pre-determined number of times (section 3.4.1). The system consists of sampling the headspace of the sample vial and room air. The room air, when selected, allowed the sensor array to stabilise its response for recovery. The sequence of valve activations that was adopted in the LabVIEW program for each cycle was; valve 1 & 3 first for the air and valve 2 for odour sample. The valves 1 and 3 were activated together for the fast recovery after sampling from the headspace of the sample vial. If valves 1 and 3 were open, gas flow-rates of the two chambers were approximately 250 ml/min for MOS chamber

and 230 ml for CP chamber. If only valve 2 was open, gas flow rates were 95 ml/min and 100 ml/min, respectively. The difference between flow-rates was caused by the different design between two sensor chambers.

There were six separate experimental runs performed on each cyanobateria culture. The CellFacts instrument (Microbial System Ltd.) was used once again to estimate the growth phase of the cyanobacteria cultures being measured. Figures 5.9 shows the profiles of the analysis of the toxic cyanobacteria samples according to the number of cell and size. Each culture was measured twice as shown in Fig. 5.9, hence two profiles per sample were produced. A label, master, means the master culture for inoculation and numbered captions represent the dates of inoculation from the master culture. The initial cell size of the master culture was about 2.82 μm. The growth curves can be drawn again from Figure 5.9. The true phases, lag, stationary and late stationary were obtained by inspecting the growth curves as shown in Figure 5.10. There was no lag phase among these samples. It was not possible to get real changes in the slope against elapsed time because of the intermittent sampling. However every culture was identified by its growth phase in the same way that was used for the continuous measurement (Chapter 4).

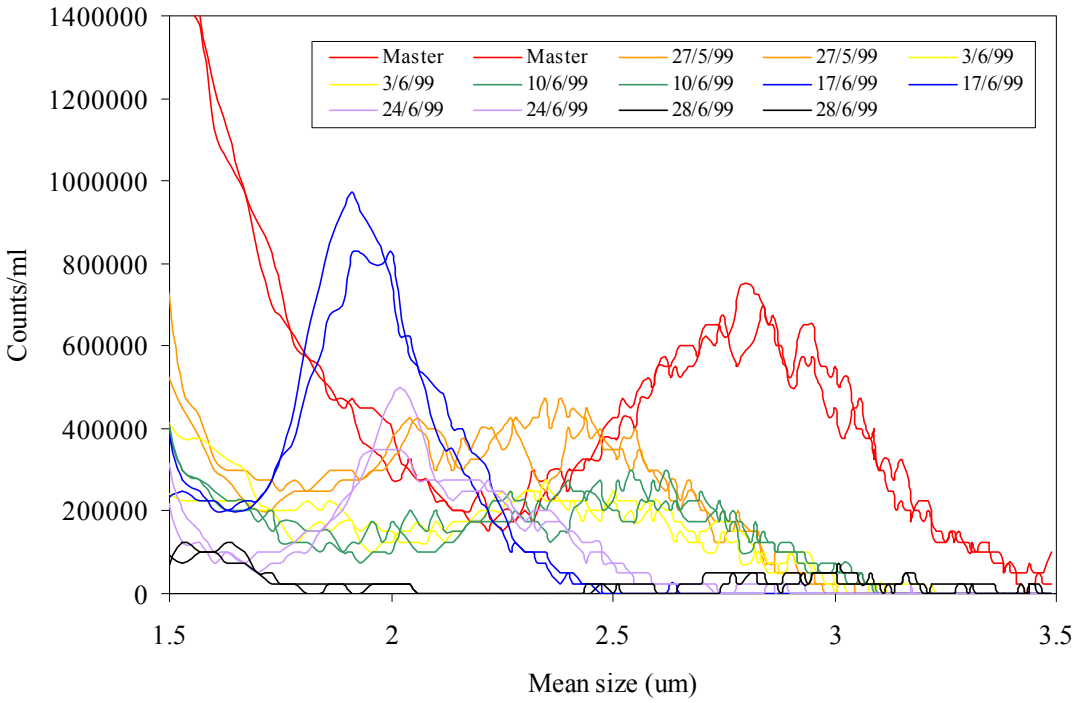

Fig. 5.9 Plot of the number cells against cell size in 1 ml of toxic cyanobacteria sample.

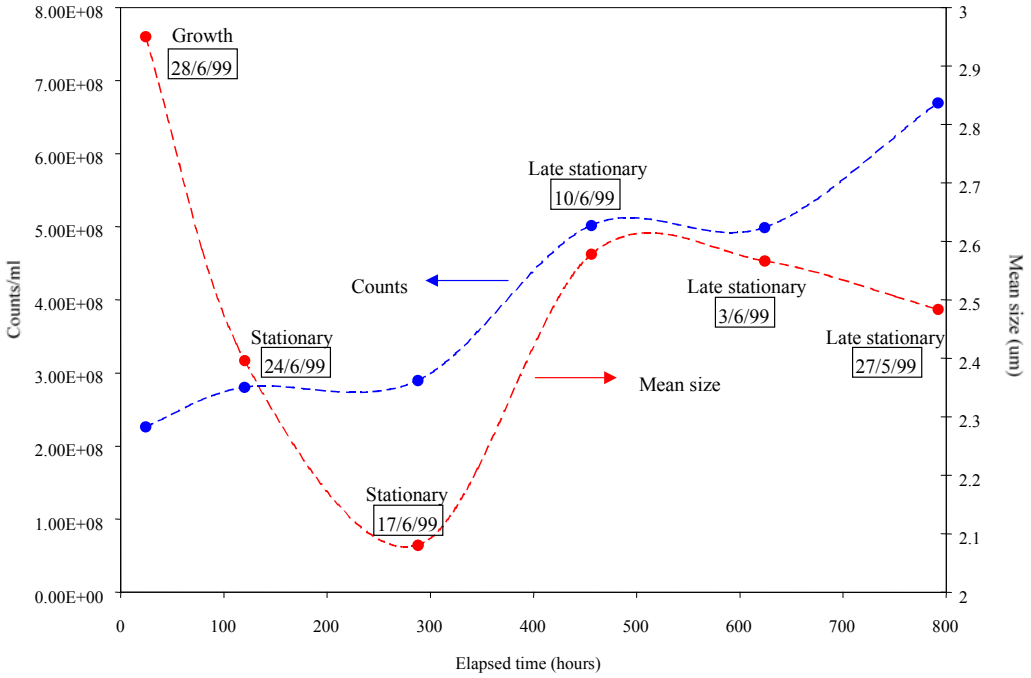

Fig. 5.10 A growth phase plot from the Cellfacts instrument showing the number of cells and cell size for cyanobacteria over a 800 hour period.

Each measurement cycle of the electronic nose system is based on two elements (room air - toxic cyanobacteria) and 1 cycle was set to 10 min. Figures 5.11 – 5.16 show the raw sensor responses from the six different stages of cyanobacteria samples in water. During the experiment, the temperatures of the MOS sensor chamber and the CP sensor chamber were 45 ºC and 35 ºC, respectively.

Unexpectedly, the sensitivity of the early growth phase was the strongest among six different cyanobacteria cultures. Output voltages of three PPy conducting polymer sensors were decreased when these were exposed to odour samples. Characterisation of discrete PPy sensors has been previously investigated by Ingleby [6]. Response data from 6 MOS and 6 CP sensors were very stable and reliable over the experimental periods with cycles.

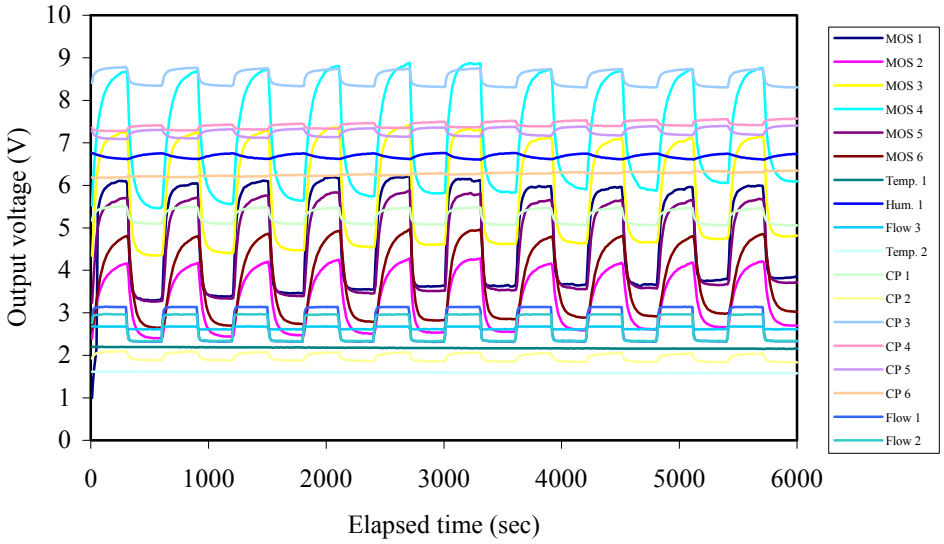

Fig. 5.11 Plot of the response from room air and toxic cyanobacteria inoculated on 28th June 1999.

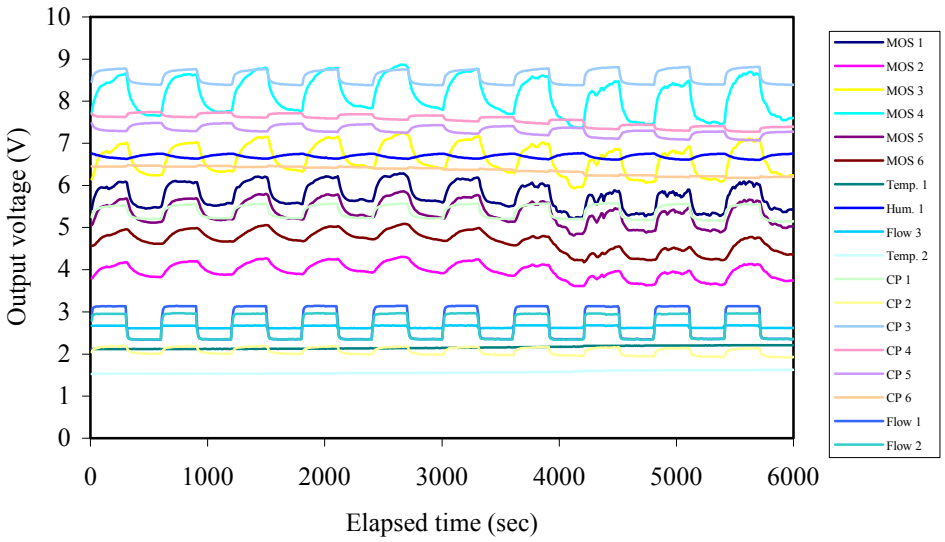

Fig. 5.12 Plot of the response from room air and toxic cyanobacteria inoculated on 24th June 1999.

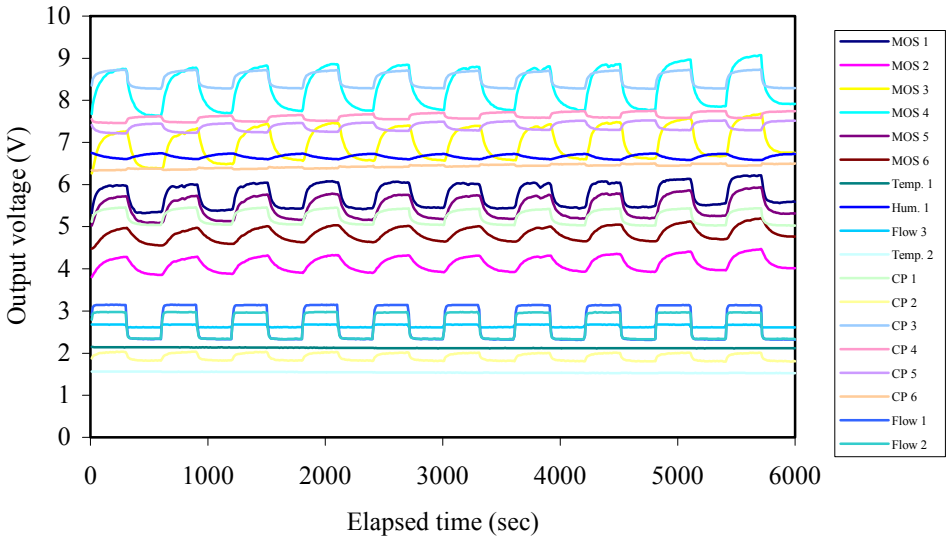

Fig. 5.13 Plot of the response from room air and toxic cyanobacteria inoculated on 17th June 1999.

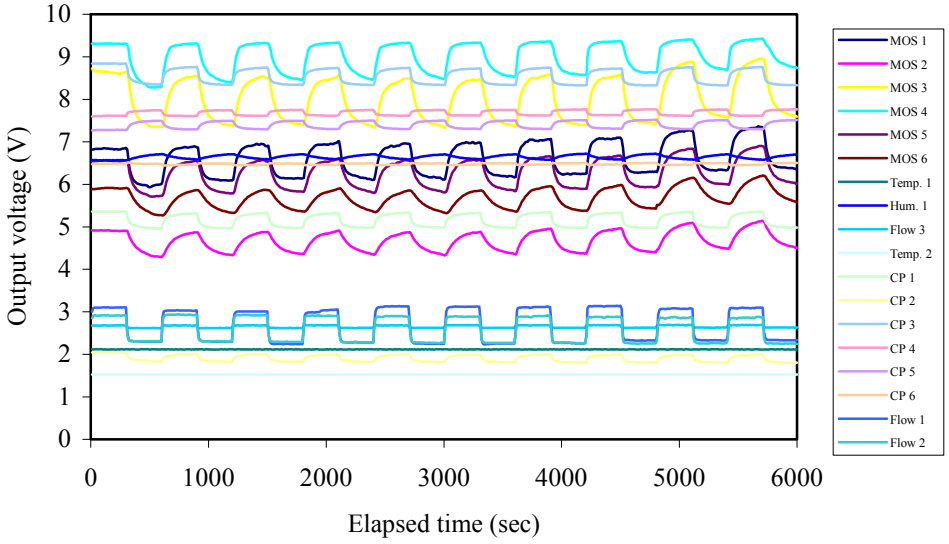

Fig. 5.14 Plot of the response from room air and toxic cyanobacteria inoculated on 10th June 1999.

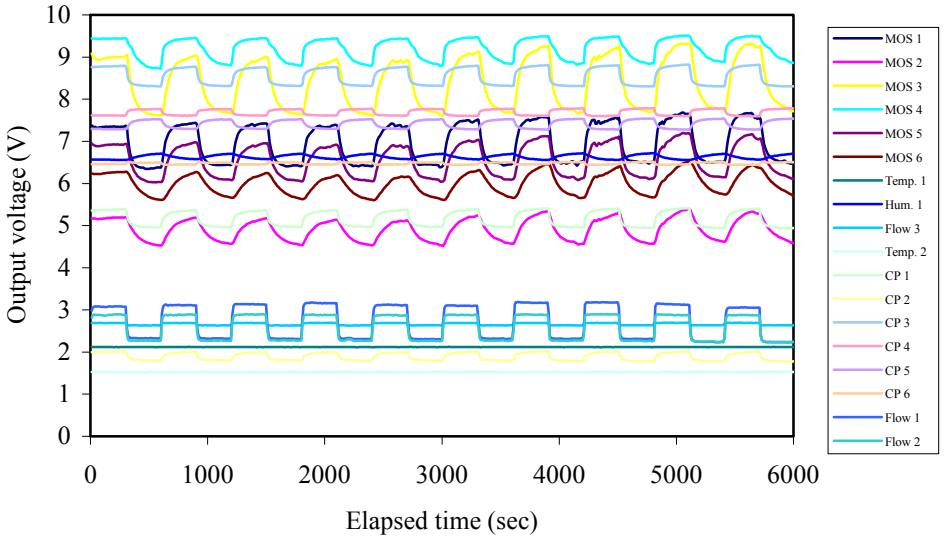

Fig. 5.15 Plot of the response from room air and toxic cyanobacteria inoculated on 3rd June 1999.

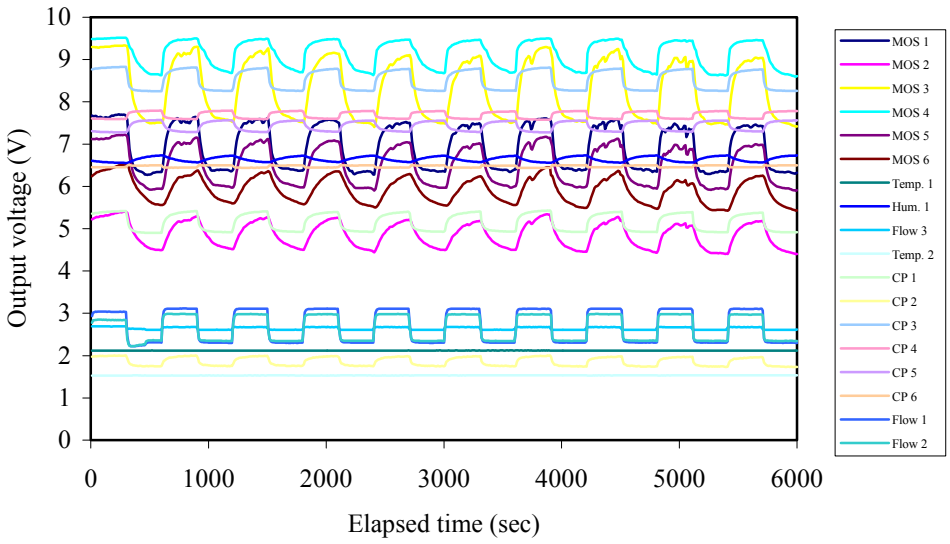

Fig. 5.16 Plot of the response from room air and toxic cyanobacteria inoculated on 27th May 1999.

Similar to the preprocessing of the standard chemicals, the average values per cycle and per element were created to reduce the number of data points. A PCA was used to see if the cyanobacteria fell into three distinct clusters of growth phase. Once again the normalised fractional difference model, which showed good results for the classification of cyanobateria strains and growth phases, was used. Figure 5.17 shows the PCA results of the response of a six-element MOS gas sensor based electronic nose to the headspace of cyanobacteria. Point 1 and point 60 represent the 1st cycle of the first cyanobacteria sample and the 10th cycle of the last cyanobacteria sample, respectively. Despite the sensor signal variance over the last stationary phases, the PCA of the normalised fractional difference algorithm exhibited good classification performance without overlap between the three phases. The stationary phase and late stationary phases have two and three different growth stages of cyanobacteria culture which have different inoculation dates (weekly base), respectively. A full separation

of these two growth stages in the stationary phase was not possible by using only one type of sensor, MOS.

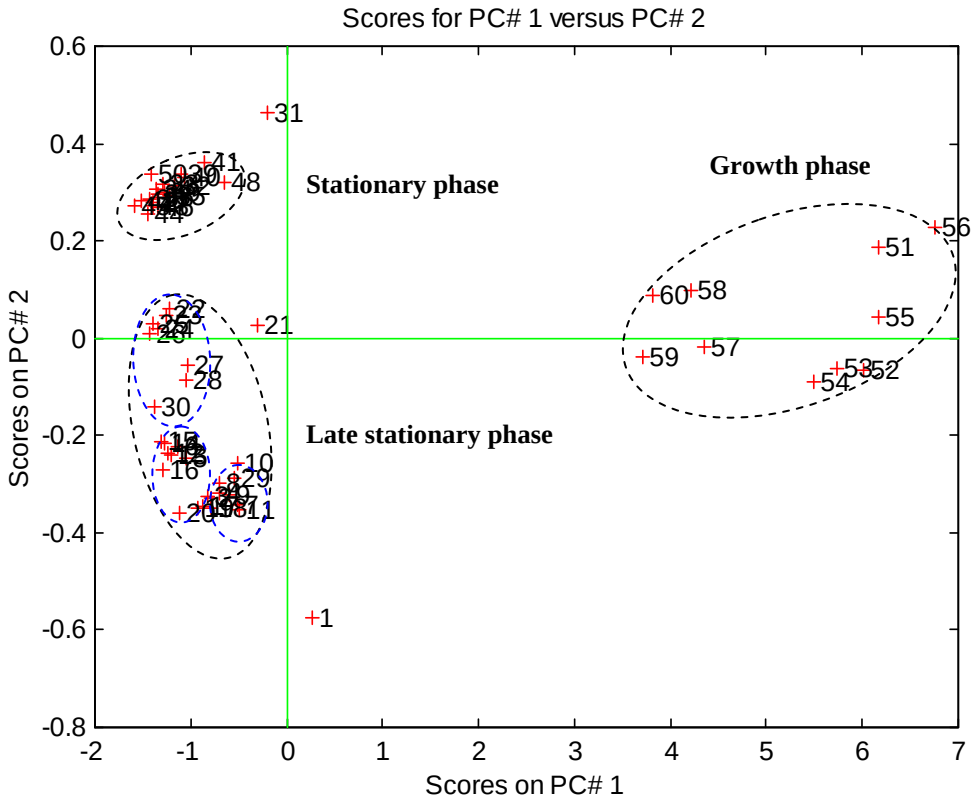

Fig. 5.17 PCA results of the response of a six-element (MOS) gas sensor based electronic nose to the headspace of cyanobacteria. The three growth phases are growth, stationary and late stationary. The response data were pre-processed by the normalised fractional difference model.

Figure 5.18 shows the corresponding PCA results of the response of a twelve-element (6 MOS + 6 CP) gas sensor based electronic nose to the headspace of cyanobacteria. Values of the MOS and CP sensor response signals are not comparable, hence standardisation and pre-processing are necessary. All six growth stages as well as the three growth phases are separated from each other. Interestingly, many of the first sample in each sequence, for example, No. 1, 11, 21, 31 in Figure

5.17 and Figure 5.18, showed discrepancies when compared with the others. This was also observed for commercial electronic noses and the HP 4440 chemical sensor (Chapter 6).

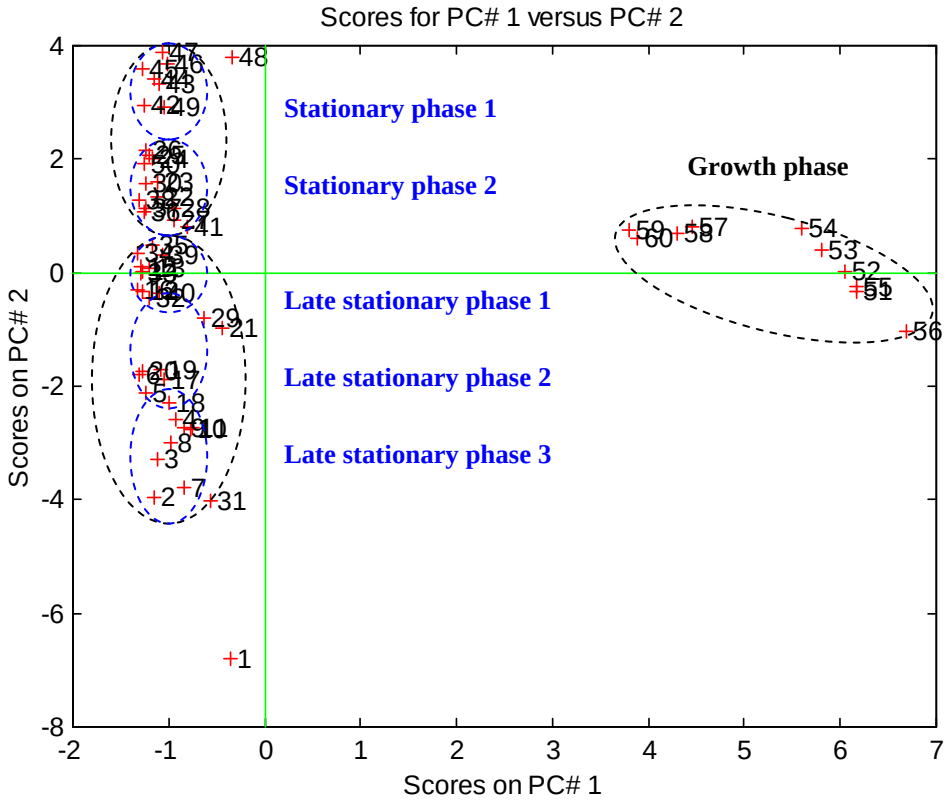

Fig. 5.18 PCA results of the response of a twelve-element (6 MOS + 6 CP) gas sensor based electronic nose to the headspace of cyanobacteria. The three growth phases are growth, stationary and late stationary. The response data were pre-processed by the normalised fractional difference model.

The first principal component accounts for 49.36%, the second for 41.89%, which shows that the first and second components are far more than the others. Table 5.3 shows the loadings that determine the correlation and prevalence of data. The same type of sensors exhibited relatively similar loading values compared to the others from different types of sensors. Following indications from Table 5.3 the

signals from 12 sensors can be reduced to seven or eight from a combination of MOS and CP sensors because similar non-zero values indicate strong collinearity.

Table 5.3 The eigenvectors of the correlation for the application of PCA to the normalised fractional difference model of cyanobacteria cultures. The variances in the principal components 1, 2 and 3 are 49.36%, 41.89%, and 7.21%, respectively.

Eigenvector, coefficient of the principal components	Principal component 1	Principal component 2
X_1	0.4064	-0.0413
X_2	0.4083	-0.0464
X_3	0.4037	-0.0769
X_4	0.4034	0.0315
X_5	0.4080	-0.0483
X_6	0.4086	-0.0335
X_7	-0.0325	-0.4261
X_8	-0.0280	-0.4246
X_9	-0.0698	-0.4270
X_{10}	0.0302	0.4182
X_{11}	0.0317	0.4345
X_{12}	0.0197	0.2793

5.5 Summary

The final modification of the electronic nose system was performed to produce a hybrid e-nose system. Using the newly modified system, data were gathered on six different cyanobacteria cultures for the classification of growth phase. All sensors including solenoid valves, gas sensors, temperature sensors, humidity sensor, and flow sensors were controlled satisfactorily using the computer software, LabVIEW. Overall the experiments were very reliable and the PCA showed excellent results.

Although a mono-type MOS sensor array was good for the simplicity of the electronic nose system (Chapter 4) it had the limitation of signal output for the broad spectrum of application.

The hybrid resistive nose based on 6 MOS and 6 CP sensors showed high resolving power to discriminate six growth stages as well as three growth phases. Thus it is expected that this further development of the electronic nose system will be applicable to a large number of environmental monitoring systems more effectively. It leads to greater flexibility with the general aim of improving the analytical performance of the total electronic nose system.

5.6 References

1. J.W. Gardner, and P.N. Bartlett, Electronic Noses, (Oxford Science Publications, (1999).
2. M. A. Craven, Bacteria classification with an electronic nose employing artificial neural networks, Ph.D. thesis, University of Warwick, UK (1997).
3. T.C. Pearce, Sensor-based Machine Olfaction: Instrumentation for the Analysis of Beer, Ph.D. thesis, University of Warwick, (1997).
4. N. Blair, The Development and Characterisation of Conducting Polymer Based Sensors for use in an Electronic Nose, Ph.D. thesis, (1994).
5. J. W. Gardner, T. C. Pearce, S. Friel, P. N. Bartlett and N. Blair, A Multisensor System for Beer Flavour Monitoring Using an Array of Conducting Polymers and Predictive Classifiers, Sensors and Actuators B, 18 - 19 (1994) 240 - 243.
6. P. Ingleby, Modelling and characterisation of conducting polymer chemoresistors, Ph.D. thesis, University of Warwick, UK (1999).

Chapter 6

Analysis of Odorous Headspace by Mass Spectroscopy

The hybrid sensor system [1, 2], comprising of a MOS sensor array and a CP sensor array, has lead to a system with larger flexibility (Chapter 5). This chapter describes the use of the Hewlett-Packard (HP) 4440 chemical sensor, including a modified HP 7694 automated headspace sampler, for the discrimination of various samples. These experiments were performed to help characterise the composition of the odorant headspace and relate its nature to the sensor data.

6.1 HP 4440 Chemical Sensor

Classical gas chromatography (GC)/mass spectroscopy (MS) techniques separate, quantify and identify individual volatile chemicals. The direct combination of high resolution gas chromatography with the mass spectrometer has become routine in chemical analysis and is usually PC driven with both the chromatograph and the mass spectrometer controlled from the keyboard [3, 4]. These systems are typically based on a simple quadrupole or ion trap analysers. They are fitted with modern turbo pumps or diffusion pumps, which can easily handle the flows from

conventional capillary columns without the need for any further interface device. Mass spectrometry [5, 6] is based upon the ionisation of solute molecules in an ion source, and the separation of the ions is generated on the basis of their mass/charge ratio by an analyser unit. Ions are detected by a dynode electron multiplier. Although gas chromatography (GC) is among the most important and powerful techniques in analytical chemistry with a wide range of applications, it requires a long time for precise data acquisition and analysis. For example, the flavour complexity of a larger required a run-time of 225 minutes, resulting in a total of 159 separately identifiable peaks [7]. The HP 4440 chemical sensor has no GC but it is a simple, fast and reliable sample screener, which comprises of a HP 7694 headspace autosampler, a HP 5973 mass selective detector (MSD) and Pirouette chemometrics software by Infometrix (Figure 6.1) [8].

Fig. 6.1 Photograph of the HP 4440A Chemical Sensor.

6.1.1 HP 7694 Headspace Autosampler

The autosampler provides a constant heating time for each sample to assure good reproducibility. Samples are placed into 10 or 20 ml vials and sealed with a crimp cap and a PTFE-coated silicon rubber septum. When 10 ml vials are used, spacers must be placed in the sample tray and the headspace oven (in all six positions). At least 1.5 cm at the top of the vial must remain empty to leave room for the headspace autosampler needle. All kinds of odorant samples can be analysed, e.g., water, foods, gases, bacteria, and soil. These samples are heated for between 5 and 30 minutes for the equilibrium at the range of oven temperature (40ºC–195ºC) depending on the samples. After equilibration, a needle pierces the septum, and the vial is pressurised with an inert gas, helium. The headspace vapour is then allowed vent back through the needle and a sampling loop.

6.1.2 HP 5973 Mass Selective Detector (MSD)

The volatiles from the headspace autosampler pass through the mass selective detector in 10-15 seconds. The vapour phase molecules are ionised and fragmented, and the charged fragments are drawn into an ion detector. The quadrupole mass sensor scans and monitors the ion detector's current, as a function of mass-to-charge ratio (m/z). Default mass sensor temperature settings are 150 °C for the quadrupole and 230 °C for the ion source. The mass sensor does not have a problem analysing samples with varying humidity levels, but autotuning of the mass sensor is required once a week to do a quality check on the responses of the mass sensor. The ionisation and fragmentation processes are reproducible to pinpoint certain ions.

6.1.3 Pirouette Chemometrics Software

When a set of samples has been analysed, the individual MS patterns are automatically appended to a single file with the extension .dat in preparation for multivariate data processing. The chemometrics software decides whether the sample's MS patterns match or differ significantly from the patterns of previously analysed samples. The Pirouette contains comprehensive data analysis tools such as Exploratory Analysis, the PCA and SIMCA algorithms, outlier detection, and model optimisation and validation. Exploratory analysis is the computation and graphical display of patterns of association in multivariate data-sets. Once a data-set is determined to be suitable, a multivariate algorithm is employed to create a pattern recognition model.

6.2 Experiments using HP 4440 Chemical Sensor

A HP 4440 chemical sensor was used to analyse various odorous samples. Table 6.1 lists the samples tested in the Sensors Research Laboratory (SRL).

Table 6.1 Sample types analysed by HP 4440 Chemical Sensor.

Samples analysed	No. of samples
Ground coffees from Costa Rica, Columbia and Kenya	42
Tap water, DI (de-ionised) water and BG-11 medium	9
Ethanol, methanol and yeast	15
Pure perforated compound (FC43)	6
Polyethylene (PE) pellets with 3 different odour levels	33
Cyanobacteria with different growth phases	35

Each sample was placed into a 10 or 20ml vial and heated in an oven for reproducibility. Standard chemical sensor methods and experimental sequences were

set up. The headspace autosampler was configured from a keypad on the front. Table 6.2 shows the autosampler parameters for coffee and cyanobacteria samples in water analysed.

Table 6.2 Experimental parameters of the headspace autosampler.

Parameter		Range and Condition	Set Value	
			Coffee	Liquid
Temperatures	Oven	40 to 195 °C	60 °C	40 °C
	Loop	200 °C max; 5-10 °C > oven	70 °C	50 °C
	Transfer line	220 °C max; 5-10 °C > loop	80 °C	60 °C
Pressure	Carrier gas	4-8 psi	2.5	4.5
	Vial	12-18 psi	14	16
Event times	HS cycle time	3-5 min; longer when vial equilibration time is long	4 min	
	Vial eq. time	> 10 min for solids and liquid volumes > 1 ml	15 min	
	Pressurisation time	0.10-0.50 min	0.30 min	
	Loop fill time	0.10-0.30 min	0.15 min	
	Solvent delay time	Pressurisation time + Loop fill time	0.45 min	
	Loop eq. time	0-0.10 min	0.02 min	
	Inject time	0.20-0.50 min	0.30 min	

6.2.1 Coffee Samples

For the first set of experiments, three kinds of ground coffee samples were placed into 10 ml headspace vials with a rubber septum. Each vial contained the same

weight (2 g) of coffee and underwent the same preconditioning steps. The vials were pressurised to 2.5 psi with the carrier gas for 0.3 minutes, and heated to 60°C for 15 minutes, in the internal oven of the autosampler. The headspace was transferred from the sampler to the quadrupole mass sensor through a heated transfer line. It is known that coffee has over 670 different compounds, which play a role in determining the coffee flavour [9]. The typical mass responses taken from three kinds of coffee and a blank vial are shown in figure 6.2, with 18 significant peaks.

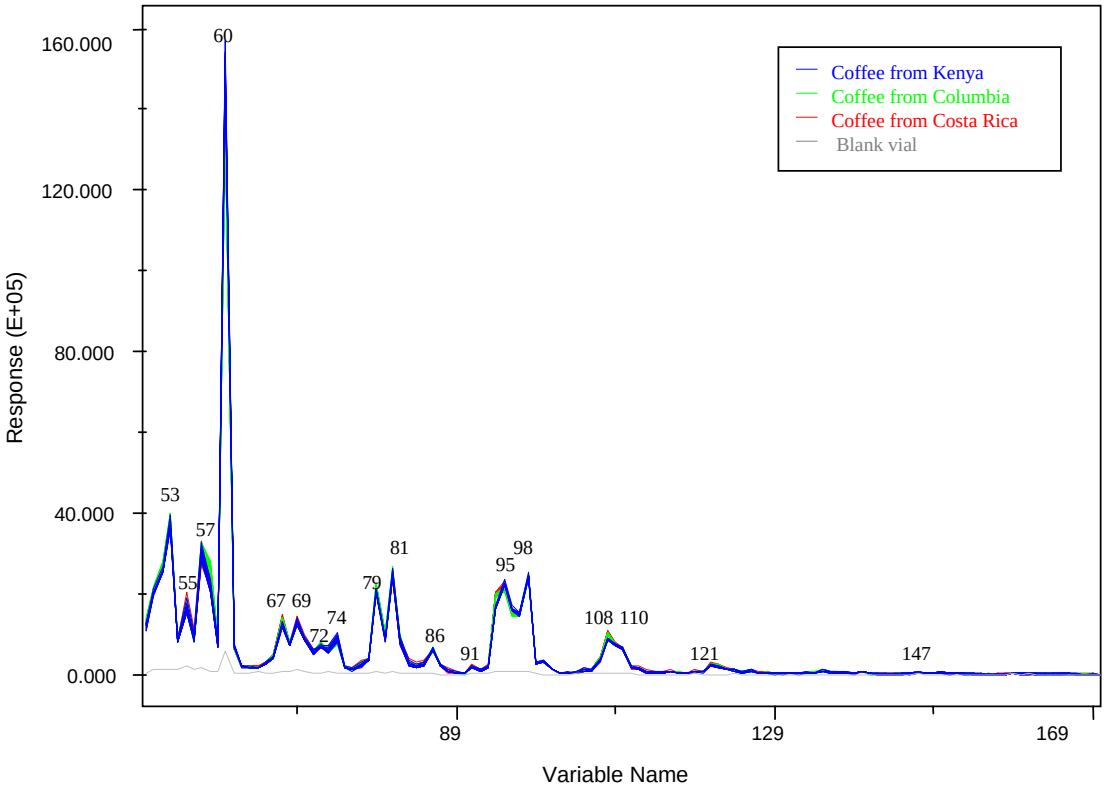

Fig. 6.2 Line plots of mass responses of 42 ground coffee samples and a blank vial.

A low mass value for the mass sensor was set to 50 to avoid signals from water (M = 18), air (M =28 or 32) and CO_2 (M = 44). From the mass responses, the graphical display patterns (Chapter 2) such as CA (cluster analysis) and PCA (principal components analysis) can be produced to explore and discriminate the

coffees. Figure 6.3 shows the analysis result of HCA (hierarchical cluster analysis) which facilitates the visual recognition of such categories.

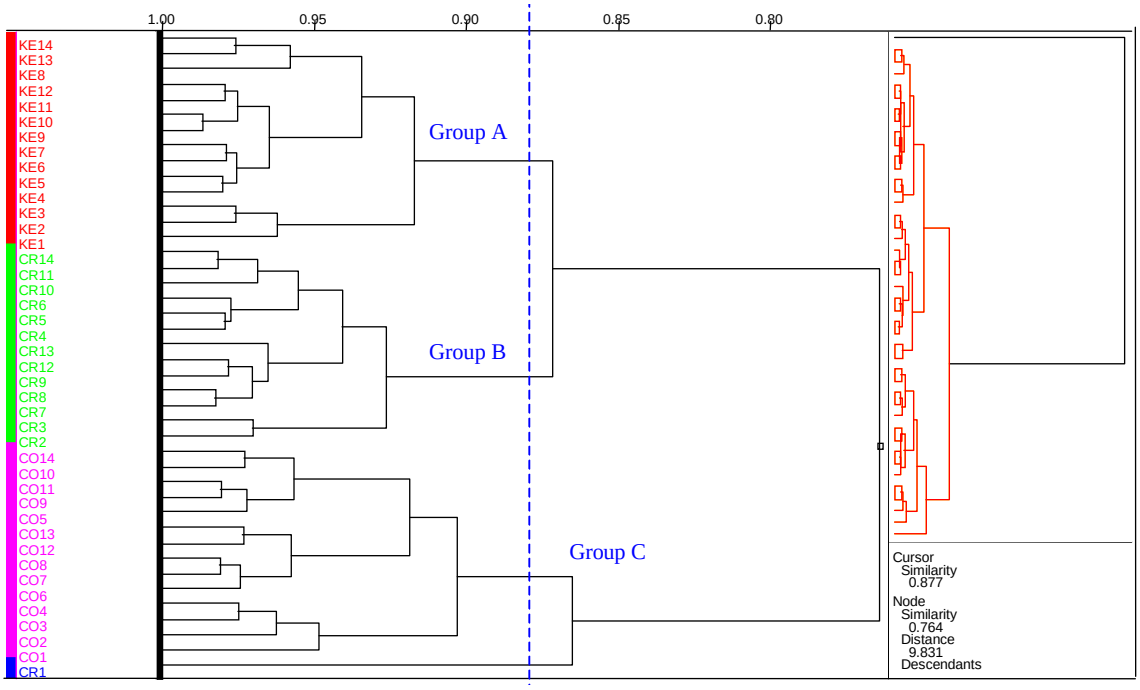

Fig.6.3 HCA result (Euclidean metric) for the classification of three kinds of coffee from Costa Rica (CR1 – CR14), Columbia (CO1 – CO14) and Kenya (KE1 – 14). Complete method was used for linkage. The first measurement CR1 was misclassified.

Each group of coffee is plotted in a different colour, emphasising category distinctions in the mass responses. The flavour complexity of the coffee was separated into single m/z (mass/charge) ratio's. The proximity is represented by a similarity index, which normalises the values to lie between 0 and 1 and takes a value of zero for the vectors furthest apart and a value of unity for identical vectors. Similarity is expressed in terms of inter-sample distances.

$$\text{Similarity}_{ab} = 1 - \frac{d_{ab}}{d_{max}} \quad (6.1)$$

where d_{max} is the largest distance in the data set (1 = identical samples, 0 = the most dissimilar samples) and d_{ab} is the multivariate distance between two sample vectors, **a** and **b**. When distances between samples are relatively small, this implies that the samples are similar. A complete link method was used for the linkage of samples. It is the farthest neighbour linkage, which assigns a sample to the cluster, whose farthest neighbour is closest to that sample. The distance between a newly formed cluster A-B and a previously existing cluster C is calculated as follows.

$$d_{AB\Rightarrow C} = 0.5d_{AC} + 0.5d_{BC} + 0.5\left| d_{AC} - d_{BC} \right| \quad (6.2)$$

Three kinds of coffee could be discriminated successfully but every first sample of a run sequence showed a discrepancy compared with the others when the sample positions were randomised. An outlier, Costa Rica 1, was the first sample of the run sequence. For outlier diagnostics, a Mahalanobis distance (MD) is computed from a k factor score of each sample:

$$MD_i = (\mathbf{t}_i - \mathbf{t})^T \mathbf{S}_k^{-1} (\mathbf{t}_i - \mathbf{t}) \quad (6.3)$$

where **S** is the scores covariance matrix and **t** is the mean score vector. If the MD of a sample exceeds a critical value MD_{crit} then the sample may be an outlier. The MD_{crit} can be determined from a chi squared distribution with k degrees of freedom in the

software package, Piroutte [10]. Figure 6.4 shows the results of the outlier diagnostics with two samples, CR1 and blank, lie in beyond the threshold.

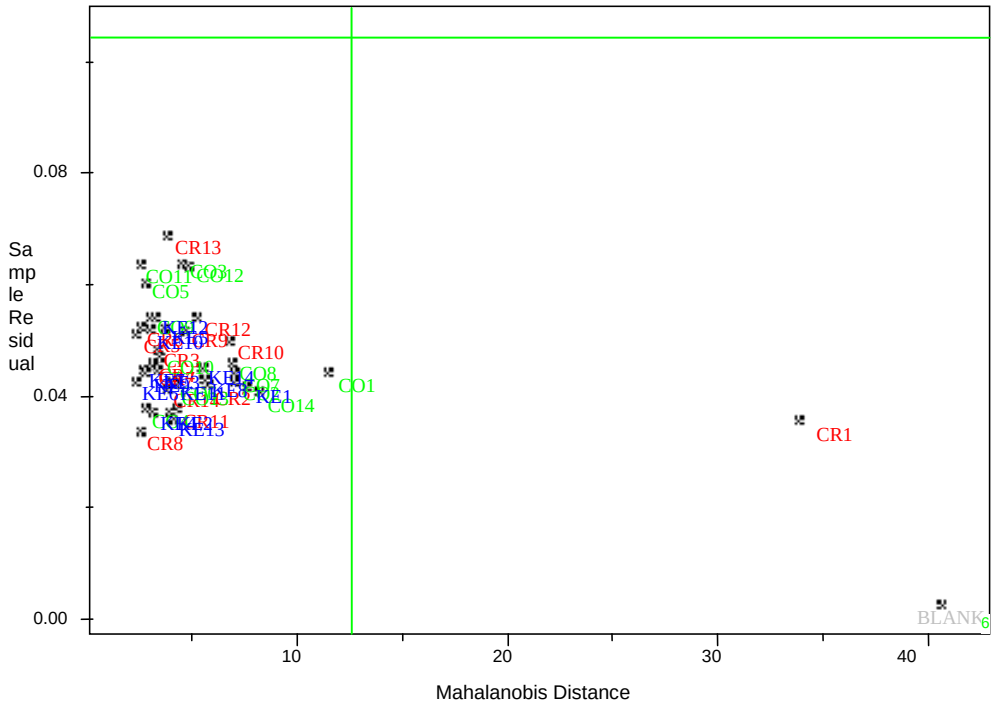

Fig. 6.4 Outlier diagnostics of Costa Rica (CR1 – CR14), Columbia (CO1 – CO14), Kenya (KE1 – 14) and a blank vial. The Mahalanobis distance (MD) was used as a diagnostic model.

Table 6.3 and figure 6.5 represent the PCA results for the normalised responses of the coffee samples. It can be seen clearly the boundaries between clusters. The first principal component accounts for 77.06% and the second for 18.89%, this shows that the first and second components have far more significance than the others.

Table 6.3 PCA results of the normalised responses of three different coffee samples; by ranking the PCs in order of the % of cumulative variance.

PC No.	Variance	Percent (%)	Cumulative percent (%)
1	1621.193970	77.059288	77.059288

2	397.386780	18.888758	95.948044
3	43.779938	2.080967	98.029007
4	19.878923	0.944893	98.973900
5	6.412197	0.304787	99.278687
6	4.242783	0.201670	99.480354

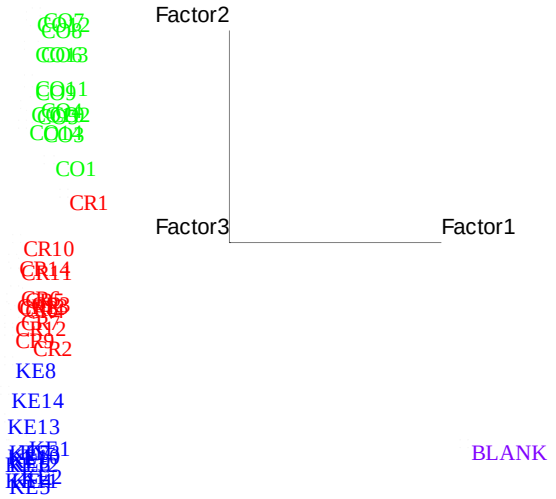

Fig. 6.5 PCA plots of normalised mass responses of three different coffee samples from Kenya (KE), Columbia (CO) and Costa Rica (CR).

Figure 6.6 plots the loadings that determine the correlation and prevalence of the coffee data. The 18 mass numbers which showed significant mass responses, in figure 6.2, have been distinguished from other mass numbers.

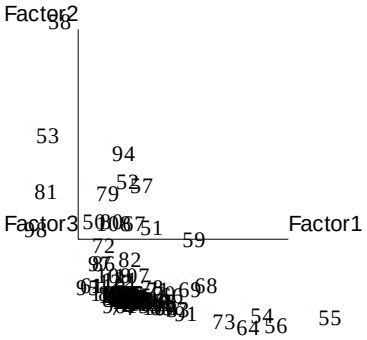

Fig. 6.6 Loading plot of normalised mass responses of three different coffee samples from Kenya (KE), Columbia (CO) and Costa Rica (CR) at the range of mass, 50 to 170.

This work was performed to ascertain a qualitative discrimination of different odour samples and to compare with the previous work using sensor arrays [11].

6.2.2 Water Samples

This experiment was performed to discriminate between a number of non-volatile water samples. Three water samples (5 ml each) of tap water, DI (de-ionised) water and BG-11 medium, were poured into 20 ml headspace vials, with a rubber septum. The vial pressure was set to 14 psi and the oven temperature 40°C. The headspace was finally transferred from the sampler to the quadrupole mass sensor through the heated transfer line.

Figure 6.7 shows the 2D PCA results of the analysis. DI water and BG 11 medium categories were mixed on the PCA plot. It was difficult more to discriminate these two water samples than the coffee samples because of non-volatile components in the water. The mass range for scanning was 45 to 200, thus the scanning rate was 8.39 scans/sec.

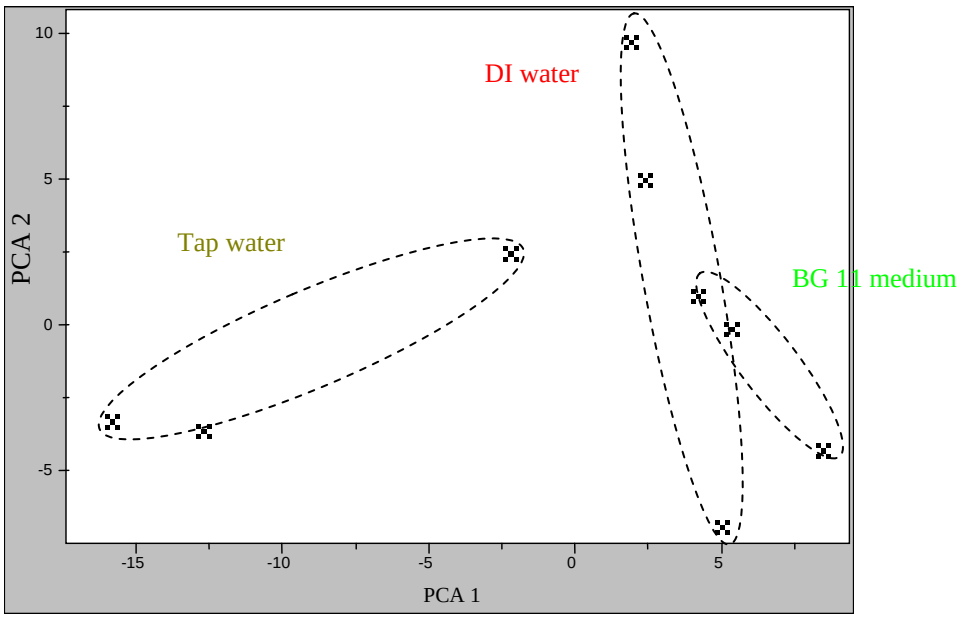

Fig. 6.7 PCA plots of mass responses of three water samples, tap water, DI water and BG-11 medium.

6.2.3 Ethanol, Methanol and Yeast Culture

Mass spectroscopy was used to discriminate ethanol, methanol and yeast culture. A low mass number was set of 30 to get mass responses of pure ethanol (M = 46) and methanol (M = 32). Figure 6.8 shows the line plot of mass responses and the PCA result. Each type of chemical sample was plotted in a different colour and grouped on a PCA plot.

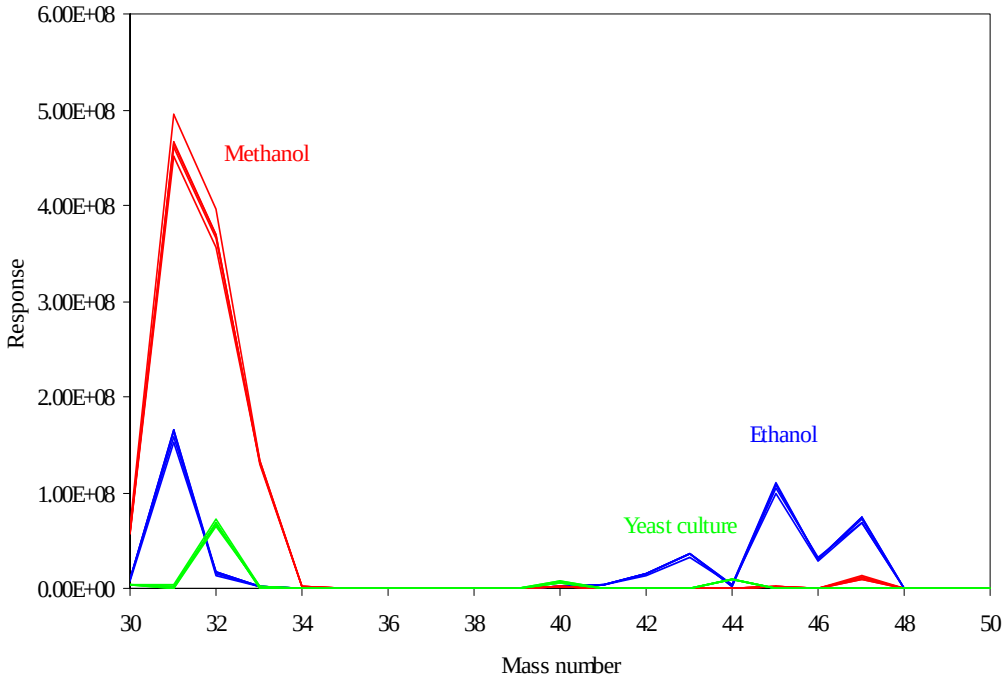

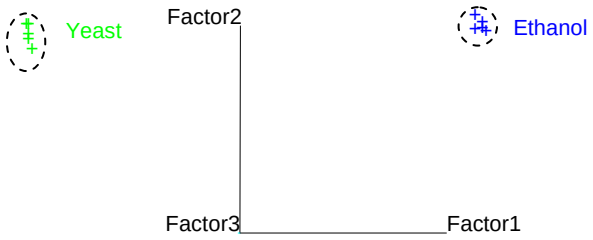

Fig. 6.8 Results of mass responses and PCA analysis of ethanol, methanol and yeast culture.

Pre-processing was set to the mean-centre, in the algorithm options and the raw mass responses were normalised. A mean-centre, $x_{ij(mc)}$, was produced with mean value, $\bar{x}_j$.

$$x_{ij(mc)} = x_{ij} - \overline{x}_j \tag{6.4}$$

Samples can be easily visualised by mean-centring. This process shifts the origin of data without altering relative inter-sample relations. The normalisation used is a vector length normalisation:

$$f_i = \sqrt{\sum_j^N x_{ij}^2} \tag{6.5}$$

where f_i is the normalisation factor for the *i*th sample and *N* is the number of feature vectors. Raw mass responses were normalised so that a sample's largest feature was equal to 100. The PCA results of these samples were extremely clear and reproducible here (see Fig. 6.8).

6.2.4 Pure Perforated Compound (FC43)

The analysis of the pure perforated compound (FC43) containing 10 μl of PFTBA, was performed over a two days period. These samples were provided by Alpha MOS (France) for reliability tests. The vials were pressurised to 3 psi of the carrier gas, for 0.3 minutes, the vials as components of the headspace autosampler reached stable conditions by heating the sample to 40 °C for 2 minutes. The headspace was finally transferred from the sampler to the quadrupole mass sensor through a heated transfer line. The low mass value for the mass sensor, was set to a higher value than 44, to avoid signals from water, air and CO_2. The highest mass

value was 505, with a scanning rate of 3.18 scans/sec. Mass sensor responses (No. of ions) were converted into a spectral view, as shown in figure 6.9.

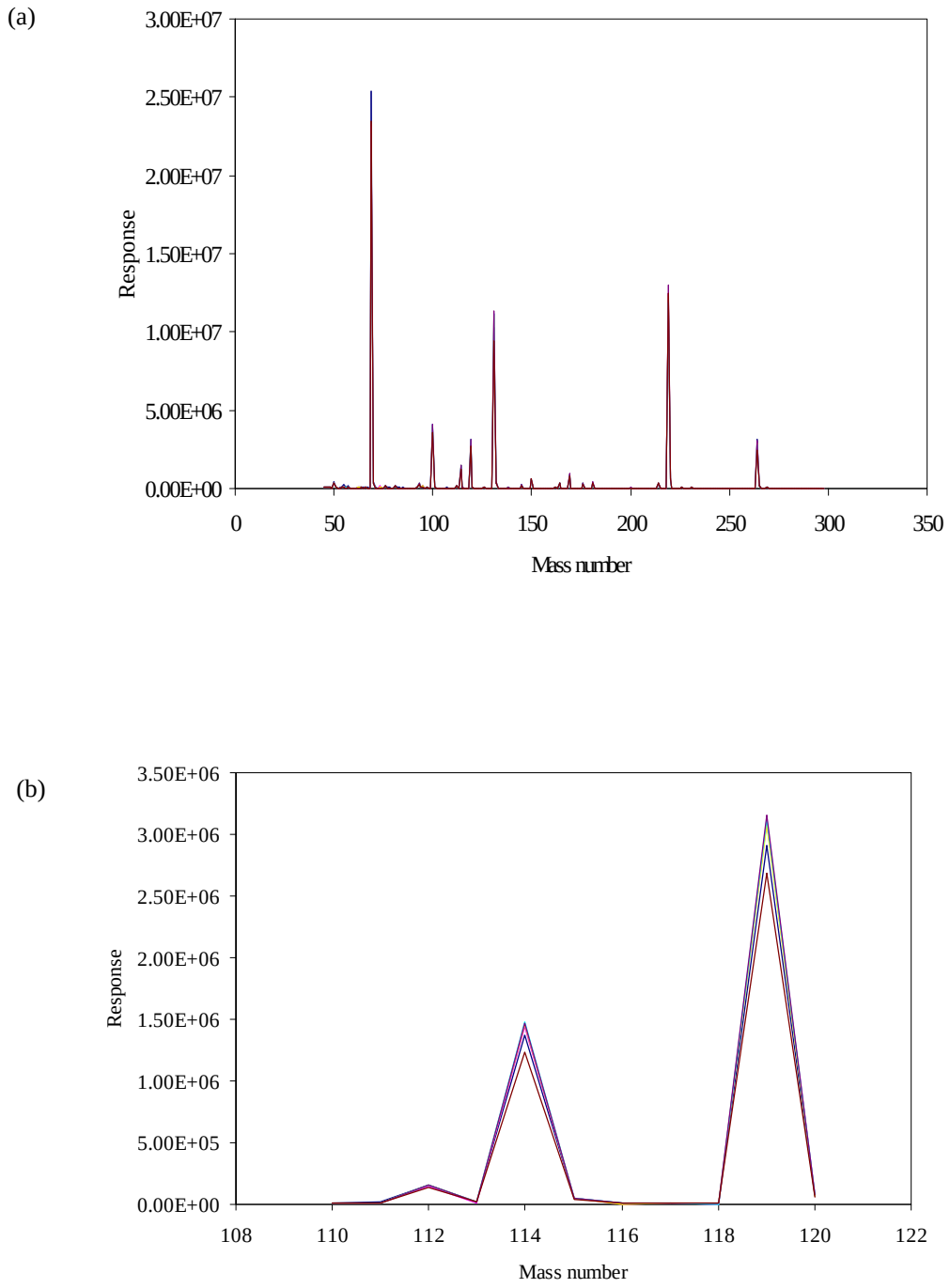

Fig. 6.9 Line plots of mass responses of 6 FC43 samples. (a) Line plot at mass range, 45-350, (b) the magnified line plot at mass range, 110-120.

The overlying line plots are fairly homogeneous and do not show outliers. Figure 6.9(b) shows the line plots of the mass responses for 6 FC43 samples with good consistency at mass ranges, 110 to120.

6.2.5 PE (polyethylene) Pellets with 3 Different Odour Levels

These sets of experiments are designed to test the quality of polyethylene for the packaging industry. Many volatile additives in PE pellets are combined with polymer to give the material specific properties, which can impart unpleasant odours to the final product. Three kinds of PE pellet (2 g) were provided by Alpha MOS and were filled in 10 ml headspace vials with a rubber septum. Three kinds of samples were previously classified to three different odour levels by a sensory panel. The optimal temperatures of the oven, loop and transfer line were 100, 105 and 110°C, respectively. The mass range for scanning was 45-200 and the scanning rate was 8.39 scans/sec. Sampling positions were randomised as for the previous experiments.

Fig. 6.10 shows the abundance and PCA plots of mass responses of PE pellets, with 3 different odour levels. The line plot shows about 10 significant peaks of mass responses. The top 10 masses were 48, 55, 57, 64, 69, 71, 77, 83, 85 and 94. The PCA results showed a good repeatability and all samples were successfully grouped associated with different odour levels in PE pellets, as shown in Figure 6.10(b). It demonstrates that the HP 7694 headspace autosampler provides repeatable headspace conditions and the HP chemical sensor can be used to assess the quality of packaging material, polyethylene associated with odour levels.

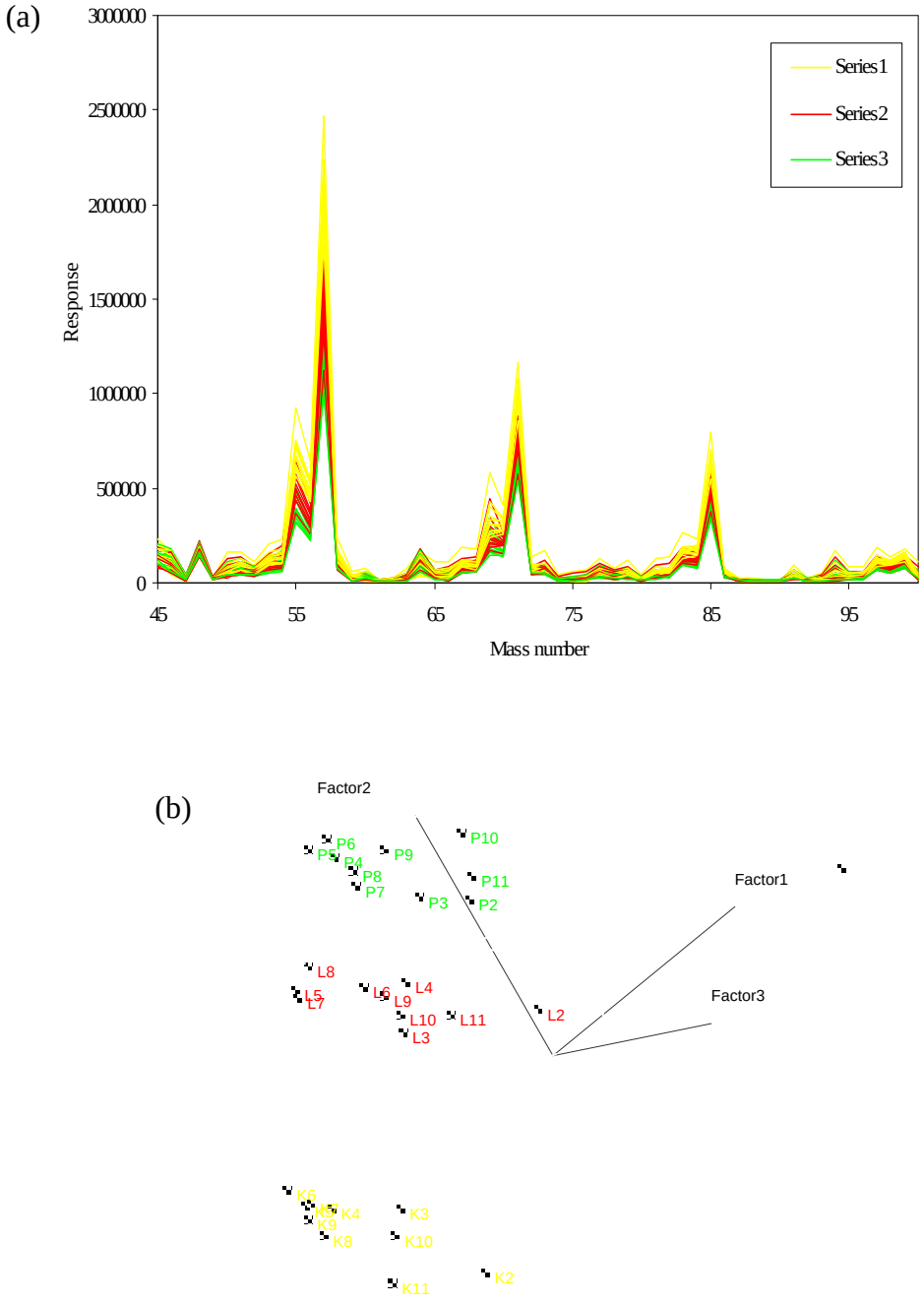

Fig. 6.10 Abundance and PCA plots of mass responses of PE pellets with 3 different odour levels. (a) Line plot of mass range, 45-100 (b) PCA plot.

6.2.6 Cyanobacteria with Different Growth Phases

The HP 4440 was used to discriminate cyanobacteria with different growth phases. The same cultures used in the electronic nose (Chapter 5) were used again hence have same profiles on analysis of the toxic cyanobacteria samples according to the number of cells and size as shown in fig. 6.11. Numbered captions represent the dates inoculated from the master culture. Phases a (27/5/99), b (3/6/99) and c (10/6/99) were late stationary phases. Phase d (17/6/99) and e (24/6/99) were stationary phases and phase f (28/6/99) was a growth phase. There was no lag phase among these samples because the cultures inoculated grew so quickly in early summer.

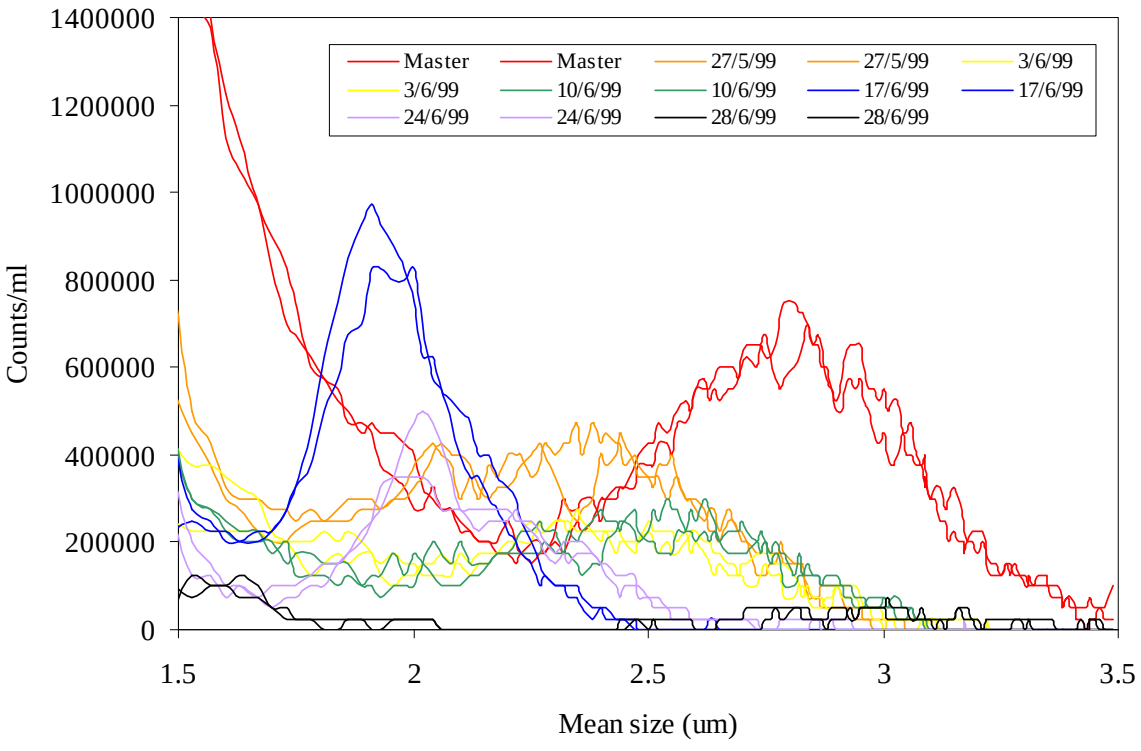

Fig. 6.11 Plot of the number of cells against cell size in 1 ml of toxic cyanobacteria sample.

First of all, pre-scanning of the cyanobacteria sample was performed at the range of mass number, 45-550 (Figure 6.12). Most of the big mass responses were detected at the range of mass values, 45-130. Low mass values ≥ 45 was to avoid signals from water (M = 18), air (M = 28 or 32) and CO_2 (M = 44).

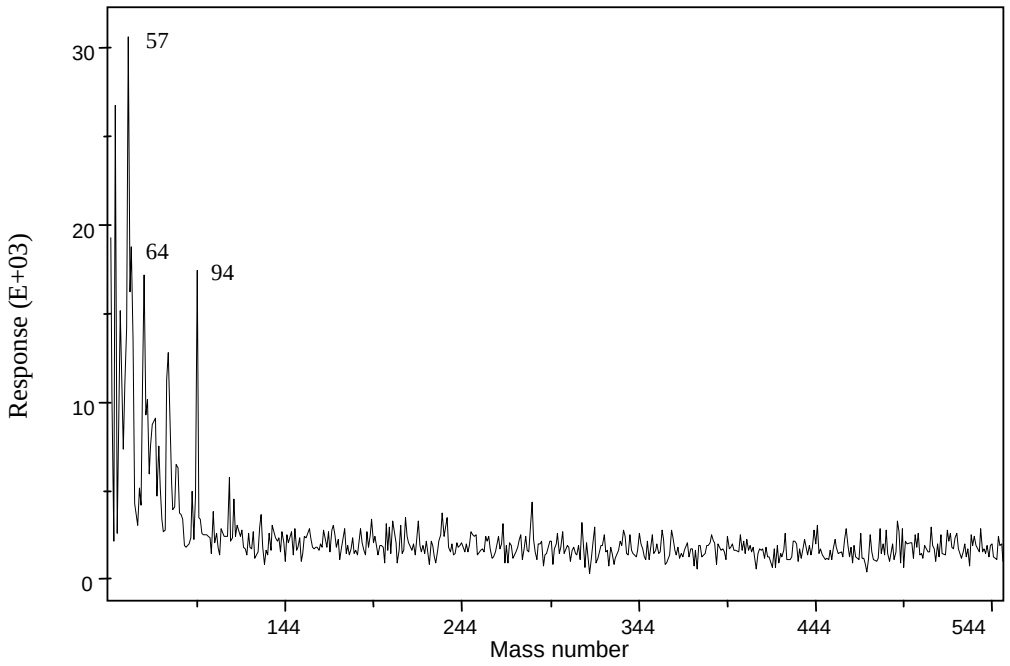

Fig. 6.12 Line plot of raw mass responses of cyanobacteria.

Figure 6.13 shows the line plot of the raw mass responses from the cyanobacteria with 6 different cultures. Each growth culture of the cyanobacteria is plotted in a different colour, emphasising category distinctions in the mass responses as shown in Figure 6.13. From the line plot of the raw mass responses of the cyanobacteria, a 2D multiplot can be plotted to reveal correlations between variables. Figure 6.14 shows the 2D multiplot indicating many 2D bi-variable combinations of mass numbers (48, 50, 54, 57, 64, 68, 73). The Cyanobacteria cultures showed distinctive responses at these mass numbers throughout the experiments. Two subplots, 54 vs 64 and 64 vs 94, are highly correlated.

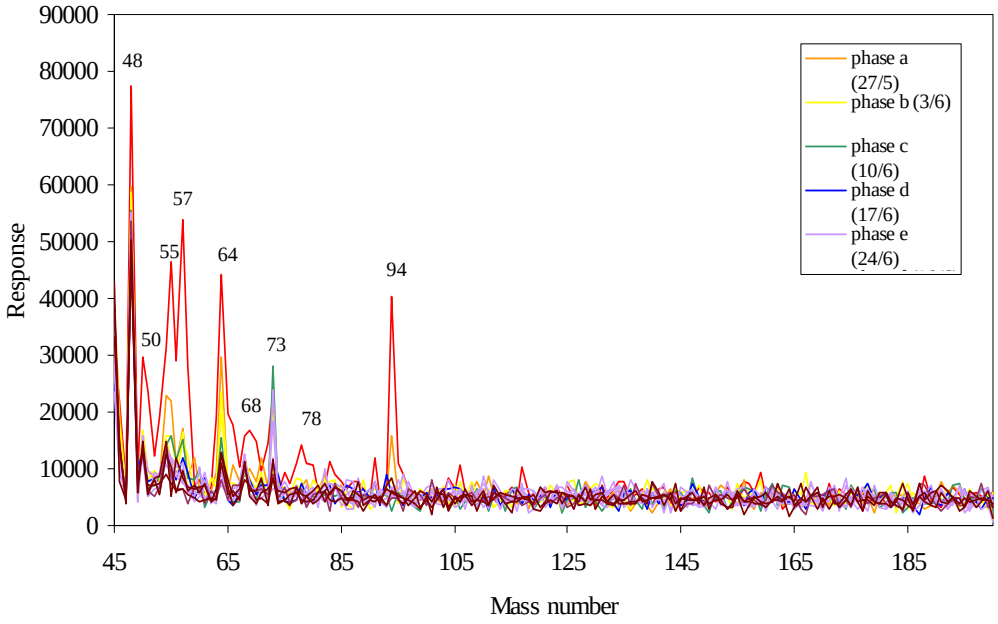

Fig. 6.13 Line plot of raw mass responses of cyanobacteria with 6 different cultures, a to f.

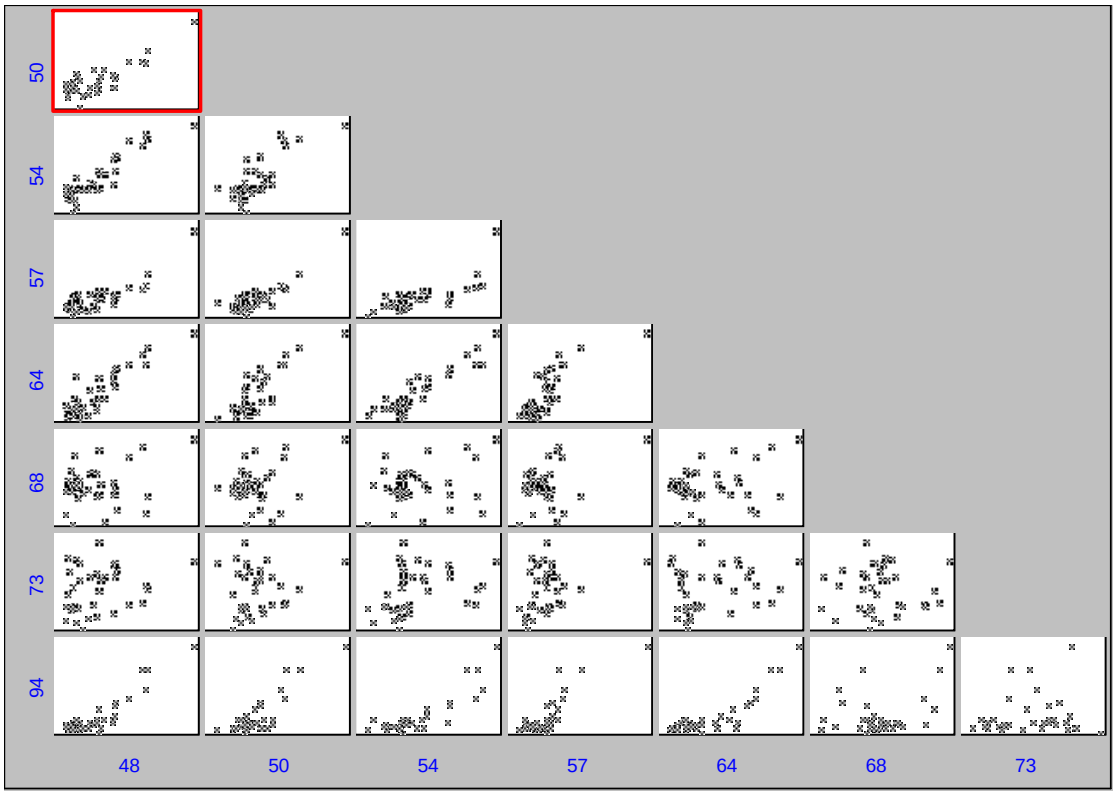

Fig. 6.14 Multiplot with correlated mass numbers in several subplots.

Figure 6.15 and Table 6.4 show the PCA results of the normalised mass data from analysis of the headspace of cyanobacteria. The number of samples per different culture was five. The first principal component explains 30.66% of the total variance and less than 60% of the variance is captured by the first 5 principal components. The PCA results after vector length normalisation exhibited good discrimination without overlap between three phases, growth phase, stationary phase, and late stationary phase but a full separation of two stationary phases, d (17/6/99) and e (24/6/99), was not clear as shown in Figure 6.15. These results were not so good compared the PCA results of the response of the sensor- based electronic nose (section 5.4).

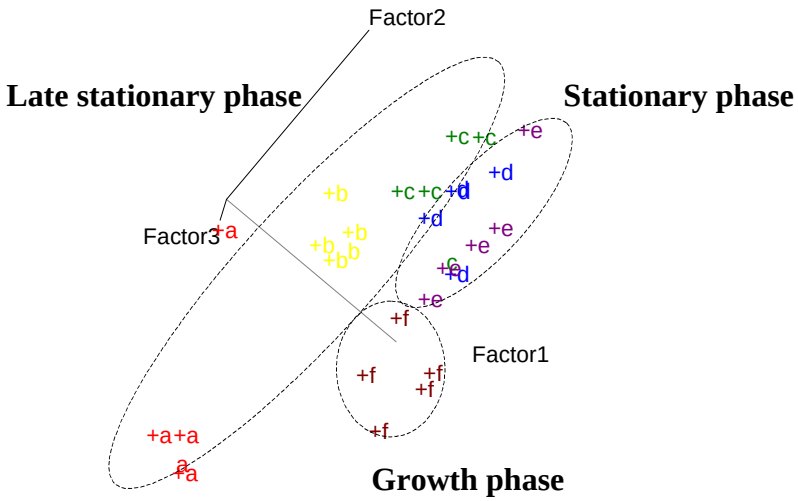

Fig. 6.15 PCA plot of cyanobateria samples with 6 different cultures.

Table 6.4 PCA results of the normalised responses of six different cyanobacteria cultures by ranking the PCs in order of the % of cumulative variance.

PC No.	Variance	Percent (%)	Cumulative percent (%)
1	5334.003906	30.657776	30.657776
2	2552.285400	14.669542	45.327316
3	1367.602539	7.860446	53.187763
4	585.344788	3.364334	56.552097
5	575.312927	3.306674	59.858772

Figure 6.16 shows the results of the outlier diagnostics by Mahalanobis distance and the first sample a lies beyond the threshold.

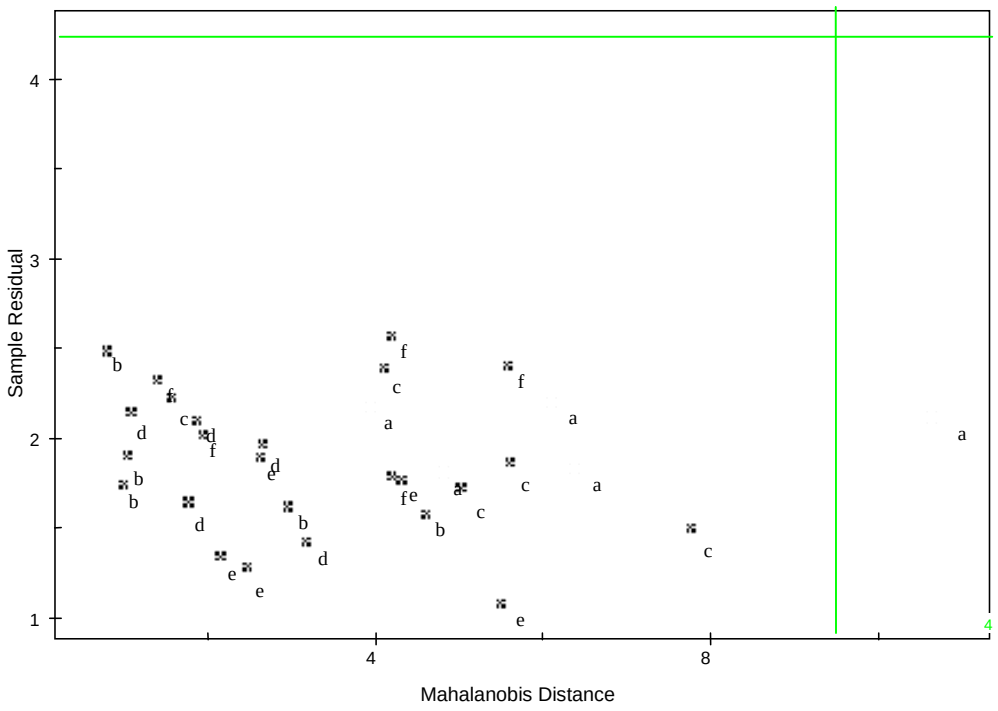

Fig. 6.16 Outlier diagnostics of 6 different cyanobacteria cultures, a to f.. The Mahalanobis distance (MD) was used as a diagnostic model.

Figure 6.17 shows the 2D and 3D plots of the loadings of the cyanobacteria data. The 18 mass numbers were distinguished from the other mass numbers. These significant 18 masses were used to improve the PCA analysis for the discrimination of six different cyanobacteria cultures.

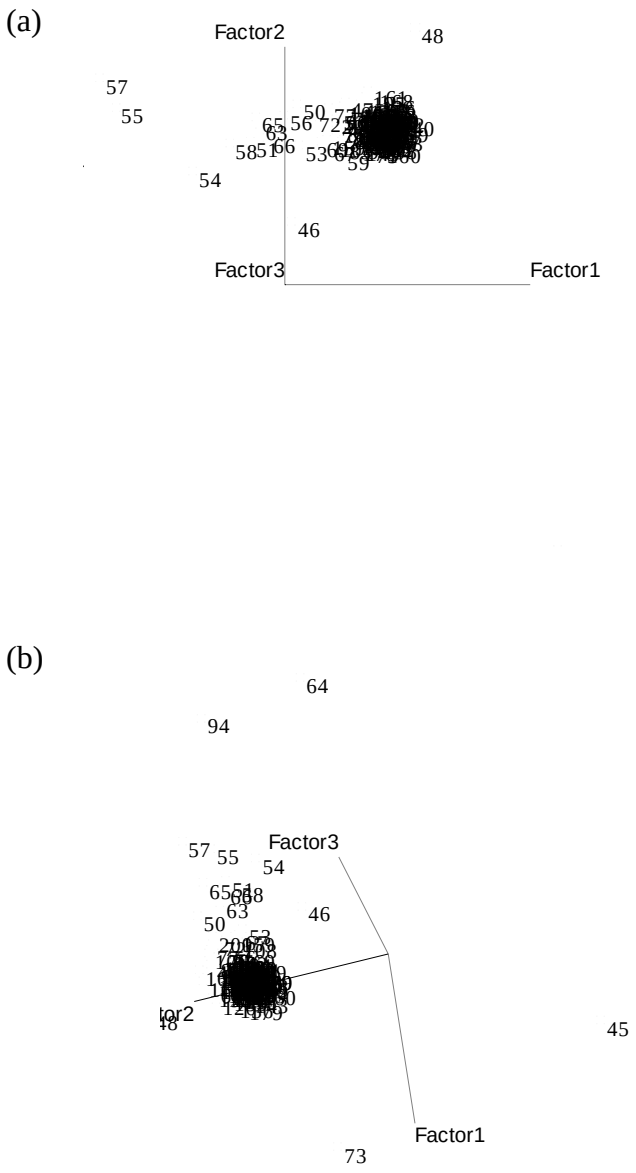

Fig. 6.17 (a) 2D and (b) 3D plots of loadings of cyanobacteria data.

Figure 6.18 and Table 6.5 show the PCA results of six different cyanobacteria cultures using 18 masses (45, 46, 48, 50, 53, 54, 55, 56, 57, 58, 59, 63, 64, 65, 66, 68, 73, 94) only. The first 5 principal components explained 84.14% of the total variance. The PCA results (fig. 6.18) were improved to discriminate six different growth stages due to the decrease of the noise level using 18 significant masses only.

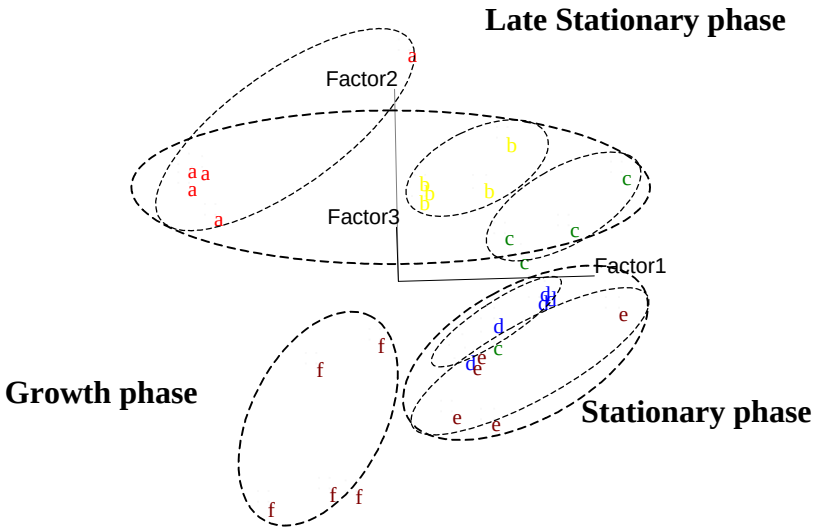

Fig. 6.18 PCA plot of 6 different cyanobateria cultures using 18 masses only.

Table 6.5 PCA results of the normalised responses of six different cyanobacteria cultures using 18 masses by ranking the PCs in order of the % of cumulative variance.

PC No.	Variance	Percent (%)	Cumulative percent (%)
1	2811.507080	35.027863	35.027863
2	1989.381714	24.785210	59.813072
3	1348.818970	16.804598	76.617668
4	334.488953	4.167315	80.784981
5	269.216675	3.354103	84.139084

Finally, the same six different cultures were used again in a mass analysis to see the repeatability after the first experiment. The cyanobacteria cultures in vials were changed in the oven (40ºC) after first run of mass analysis, therefore showed different mass responses during the second run of mass analysis as shown in figure 6.19. Therefore it was not possible to classify different growth phases for the second test. All samples seemed to turn to the identical stage, the death phase, which shows only two main peaks at mass numbers 73 and 143. Therefore careful sample treatment and analysis are required for thermally sensitive samples such as cyanobacteria in water.

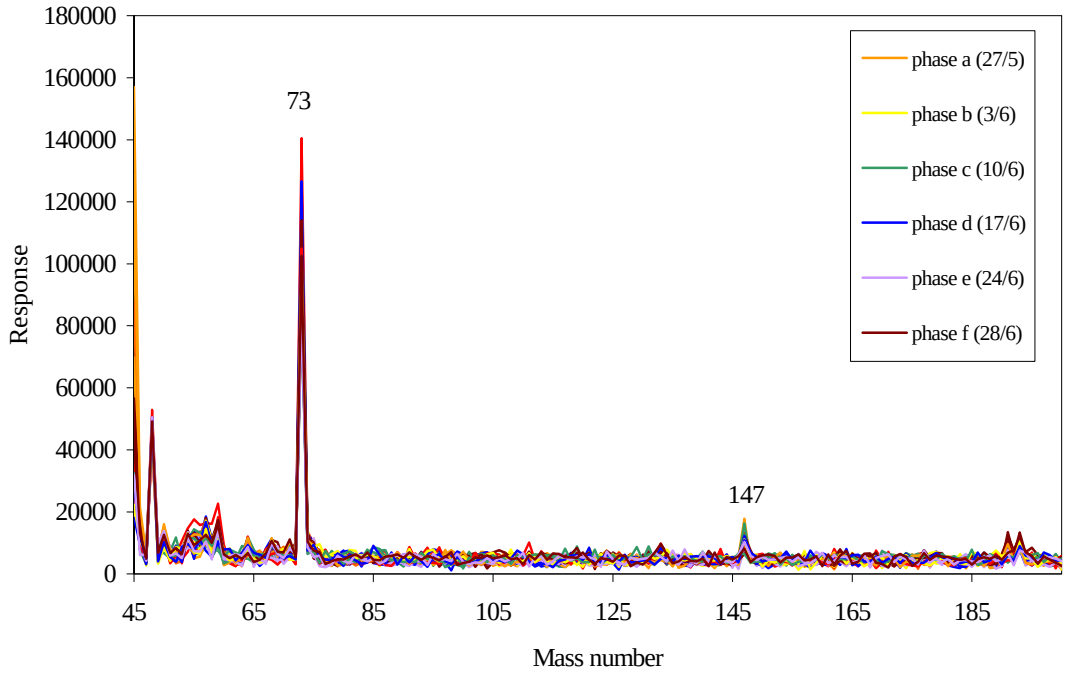

Fig. 6.19 Line plot of mass responses of cyanobacteria with 6 different cultures, a to f. This is the result from the second run of mass analysis with the same samples.

6.3 Summary

In this chapter the HP 4440 chemical sensor was used to discriminate various samples and compare with the sensor-based electronic nose.

The HP 4440 chemical sensor and the electronic nose use different sensing techniques but the PCA results for the mass sensor showed similar PCA results of the response of a six-element (MOS) gas sensor based electronic nose. The hybrid resistive nose based on 6 MOS and 6 CP sensors showed better resolving power to discriminate six growth stages as well as three growth phases compared to the HP 4440 chemical sensor (section 5.4). These investigations highlight a relationship between cyanobacteria culture and odour, since the strain and growth phase of the cyanobacteria could be predicted from the headspace of culture in water. Whilst the mass analyser detects individual volatile chemicals accurately, it proves no indication of whether the volatile substance is an odour (section 2.2.1).

The mass spectrometry-based sensor system is becoming a key approach to odour analysis. However, its use is highly dependent on application. The mass selective detector also needs regular autotuning to maintain optimal conditions and the photomultiplier voltage should be within set tolerance levels. Although this instrument-based analysis measures only one aspect of the quality of odour, it can improve and confirm the capability of the electronic nose system if it can be closely correlated to the odorant headspace.

6.4 References

1. H. Ulmer, J. Mitrovics, G. Noetzel, U. Weimar, and W. Göpel, Odours and flavours identified with hybrid modular sensor system, Sensors and Actuators B, 43 (1997) 24-33.
2. J.W. Gardner, and P.N. Bartlett, Electronic Noses, (Oxford Science Publications, (1999).
3. R. L. Grob, Modern practice of gas chromatography, John Wiley & Sons Inc. (1995).
4. I. A. Fowlis, Gas Chromatography, John Wiley & Sons Inc. (1995).
5. R. Brymner, and J. R. Penney, Mass Spectrometry, Butterworth & Co. Ltd. (1967).
6. C. A. McDowell, Mass spectrometry, MaGraw-Hill Book Co, Inc. (1963).
7. T. C. Pearce, Sensor-based machine olfaction: Instrumentation for the analysis of the flavour of beer, PhD thesis, University of Warwick, UK, (1997).
8. The HP 4440 Primer, Hewlett-Packard Company, (1998).
9. C.-T. Ho, H.-I. Hwang, T.-H. Yu, and J. Zhang, An overview of the Maillard reactions related to aroma generation in coffee, Proceedings of 15th International Scientific Colloquium on Coffee, Vol. II (1993) 519-527.
10. Piroutte: Multivariate data analysis for window 95/98 and NT, Infometrix, Inc., (1998).
11. T. Aishima, Aroma discrimination by pattern recognition analysis of responses from semiconductor gas sensor array, J. Agric. Foof Chem., 39 (1991) 752-756.

Chapter 7

Conclusions and Future Work

7.1 Conclusions

The main objective of this research was to develop a hybrid electronic nose system suitable for monitoring the quality of potable water. A special goal was the classification and early warning of toxic cyanobacteria in water. The approach taken to discriminate not only different strains, but also the growth phase, of cyanobacteria involved the investigation of both MOS and polymer sensor technology and neural network analysis. Previous work at Warwick had shown the potential of an electronic nose to detect micro-organisms based upon their gaseous headspace. This real-time analysis, including on-line monitoring, is of importance in the natural environment. This research highlights the potential importance of the electronic nose employing gas sensors for the monitoring of environmental problems such as water enrichment.

A number of different gas sensor technologies, signal processing and PARC techniques were investigated. The response of two prototype research-based silicon devices, SRL 125/MOS and IDC 10, were characterised with an automated gas sensor test system. The results were encouraging, with respect to the detection of CO, and low-power consumptions of micoheaters, 75 mW (SRL 125/MOS) and 60 mW (IDC 10) at

300 °C. The fast thermal response permits the use of a pulsed-mode operation and hence lower average power of *ca*. 1 mW. These silicon devices offer a low-cost option, due to the use of standard silicon fabrication techniques, and operation within a battery-powered hand-held instrument.

MOS thick-film gas sensors have very good sensitivity, stability and are relatively easy to make. CP gas sensors are readily grown by electrochemical polymerisation and operate at room temperature with fast reversible change in conductivity. MOS and CP sensors were employed in the hybrid sensor system, because of their attractive characteristics. Pre-processing techniques were able to reduce the sampling errors and base-line drift of the sensors, and so optimised the classification process. Autoscaling and array normalisation were employed to give equal weighting to each sensor and thus compensated for the absolute differences in the magnitudes of the signals. PCA was chosen to explore clusters within the data. It is a most effective classical statistical method to show the visualisation of pattern recognition before neural networks. The artificial neural network was biologically inspired from studies of neural organisation in the brain. Three supervised classifiers, MLP, LVQ and Fuzzy ARTMAP neural networks were used and compared in the classification of both the strain and growth phase of the cyanobacteria grown in water.

The desire to monitor on-line the growth phase of cyanobacteria culture led to the construction of an automated measurement system. It consists of three main stages: the odour sampling system, an electronic nose and a Cellfacts instrument that analyses liquid samples. The temperature of the main chamber varied by around ±0.1 °C during the test and it was found to have a negligible effect on the classification results. All sensors including solenoid valves, gas sensors, temperature sensors, the humidity sensor, and flow sensors were controlled using a commercial computer

software package, LabVIEW (National Instrument Inc.). The software was structured with a main Virtual Instrument (VI) capable of calling and dismissing the sub VIs. Finally, a HP 4440 chemical sensor (Hewlett-Packard) was used to validate the electronic nose results. The main results of cyanobacteria experiments are as follows.

7.1.1 A Six-element Metal Oxide based E-nose

The Warwick e-nose has been used for the continuous monitoring of the growth of cyanobacteria over a period of 40 days. The normalised fractional difference method gave the best PCA result. Three supervised neural networks, multi-layer perceptron (MLP), learning vector quantization (LVQ) and Fuzzy ARTMAP were used to classify both strain and different growth phases of cyanobacteria (i.e. lag, growth, stationary and late stationary). Conventional water analysis takes several days to classify toxic and non-toxic strains of cyanobacteria but the electronic nose was able to classify two different strains in a few hours. The best results show that the toxin strain of cyanobacteria was correctly predicted with an accuracy of 100%, and that the accuracy of MLP, LVQ and Fuzzy ARTMAP algorithms with 4 different growth phases of toxic cyanobacteria was 92.3 %, 95.1 % and 92.3 %, respectively.
The number of training iterations of Fuzzy ARTMAP was found to be typically more than an order of magnitude less than those for the MLP and the LVQ networks. Therefore Fuzzy ARTMAP gave the best performance overall. Unfortunately, the performance of the generalisation was not so good and the classification rate for LVQ and Fuzzy ARTMAP was 70%. It was difficult to recognise the growth phase of an unknown culture that had a different trend from other cultures used for training. The majority of the classification error is associated with the different growth trend of the

cyanobacteria culture, and so it could be reduced significantly if the neural network was trained on-line.

7.1.2 A Hybrid E-nose based on 6 MOS and 6 CP

Although a mono-type MOS sensor array was found to perform well, it does have limitations of signal output for the broad spectrum of applications. Therefore a mixed or hybrid array comprising different types of sensor, 6 MOS and 6 CP, was also investigated. The final modification of the Warwick electronic nose system was performed to produce a hybrid e-nose system. Using the newly modified system, data were gathered on six different cyanobacteria cultures, for the classification of growth phase. Overall the experiments were very reliable and the PCA showed excellent separation. The hybrid resistive nose based on 6 MOS and 6 CP showed high resolving power to discriminate six growth stages as well as three growth phases. Even though time did not permit many series of the continuous monitoring, because of the relatively long life span (30–40 days) of cyanobacteria, improved results proposed the use of a multi-sensor array rather than MOS sensor array only. It would be expected that this hybrid e-nose should be applicable to a large number of environmental monitoring more effectively and leading to a larger flexibility in the determination of independent sensor responses of the total electronic nose system.

A HP 4440 chemical sensor was also used for the discrimination of six different cyanobacteria samples and the comparison with the electronic nose was made. The results showed some ability to classify the cyanobacteria cultures. The PCA results from the mass spectra were very similar to the results obtained from a six-element (MOS) gas sensor based electronic nose. The hybrid resistive nose based on 6 MOS and 6 CP sensors showed the better resolving power to discriminate six

growth stages as well as three growth phases rather than the HP 4440 chemical sensor.

This work reports the first major study of the use of an e-nose to monitor water enrichment. The main research objectives have been achieved successfully. These investigations highlight a clear relationship between a cyanobacteria culture and its headspace, since the strain and growth phase of the cyanobacteria could be predicted from a headspace analysis. The HP 4440 chemical sensor confirmed the capability of the Warwick hybrid e-nose for a broad spectrum of applications in the water industry. It can be concluded that e-nose technology can be applied to analysing potable water quality.

7.2 Future Work

This work can be extended in the following manner:

- A hybrid e-nose for the continuous monitoring of microbial situations: The improved hybrid e-nose could be used for the continuous monitoring of human pathogens such as *Staphylococcus* as well as toxic cyanobacteria. The HP 4440 chemical sensor could be used to collect useful data and confirm the results of the hybrid e-nose.

- Development of an intelligent portable e-nose using thin film sensor arrays: A low-power interface ASIC chip and thin film sensor array could provide the development of an intelligent portable e-nose. This would need MOS and CP silicon sensors.

- Portable e-nose for the detection of real samples in lakes or water reservoirs: Portable e-nose should be applied for the detection of real samples in their natural environment.

- Development of novel neural network algorithms to improve the boundary identification and growth change: Other neural network algorithms such as recurrent networks could be considered and tested to reduce errors in the phase boundaries. Fuzzy one-of-N codes or Gradient one-of-N codes methods could be used for monitoring the characteristic transition of cyanobacteria.

- Application of dynamical signal processing: Dynamical models could be applied to the raw data for the analysis of transient sensor responses, which can improve the overall classification rate. Preliminary results in this area look promising [1].

7.3 Reference

1. J. W. Gardner, C. S. Dow, H. W. Shin, G. Searle, and M. J. Chappell, Dynamical signal processing techniquesfor bioprocess monitoring, The 6th International Symposium, Olfaction & Electronic Nose 99, Tübingen, 20-22 September (1999) 331-335.

Appendix A

Hybrid E-nose with Virtual Instrumentation Programs

The Warwick hybrid e-nose consists of a MOS chamber, a CP sensor chamber, a sampler, interface boards and power supply units. Following sections show operation procedures with VI program details.

A.1 Main System

Switch on the e-nose units including a diaphragm pump and set the MOS sensor heater switches to the appropriate positions. The heater voltages can be selected as 4 V, 5 V or 6 V (sensor cleaning voltage). Allow 30 minutes for the MOS sensor chamber to reach thermal stability.

A.2 Labview Programs

Originally, Craven (Chapter 3) developed the VI programs for the operation of the Warwick e-nose but the modified Warwick hybrid e-nose required more advanced additional VI design. There were three library files, Shin2, Bargraph, Tempsys, to run the

hybrid e-nose. The main library file, Shin2, has four control VIs, LPM Port Test, Temperature System 0.1, CP control2, Advanced V1.93.

A.2.1 LPM Port Test.vi

This program checks the digital output lines from the LPM-16 I/O card before running whole experiment. Each switch corresponds to a pair of digital output and it is necessary to open solenoid valve 1 before running of main control VI, Advanced V1.93 as shown in Figure A.1.

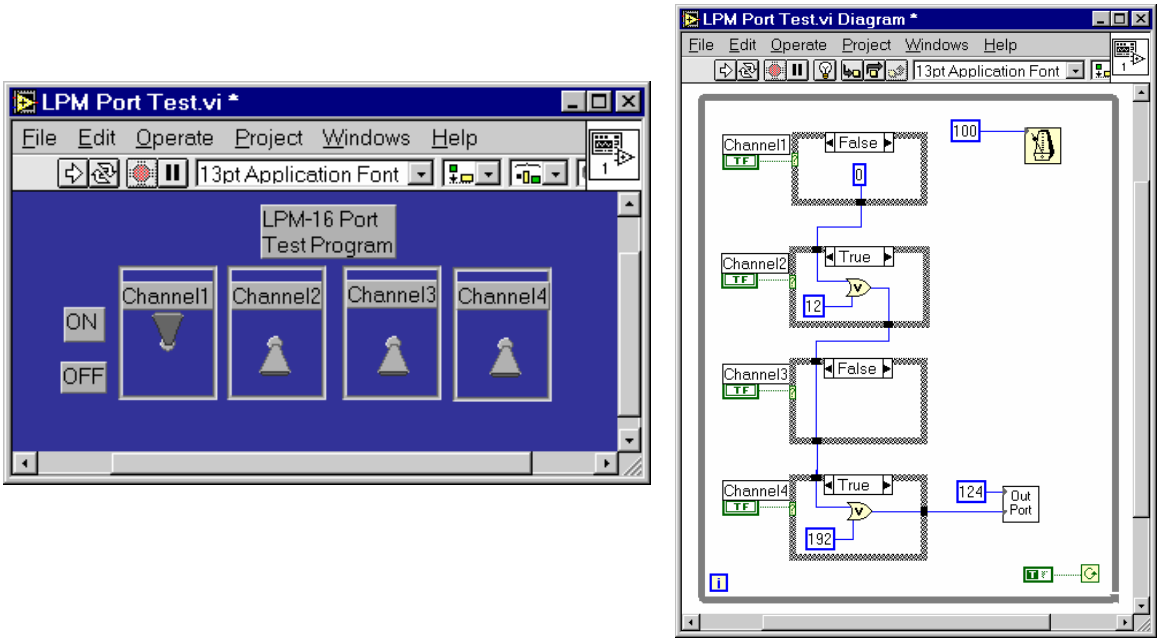

Fig. A.1 LPM Port Test.vi and its block diagram.

A.2.2 Temperature System 0.1.vi

The temperature control vi was updated to the temperature system 0.1vi because the second thermofoil heater (model:HK5547R47.4L12A) was attached in top layer of new CP sensor chamber. The temperatures of MOS and CP chambers were controlled by a on-

off controller using LPM-16 as previous design. Figure A.2 shows the design of the temperature system 0.1.vi. It is necessary to control the target temperature for each chamber using 'Target Temps'. Set to the nominal temperature and run by clicking on running button. This program runs as a background task all the time. The values of offset and ratio are for the conversion of temperature sensor output voltage into degrees centigrade.

A.2.3 CP control2.vi

Figure A.3 shows the program design and block diagram of main CP control2.vi, which was designed as a sub VI of Advanced V1.93.vi. The voltage output from each CP sensor was saved as within a text file and the voltage outputs from flow sensors return to the real flow-rate (ml/min) through the formula node that calculates a equation inside the resizable box. Text file VI converts a 2D or 1D array of single-precision (SGL) numbers to a text string and writes the string to a new byte stream file or appends the string to an existing file. This VI was run with the valve control VI, the temperature control VI and MOS sensor array control VI together.

A.2.4 Advanced V1.93.vi

Select the main vi for the valve control and data collection. If it is activated, then a dialogue box is opened and asks for a configuration file. It simply creates new file or overwrites old file and changes configuration. Figure 3.21 shows the sampling cycle example of configuration. For the flexibility of data collection, sampling rate is changeable using a cycle division mode. Start the system control program and leave it for

a duration of particular time span. If there is an error or problem, then simply activate the exit button to stop running program.

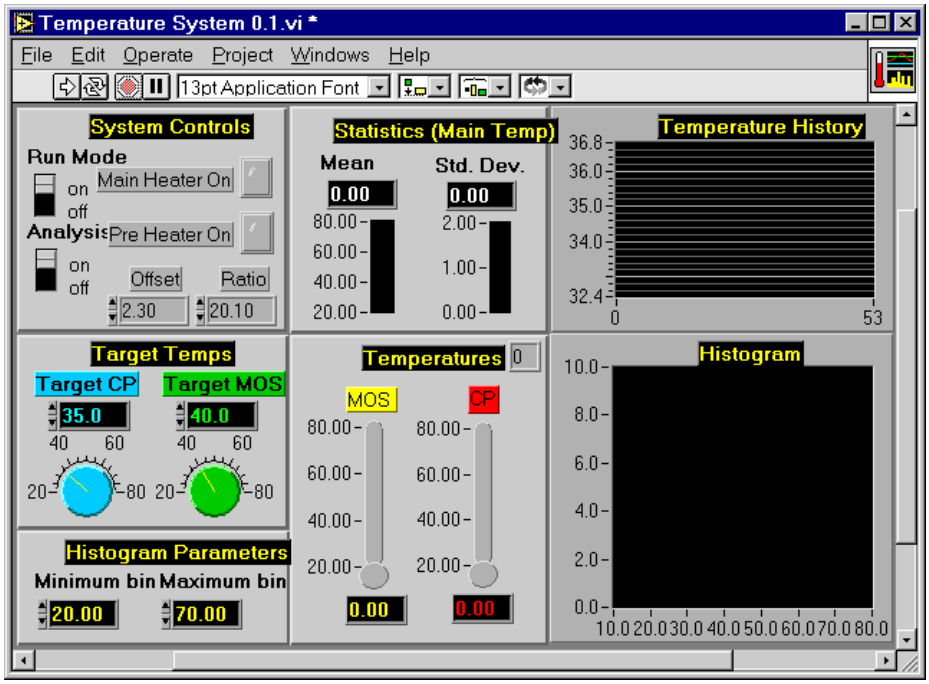

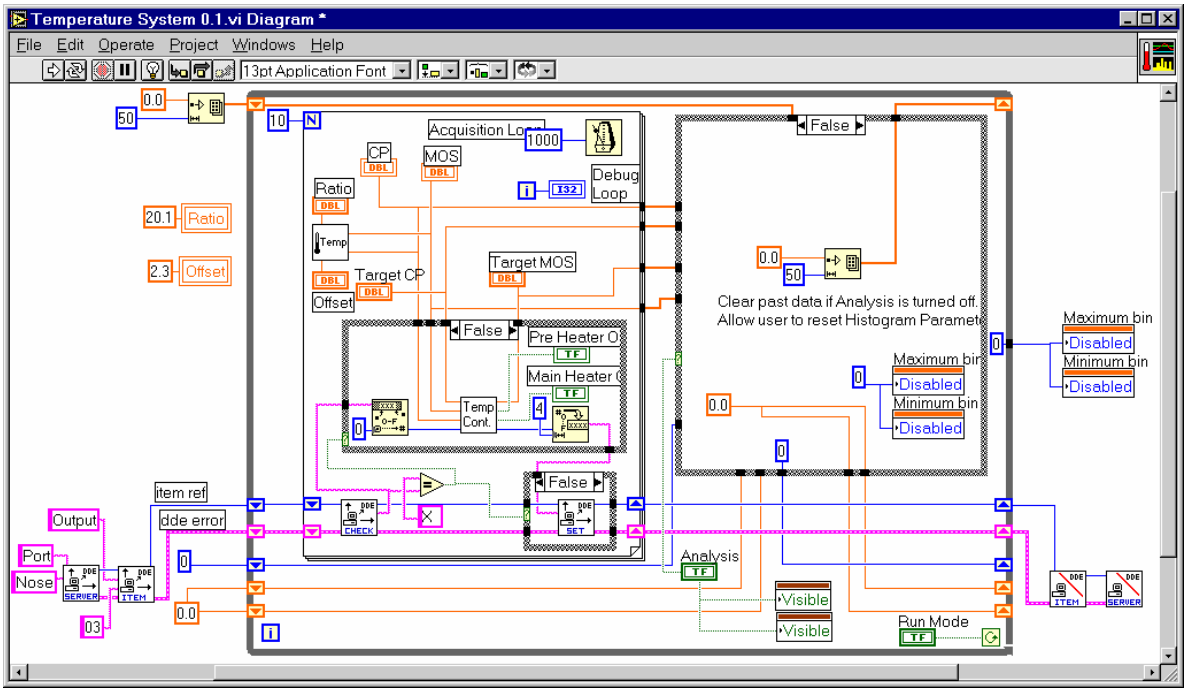

Fig. A.2 Temperature System 0.1.vi and its block diagram.

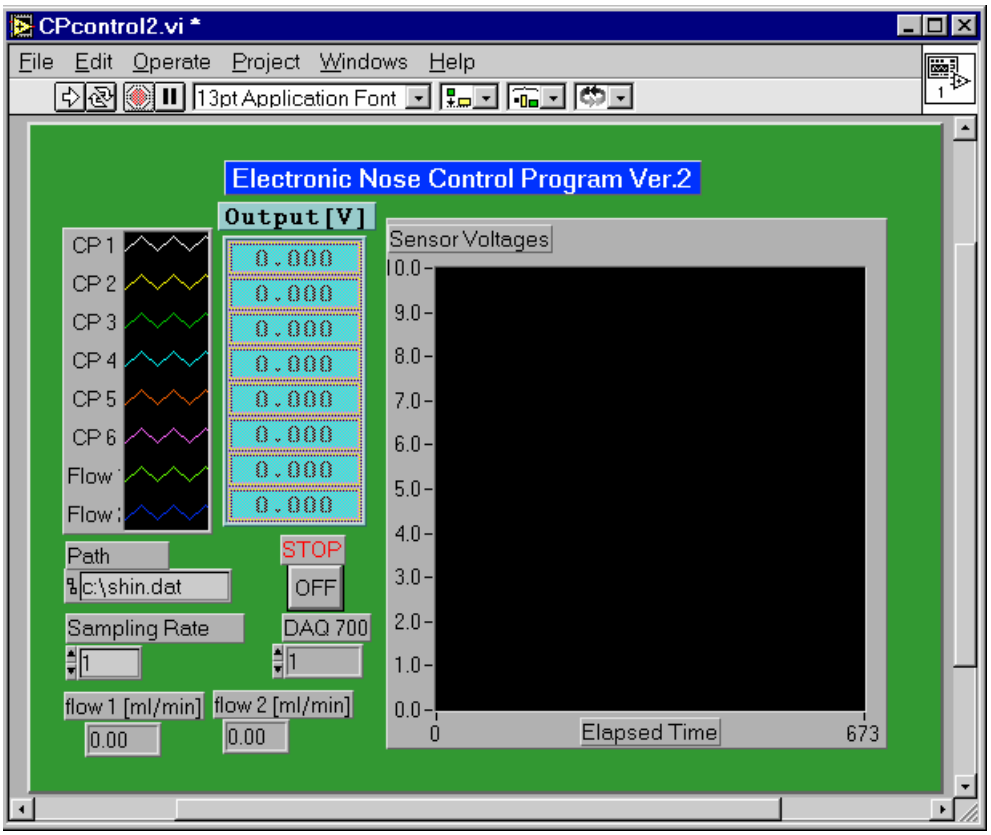

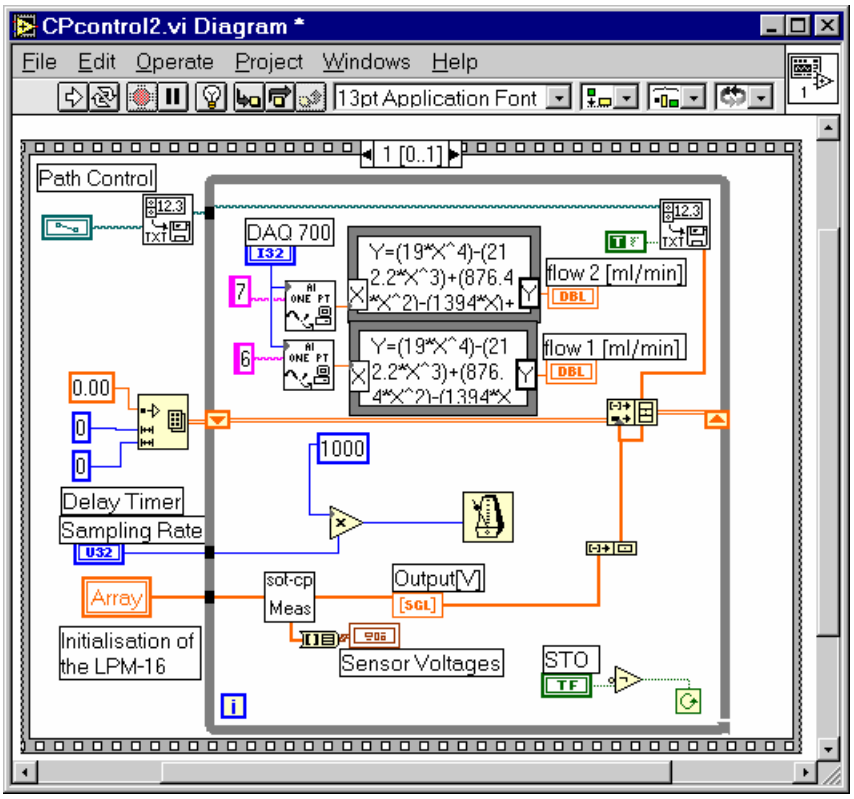

Fig. A.3 CP Control2.vi and its block diagram.

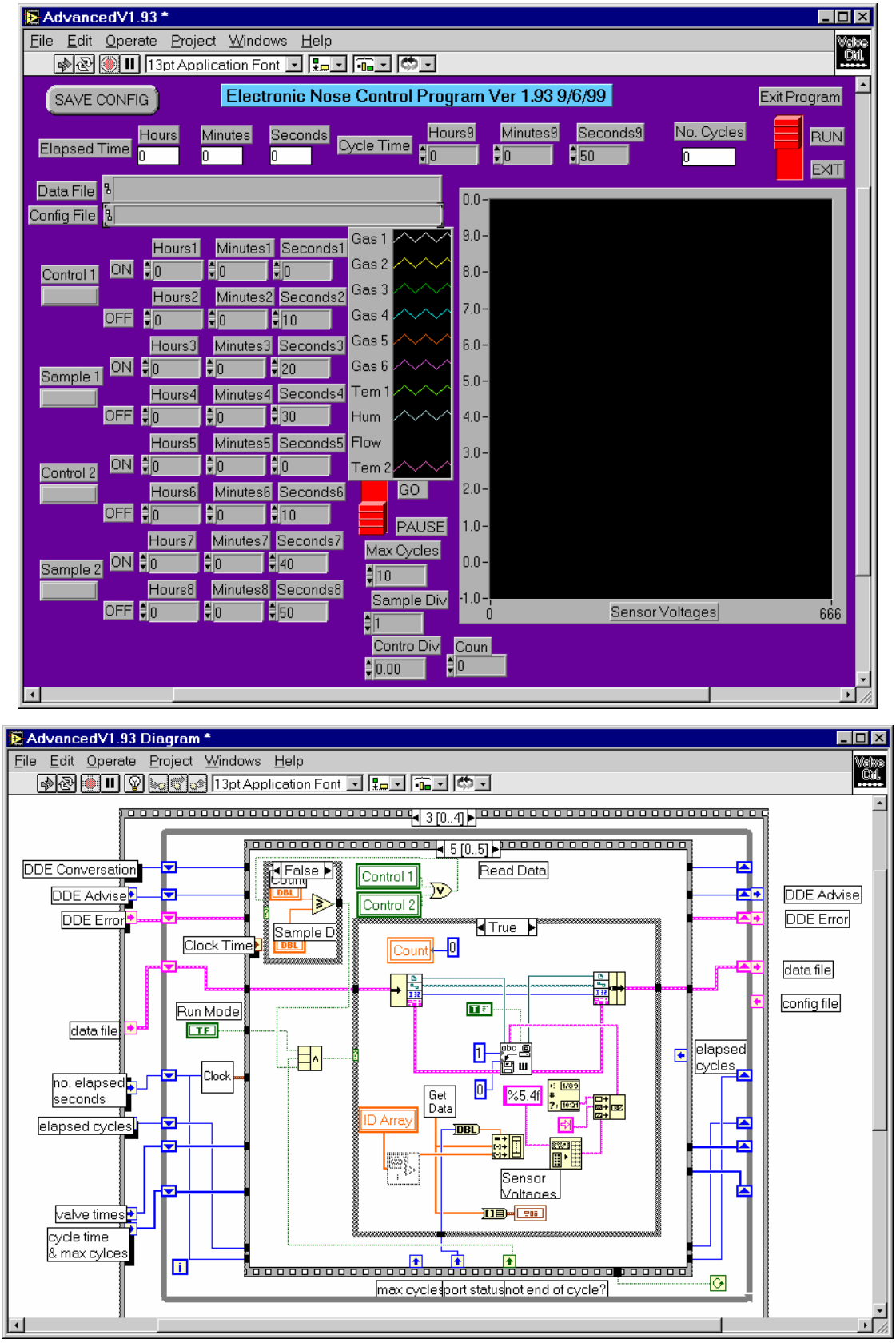

Fig. A.4 Advanced V1.93.vi and its block diagram.

A.3 Calibration of Sensor Resistance

Each MOS sensor should be calibrated before the experiment commenced. The channel is selected with a channel switch, then set the resistance switch to the desired position. Then adjust the potentiometer for that channel to give 5 V on its LED display. Return the channel select switch to its off position to switch the MOS sensor back into circuit. In CP sensor, coloured dip switches and variable resistors were used to change the resistance range of CP, then output voltage. Optimum output voltage range of sensors were 5 V to 7.5 V, otherwise results may not be accurate.

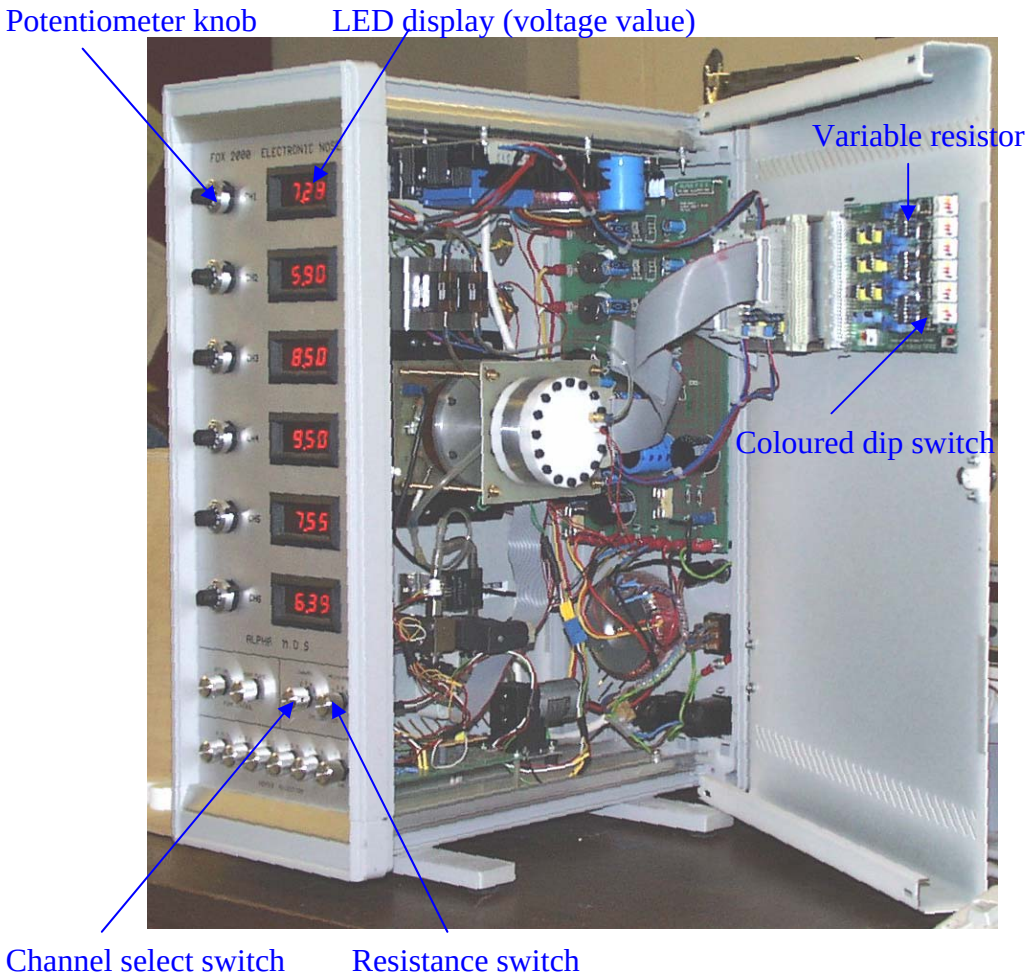

Fig. A.5 Photograph of the Warwick hybrid electronic nose system.

Appendix B

Interface Circuit Diagram of CP Sensor Array

The additional interface card was produced for the interface of flow sensors and the CP interface card with a LPM-16 card (section 5.2.3). The details of circuit diagram and layout are as follow.

Appendix C

PTFE Holder for Silicon Wafer Backside Etching

Mechanical protection of the backside can be achieved with a holder. The holder was made from PTFE, which is inert with respect to the anisotropic etchants. The 3 inch wafer is fixed between teflen-coated O-rings, which are carefully aligned in order to avoid mechanical stress in the wafer by the mount (section 3.3.2). The details of design are as follow.

Appendix D

Design of CP Sensor Chamber

The new CP sensor chamber was designed to enhance the existing electronic nose's performance, because of more sensors and better dynamic response through a reduction in dead-volume (section 5.1). The precise dimensions of the chamber can be seen as follows.